REACTIVE BARRIER MEMBRANES WITH ENVIRONMENTAL APPLICATIONS

A DISSERTATION
SUBMITTED TO THE FACULTY OF THE GRADUATE SCHOOL
OF THE UNIVERSITY OF MINNESOTA
BY

ANDREW M. WARTA

IN PARTIAL FULFILLMENT OF THE REQUIREMENTS
FOR THE DEGREE OF
DOCTOR OF PHILOSOPHY

EDWARD L. CUSSLER JR., PH.D.
WILLIAM A. ARNOLD, PH.D
ACADEMIC AND RESEARCH ADVISERS

DECEMBER, 2010

Acknowledgements

I would first like to thank my family, my parents: Joe and Kathy, brothers: Matt, Chris and Alex, and sister Tori, whose loving support and encouragement have helped me more than they could ever know. My friends – who were always there to joke around with, have fun, play games and wander campus after midnight with – that have helped keep me from going crazy these last few years (some I'm sure would question whether they truly managed the last part).

I would especially like to acknowledge my best friend, soul mate, and wife, Denise Feda. No accomplishment would mean anything if I couldn't share it with you.

I would like to thank the members of the Cussler Group: Eric, Nancy, Pieter, Abhishek, Jonathan, Bill, Brian, Joe, Junshun, Quan, and Nate, and the Arnold Group: Shimo and Erin, who have helped keep the days light and upbeat despite the mountains of work that always seem to pile up. Special thanks go to Ed Cussler and Bill Arnold who have provided wonderful guidance and have instilled in me the belief that collaborations between professors can not only work, but give rise to higher levels of research and understanding. Thanks also to the faculty and staff of the University of Minnesota and University of Nebraska, who have always been willing to lend their expertise, and an extra hand when needed.

To the people of the Heppner Garden Level, Neihardt Council, UNL RHA, NRHH, my MACURH Bid Team, MACURH, NACURH, COGS, and GAPSA who taught me so much about myself, I give a huge thank you. From them I learned the power of being a member of a group yet keeping an individual perspective and outlook; to mesh your abilities with those around you and to build on the strengths of others. (They also taught me it is possible to only sleep 8 hours in 8 days). Chuck and Jefe, who helped so much in bringing out leadership qualities I never would have guessed I had, to you I also say thank you.

And finally, to all those who I haven't mentioned above but have touched my life through all these years, thank you all.

Dedication

I dedicate this thesis to everyone who has helped me become the person I am. Without all of you, this document could never exist.

Abstract

Addition of reactive groups to a barrier membrane can increase lag time for specific contaminants. Loading polyvinylalcohol (PVA) with a cesium-selective crystalline silicotitanate (CST) is shown to greatly increase lag time for cesium ion when upstream concentration is constant. Experiments are reproducible. Results can be generalized to real-world environmental applications.

Loading powdered activated carbon (PAC) to PVA is shown to greatly increase lag time for 1,2,4-trichlorobenzene (1,2,4-TCB), a model for polychlorinated biphenyls (PCBs). Flow-through diffusion cell tests are performed challenging a PAC loaded barrier membranes with varying upstream concentrations. Desorption from a loaded PAC barrier membrane is shown to depend on the square root of time.

Theoretical models are derived for four cases where a reactive volume degrading a contaminant in series with a sorbing, carbon-containing volume. Reactions following first-order kinetics allow more contaminant to escape from the modeled systems than reactions following zero-order kinetics.

Results are summarized and potential future work is suggested.

Table of Contents

List of Tables

List of Figures

Chapter 1

Introduction and Goals

This chapter explains why this research is being done. In particular, the environmental concerns addressed by this project are emphasized. By the end of this chapter a reader should have a clear view of the applications and potential impacts of barrier membranes studied in this research.

1.1 Motivation

1.1.1 Cesium-137 pollution

Cesium-137 (^{137}Cs) containment is a high priority of radioactive waste treatment facilities because ^{137}Cs emits gamma radiation, has a long half-life, and has a high mobility in the biosphere (Moore, 1993). A fission product of uranium and plutonium production, ^{137}Cs is a radioactive isotope of the element cesium. The relatively long half-life of 30 years for ^{137}Cs is cause for environmental concern because of the radioactive decay process. ^{137}Cs undergoes beta-minus decay to ^{137}Ba which quickly emits a 660 keV gamma particle as shown in Equation 1.1.

$$^{137}Cs \underset{30\,yr}{\rightarrow} {}^{137}Ba^{*} + \beta^{-} \underset{2.6\,\mathrm{min}}{\rightarrow} {}^{137}Ba + \gamma_{660keV} \qquad (1.1)$$

Cesium shares many of the same chemical properties as other Group I metals, such as sodium and potassium, and undergoes the same reactions in the environment. This is of concern in biological systems where sodium and potassium are part of the muscular and nervous structures of organisms. ^{137}Cs atoms can undergo radioactive decay while bound inside living organisms, which can lead to loss of cell function, cell mutation, or cell death. Radioactive cesium may enter the environment by leaking into groundwater and other natural waterways surrounding containment zones. Hanford, WA is an example of a containment area which may unintentionally release ^{137}Cs into the environment.

The Hanford Site, in the south-central part of Washington State, was used by the U.S. for plutonium processing starting in 1944. Nine reactors were used at the site up until 1986. Currently, nuclear waste is stored underground in the 200 Area of the Hanford Site where ^{137}Cs constitutes 40% of the radioactivity in nuclear waste containers

(McKinley, 2001). This ^{137}Cs, in the supernatant of canisters, can leak into surrounding soil (Gephart, 1998). Of the approximately 28 MCi of ^{137}Cs stored in the 200 area, an estimated 0.08 MCi has already leaked into the ground below the containment zone (Garten, 2000). This leakage is of particular environmental concern because of the proximity of the Columbia River to the Hanford site, shown in Figure 1.1.

1.1.2 Polychlorinated biphenyl pollution

Polychlorinated biphenyls (PCBs) were a class of molecules widely used in industry for their physical and chemical properties starting in 1929 until their use was banned in the US in 1978 (Abramowicz and Olson, 1995, Wiegel and Wu, 2000). Relatively inert, these molecules are flame resistant, have low vapor pressure and water solubility, excellent dielectric properties, and are stable to oxidation (Kimbrough and Jensen, 1989). Of the more than 1.2 billion pounds (627,000 tons) of PCBs used in North America, more than 280 million pounds (143,000 tons) are in landfills and dumps, and more than 150 million pounds (77,000 tons) of PCBs have been leaked into the environment (Buckley, 1982).

Polychlorinated biphenyls have been shown to cause organ damage, specifically liver damage. The amount of chlorination of the compounds was found to determine the degree of systemic toxicity (Drinker *et al.*, 1937). Two cases demonstrating the dangers of PCBs and other chlorinated compounds involving rice oil have occurred. The first, in Western Japan in 1968, involved over 1850 people. The second, in Taiwan in 1979 involved over 2000 people. These incidents resulted in health problems including acne like pustules, respiratory and liver irregularities, chronic bronchitis, and severe ocular problems of the meibomian glands such as irregular arrangement, atrophy, and "secretion of cheese-like material" more than ten years after ingesting the chlorinated compounds (Kuratsune *et al.*, 1972, Kuratsune, 1972). Children born to mothers who consumed contaminated rice oil in Taiwan were more likely to develop middle-ear diseases (Chao *et al.*, 1997), musculoskeletal changes (Guo *et al.*, 1994), ectodermal defects and developmental delay (Chen *et al.*, 1992).

1.2 Goals and Applications

The primary goal of this research is to create reactive barrier membranes to selectively contain contaminant compounds, specifically cesium and PCBs. Past research has shown barrier effectiveness can be increased by a factor of 10 to 1000 by incorporating reactive groups into the barrier matrix (Yang *et al.*, 2001). Yang *et al.* also present the mathematical theory governing this increase for reversible and irreversible reactions.

The barrier membranes synthesized in this project incorporate ion-exchanging and adsorptive materials such as crystalline silicotitanate (CST), which was designed to specifically bind cesium from aqueous solution, and powdered activated carbon (PAC), a sorbent for organic compounds. Loading barrier membranes with these materials should greatly hinder breakthrough of selected contaminants. The results of this work are compared to the theory of Yang *et al.* and where necessary, new theories are developed.

Two main applications are envisioned for cesium-selective barrier membranes. First, they can be used as a removable liner placed around areas contaminated with ^{137}Cs. Not only would these liners prevent radioactive cesium from diffusing into groundwater, but also the liner may simply be removed and replaced if damaged or saturated with cesium. The ability to place a selective barrier in areas known to have high concentrations of cesium can aid in preventing further contamination.

Second, cesium-selective barrier membranes may be used as secondary containment for vessels containing radioactive cesium. As discussed above, canisters containing ^{137}Cs in the supernatant at the Hanford, WA site have been known to leak. Surrounding canisters with one of these barriers could contain any leaks that develop while crews repair or replace the breached container, preventing additional subsurface contamination. If a geological depository for nuclear waste becomes reality, waste will need to be transported across the country (Garrick, 2003). The extra containment offered by these cesium-selective barrier membranes could increase transport safety.

Powdered activated carbon (PAC) containing barrier membranes could be used in similar situations to those described above for organic pollutants such as PCBs and other chlorinated compounds. Additionally, this research investigates other possible uses for

barriers utilizing adsorptive reactive groups including damping concentration fluctuations and controlled release of reagents, which may prevent toxic shocks to bacteria used in the biodegradation of contaminants.

Before potential applications are thoroughly explored, proof of the principle must be given. The work discussed in the next few chapters shows the background and experimental expertise necessary to proceed.

1.3 Thesis Arrangement

The following four chapters address three main points: background and theory, new experimental research, and correlation of this research to theory. Each chapter builds upon the ideas and experiments presented in the previous chapter.

Chapter 2 focuses on the theory of mass transport through homogeneous and heterogeneous membranes. Diffusion cell experiments yielding measurements of lag times and how they change with different reacting systems are emphasized. Diffusion properties of contaminants through flake-filled barriers are discussed.

Chapters 3 and 4 focus on the tools and procedures used to carry out this research, as well as its results. Chapter 3 discusses barrier membranes containing ion-exchange materials for specific contaminants (cesium and chloride) and the resulting increase in breakthrough times for these contaminants in diffusion cell tests. Results primarily focus on constant upstream concentrations.

Chapter 4 discusses barrier membranes containing materials that adsorb contaminants. Increased breakthrough times for constant upstream concentrations are shown. Experiments in which the upstream concentration is varied are also performed. Results primarily focus on membrane response to varying upstream concentration. Theories to approximate these results are derived and discussed.

Chapter 5 summarizes the results of this thesis, and suggests ideas that could build upon this research.

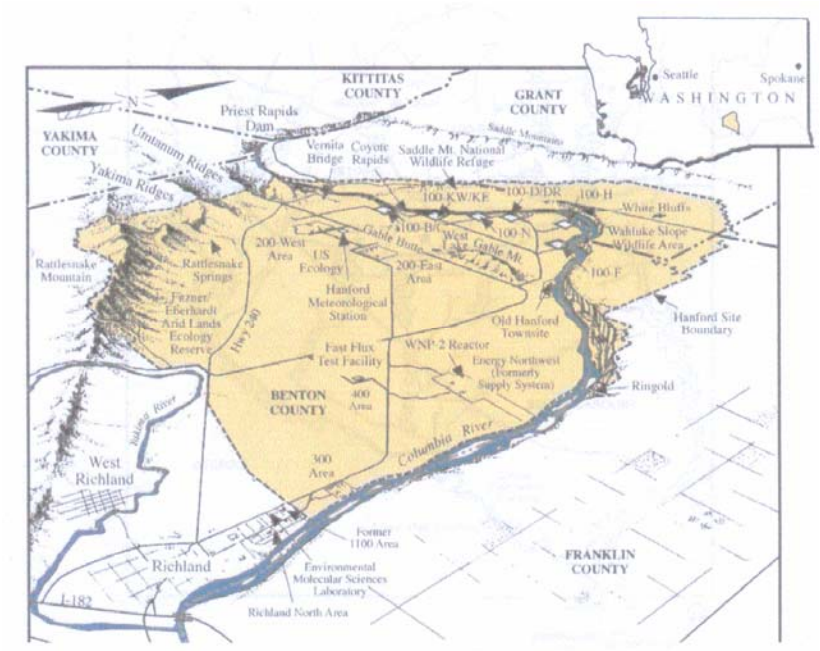

Figure 1.1: Site map of the Hanford Site in Washington State. The Columbia River flows through the complex and forms much of the southern and eastern border. (Garten *et al.*, 2000)

Chapter 2

Background for Barrier Membranes

This chapter establishes the theoretical groundwork for this thesis. The discussion focuses on the existing knowledge of barrier membranes and the chemistry relevant to this work. The principles of ion-exchange and detection using ion-selective probes are outlined. The ideas covered are basic to an understanding the material presented in the following chapters.

2.1 Barrier Membranes

Membranes are used as barriers industrially in applications varying from liners for landfills to coatings for controlled release of medication. These often chemical-specific barriers are used to increase the usable life of a material, be it food in a supermarket or the wing of a fighter aircraft. Barrier membranes accomplish this by altering the transport properties of a chemical through the barrier surface. To understand how these barriers work, it is important to look closely at how transport occurs through the membrane.

In barrier membranes, transport is due to diffusion. Diffusion is the result of random motion of particles moving from an area of higher chemical potential to an area of lower chemical potential. Diffusion resulting from a concentration gradient is the easiest to visualize and measure. As time elapses, the concentration gradient between two solutions in contact with each other will lessen until the concentrations are the same.

Perhaps the most recognizable law to define diffusion is Fick's First Law

$$J_{1(z)} = -D\frac{\partial c_1}{\partial z} \qquad (2.1)$$

where $J_{1(z)}$ is the overall mass flux of species 1, c_1 is the concentration of species 1, z is distance along the direction of diffusion and D is the diffusion coefficient which will be assumed in this chapter to be independent of concentration. This one dimensional equation relates the flux of a species to its change in concentration with position. Fick also developed the following for unsteady-state diffusion:

$$\frac{\partial c_1}{\partial t} = D\left(\frac{\partial^2 c_1}{\partial z^2} + \frac{1}{A}\frac{\partial A}{\partial z}\frac{\partial c_1}{\partial z}\right) \qquad (2.2)$$

where A is the area diffusion occurs across. When the area A, is constant, Equation 2.2 reduces to the familiar form of Fick's second law

$$\frac{\partial c_1}{\partial t} = D\frac{\partial^2 c_1}{\partial z^2} \quad . \tag{2.3}$$

It is important to remember this equation implies one-dimensional diffusion of a species with constant diffusion coefficient across a constant area. With these laws of diffusion in hand, diffusion through a barrier membrane can be explained. The first barrier type to explore is for homogeneous thin-film membranes.

2.2 Homogeneous Membranes

Transport through a barrier membrane can be either steady-state or unsteady-state. Concentration profiles and fluxes for each case can be found by solving Equation 2.3 for appropriate boundary conditions. These solutions also allow for the definition of the "lag time" giving a measure of barrier membrane effectiveness. For this research, a larger lag time and/or a lower flux means a better barrier membrane.

2.2.1 Steady-State

If transport through a barrier membrane is at steady-state, the time dependence of Equation 2.3 is zero with respect to position z

$$0 = D\frac{\partial^2 c_1}{\partial z^2} . \tag{2.4}$$

Imagine a thin-film with thickness l separating two well-stirred solutions with different concentrations. The higher concentration solution is labeled the "upstream" side and the lower concentration solution is labeled the "downstream" side. For the simplest case where concentrations are equal on both sides of each solution/thin-film interface, the expected concentration profile is shown in Figure 2.1.

The linear concentration profile shown in Figure 2.1 comes from integration of Equation 2.4 with the following boundary conditions:

$$z = 0 \qquad c_1 = c_{1(0)} \tag{2.5}$$

$$z = l \qquad c_1 = c_{1(l)}\,. \tag{2.6}$$

This integration gives the concentration at any distance z as

$$c_1 = \frac{z}{l}(c_{1(l)} - c_{1(0)}) + c_{1(0)}\,. \tag{2.7}$$

The flux can be found by taking the derivative of Equation 2.7 with respect to z

$$\frac{dc_1}{dz} = \frac{1}{l}(c_{1(l)} - c_{1(0)}) \tag{2.8}$$

and substituting Fick's first law (Equation 2.1)

$$J_{1(z)} = \frac{D}{l}(c_{1(0)} - c_{1(l)})\,. \tag{2.9}$$

Equation 2.9 gives the steady-state flux within the membrane.

In the above derivation, it was assumed the concentration was constant across the solution/thin-film interface. This is not valid for many materials used as barrier membranes, where the concentration may change by orders of magnitude across the interface as shown in Figure 2.2. To relax this assumption, a partition coefficient, *H*, is introduced where

$$z = 0 \qquad c_1 = HC_{1(0)} \tag{2.10}$$

$$z = l \qquad c_1 = HC_{1(l)}\,. \tag{2.11}$$

Integrating Equation 2.4 with these new boundary conditions and again applying Equation 2.1 to the result gives the steady-state flux inside the membrane

$$J_{1(z)} = \frac{DH}{l}(C_{1(0)} - C_{1(l)}) \tag{2.12}$$

in terms of the upstream and downstream concentrations.

When designing a barrier membrane to slow or stop a contaminant from breaking through, reducing this flux is desirable. For a given $C_{1(0)}$, Equation 2.12 shows this can be accomplished by increasing membrane thickness, l, or decreasing the quantity DH, called the permeability. Increasing membrane thickness is straight-forward, though it is often undesirable to alter the thickness of an existing material. An example showing this

comes from the computer industry. Microchips need to be protected from oxygen, but space does not allow for increasing the thickness of the barrier protecting them.

Decreasing the permeability is also a possibility. To accomplish this, a different polymer membrane with a lower partition coefficient for a given contaminant is used. An example showing differing permeabilities is water-swollen polyvinylalcohol (PVA) and high-density polyethylene (HDPE). Hydrochloric acid (HCl) placed upstream of a 250 μm PVA membrane is detected on the downstream side in minutes. For the same thickness HDPE membrane, it takes days or weeks before HCl is detected downstream. The decreased permeability of HCl in HDPE is responsible for this decreased flux.

Other possibilities for reducing permeability are addition of impermeable solid particles or reactive groups to the barrier membrane polymer matrix. Each of these topics will be discussed below with emphasis placed on reactive barrier membranes.

2.2.2 Unsteady-State

To this point, the discussion has focused on steady-state transport through a thin-film. Unsteady (time dependent) transport is equally important for understanding behaviors of barrier membranes. Combining these two phenomena gives the full downstream concentration profile and allows for definition of a new parameter, the lag time.

For unsteady-state transport through a thin-film, Fick's second law (Equation 2.3)

$$\frac{\partial c_1}{\partial t} = D\frac{\partial^2 c_1}{\partial z^2}$$

is integrated with initial condition and boundary conditions

$$t = 0 \quad \text{all z} \qquad c_1 = 0 \tag{2.13}$$

$$t > 0 \quad z = 0 \qquad c_1 = c_{1(0)} \tag{2.14}$$

$$z = l \qquad c_1 = 0\,. \tag{2.15}$$

The initial condition says species 1 is not present in the thin-film. The first boundary condition is straightforward: the upstream reservoir concentration is greater than zero and does not change with time. The second boundary condition is less clear, stating the

downstream concentration remains devoid of species 1 for all time. Examination of Equation 2.12 shows if a steady-state is reached, there will be some flux of species 1 to the downstream reservoir. The solution avoids this concern by assuming the downstream concentration of species 1 is small, much less than $c_{1(0)}$.

The partial differential equation form must be solved by separation of variables. Crank (1975) shows the solution is an infinite summation

$$c_1 = c_{1(0)} - \frac{c_{1(0)} z}{l} - \frac{2c_{1(0)}}{\pi} \sum_{n=1}^{\infty} \frac{1}{n} \sin\left(\frac{n\pi z}{l}\right) \exp\left[\frac{-Dn^2\pi^2 t}{l^2}\right]. \quad (2.16)$$

The previous equations apply at steady-state; Equation 2.16 applies at all time. A measure of how much time a thin-film takes to reach steady-state has been derived by Daynes (1920) by taking the limit of Equation 2.16 at large times to get

$$\frac{c_1}{c_{1(0)}} = \frac{AD}{Vl}\left(t - \frac{l^2}{6D}\right) \quad (2.17)$$

where V is the downstream reservoir volume. This equation gives the time to reach steady-state

$$t_L = \frac{l^2}{6D} \quad (2.18)$$

where t_L is called the lag time.

The lag time can be found experimentally by a diffusion cell experiment. In a diffusion cell experiment, a thin-film is placed between two well-stirred solutions of known volume. A solute is added to the upstream solution and concentration of solute in the downstream solution is measured with time. A typical plot of downstream concentration versus time is shown in Figure 2.3. The lag time is found by linear regression of the steady-state slope to the x-axis. The time at which the regression crosses the x-axis is the lag time, which gives a parameter to compare barrier membrane effectiveness. In general, a larger lag time indicates a better barrier.

For a homogeneous membrane, Equation 2.18 shows the lag time varies with l^2 and inversely with diffusivity. Doubling the membrane thickness results in a factor of four increase in lag, while halving the diffusivity doubles the lag. Increasing thickness is

generally easy, but it is desirable to find other lag time increasing factors. Impermeable flakes may be added to the barrier membranes, but the increase to lag time is often small. Addition of reactive groups to membranes can have a much larger impact.

2.3 Heterogeneous Membranes

The previous section shows the lag time of a homogeneous membrane is a fixed ratio of membrane thickness and diffusivity. For a given homogeneous membrane material the diffusivity (permeability) is fixed, leaving only varying thickness to increase lag time. Addition of a second phase to the barrier membrane can also increase the lag time. This section looks at impermeable flake-filled membranes and addition of reacting species to increase barrier lag time with primary focus on the latter.

2.3.1 Flake-Filled Membranes

The permeability of a barrier membrane can be decreased through addition of impermeable solid flakes (Eitzman *et al.*, 1996; Lape *et al.*, 2004; Perry *et al.*, 1989; Yang *et al.*, 2004) such as mica or clay. These particles increase the path length a contaminant molecule must travel through a barrier membrane as shown in Figure 2.4.

Increased path length, or tortuosity, in a membrane leads to lower measured permeability as it takes longer for a particle to transport through the barrier. As Maxwell showed for spheres in 1881 and Rayleigh showed for cylinders in 1892, the decrease in permeability is a function of volume fraction, not particle size (Brydges *et al.*, 1975; Michaels *et al.*, 1975; Wakeman and Mason, 1979; Falla *et al.*, 1996). The presence of the flakes also decreases the area that is available for transport. Equation 2.2 shows diffusive flux is dependent on membrane area. Decreasing the area for transport decreases the flux (Cussler *et al.*, 1988).

2.3.2 Reactive Membranes

Addition of a reactive group can greatly increase the lag time of a barrier membrane. If a reaction rapidly consumes a contaminant species as it passes through a

barrier membrane, the lag time will increase. The following shows addition of a reactive group does not change the steady-state flux, but can delay steady-state significantly.

To explain this case, imagine two solutions will be separated by a reactive barrier film. A contaminant, species 1, will diffuse from the upstream side through the reactive membrane which is initially loaded with immobile species 2. As species 1 diffuses it will react with species 2. This can be modeled as a second order reaction

$$R_1 + R_2 \underset{k_B}{\overset{k_F}{\rightleftharpoons}} P \tag{2.19}$$

where R_1 is the diffusing contaminant species, R_2 is the immobile reactive species, P is the reaction product, k_F is the forward reaction rate constant and k_R is the reverse reaction rate constant.

It is necessary to solve mass balances within the barrier to find how large an increase in lag time to expect. These mass balances are

$$\frac{\partial c_1}{\partial t} = D_1 \frac{\partial^2 c_1}{\partial z^2} - k_F c_1 c_2 + k_R c_P \tag{2.20}$$

$$\frac{\partial c_2}{\partial t} = D_2 \frac{\partial^2 c_2}{\partial z^2} - k_F c_1 c_2 + k_R c_P \tag{2.21}$$

$$\frac{\partial c_P}{\partial t} = D_P \frac{\partial^2 c_P}{\partial z^2} + k_F c_1 c_2 - k_R c_P \,. \tag{2.22}$$

The boundary conditions are as follows

$$t = 0 \quad \text{all z} \qquad c_1 = 0 \qquad c_2 = c_{2(0)} \qquad c_p = 0 \tag{2.23}$$

$$t > 0 \qquad\qquad z = 0 \qquad c_1 = HC_{1(0)} \tag{2.24}$$

$$z = l \qquad c_1 = 0 \,. \tag{2.25}$$

These assume no species 1 or product present in the membrane or downstream solution initially. As before, H is a partition coefficient. Equation 2.25 shows the downstream concentration of species 1 is negligible for all times, even though species 1 will have some flux into the downstream reservoir.

Of special interest are systems where the reaction is sufficiently "fast". A fast reaction is characterized by a large Damköhler number $\frac{kl^2}{D}$, where k is the reaction rate constant, l is the membrane thickness and D is the diffusion coefficient for species 1. The Damköhler number relates the speed of reaction to the speed of diffusion. If the rate of reaction is slow compared to the rate of diffusion, it is said to be reaction limited and has a small Damköhler number. If the rate of reaction is fast compared to diffusion, it is diffusion limited and has a large Damköhler number. The following sections solve Equations 2.20-2.22 assuming large Damköhler number.

2.3.2.1 Instantaneous Reaction

A sufficiently large rate of reaction can be modeled as an instantaneous reaction. In this limit, reaction occurs immediately upon arrival of a diffusing particle. Thus species 1 and 2 cannot coexist. The following sections detail the differences of instantaneous reversible and irreversible reactions.

2.3.2.2 Reversible Reaction with Mobile Product

Many reactions are reversible, having equilibrium between products and reactants. Second order reversible reactions with a single product have the same form as Equation 2.19 with a forward and reverse rate constant. The equilibrium equation can be written as

$$c_p = Kc_1c_2 \qquad (2.26)$$

where K is the overall rate constant defined as $K = \frac{k_F}{k_R}$.

If the reaction within a reactive membrane is reversible and the product is mobile, the solution to Equations 2.20 through 2.22 is known. This most widely studied reactive membrane case is called facilitated diffusion (Cussler, 1997). The solution assumes species 2 is present in excess within the membrane. The concentration of species 2 is nearly constant and can be grouped with the overall reaction rate constant in Equation 2.26 to give

$$c_p = K' c_1 \tag{2.27}$$

where $K' = Kc_2$ is the apparent reaction rate constant. Using this relation, Equations 2.20 and 2.22 are added to give

$$(1 + K')\frac{\partial c_1}{\partial t} = D(1 + K')\frac{\partial^2 c_1}{\partial z^2} \tag{2.28}$$

which assumes diffusion coefficients for both species are equal. Applying a mass balance and solving with initial condition and boundary conditions from Equations 2.23 through 2.25 gives

$$\frac{C_1}{C_{1(0)}} = \left[\frac{DH}{l}(1 + K')\frac{A}{V}\right]\left(t - \frac{l^2}{6D}\right) \tag{2.29}$$

where V is the downstream cell volume.

This result, for facilitated diffusion, is an interesting contrast with that for diffusion without reaction. Comparing the quantity in the final set of parentheses of Equation 2.29 with that for a homogeneous membrane given in Equation 2.18 shows that lag time for facilitated diffusion is the same for that without reaction. Further comparison of Equation 2.29 with Equation 2.17 shows the homogeneous membrane permeance, defined as $\frac{DH}{l}$, has increased by a factor of $(1 + K')$. The flux of species 1 has increased because it now exists alone and bound as part of a product. Although the lag time of species 1 looks to be the same for facilitated transport and a homogeneous membrane, experiments often do not support this. Ward (1970) suggests unequal diffusion coefficients may be the cause of this discrepancy. More importantly, a reversible reaction with mobile product is not a good candidate for increasing lag time, the goal of this discussion. A better solution, keeping the reaction fast, but making the product immobile, is discussed next.

2.3.2.3 Reversible Reaction with Immobile Product

The previous section shows addition of a reacting group to a barrier membrane does not necessarily increase lag time. Luckily for this research, it is possible to design a

reactive barrier membrane with increased lag time. This is accomplished by an infinitely fast reversible reaction with immobile product.

If excess species 2 and product are immobile, the diffusion coefficients D_2 and D_P are both zero, simplifying Equations 2.20 through 2.22 to

$$\frac{\partial c_1}{\partial t} = D_1 \frac{\partial^2 c_1}{\partial z^2} - k_F c_1 c_2 + k_R c_P \tag{2.30}$$

$$\frac{\partial c_2}{\partial t} = -k_F c_1 c_2 + k_R c_P \tag{2.31}$$

$$\frac{\partial c_P}{\partial t} = k_F c_1 c_2 - k_R c_P . \tag{2.32}$$

Adding Equations 2.30 and 2.32, using a mass balance and integrating, gives the solution

$$\frac{C_1}{C_{1(0)}} = \left[\frac{DH}{l}\frac{A}{V}\right]\left(t - \frac{l^2}{6D}(1+K')\right). \tag{2.33}$$

The permeance is the same as for a homogeneous membrane, $\frac{DH}{l}$, so the steady-state flux of the reactive membrane is the same as for the homogeneous membrane. Unlike for the mobile product, reaction with immobile product leads to an increase in the lag time by a factor of $(1+K')$. For an apparent reaction rate constant of 9, Equation 2.33 suggests a lag time increase by a factor of 10. The goal of finding a reacting system to increase barrier lag time has been reached. Fast reactions lead to longer lag times.

What happens as K' goes to infinity? Even with excess species 2 present, there comes a time when the entire immobilized reagent is consumed. This implies a reaction with an infinitely large apparent rate constant will have an infinite lag time. This is not true: there is a limit to lag time increase as explained in the next section.

2.3.2.4 Irreversible Reaction

Very fast irreversible kinetics can lead to a dramatic increase in lag time. An instantaneous irreversible reaction of the form $R_1 + R_2 \longrightarrow P$ both has no reverse rate constant and here happens instantly (very large Damköhler number). There can be any

number of mobile or immobile products, but the reagent, species 2 and products are assumed immobile. Mobile products affect the steady-state flux but not the lag time.

The idea of a moving reaction front provides a basis for deriving the lag time of irreversible reactive membranes. Diffusing species 1 reacts on contact with species 2 to set up the moving front. There is no species 2 present behind the front and species 1 is diffusing with a steady-state flux as through a homogeneous membrane. Ahead of the front, no species 1 is present and species 2 has the initial concentration $c_{2(0)}$. The moving reaction front concentration profiles of species 1 and 2 are shown in Figure 2.5.

For all $z \le l'$ within the membrane, the concentration profile for species 1 is linear. The mass balance on species 1 is given by Equation 2.4, the time independent form of Fick's second law. The boundary conditions are

$$z = 0 \qquad c_1 = HC_{1(0)} \tag{2.34}$$

$$z = l' \qquad c_1 = 0 . \tag{2.35}$$

Integration gives the concentration of species 1 as

$$c_1 = HC_{1(0)}\left(1 - \frac{z}{l'}\right) \tag{2.36}$$

where l' is the advancing front location. The flux of species 1 is

$$J_1 = \frac{DH}{l'} C_{1(0)} \ . \tag{2.37}$$

Species 2 is initially present at concentration $c_{2(0)}$ throughout the membrane. This concentration remains constant where $z > l'$, everywhere else it is zero. The advancing front moves slowly, requiring an unsteady-state mass balance on the immobile species 2

$$\frac{d}{dt}\left(Al'c_{2(0)}\right) = \upsilon A \frac{DH}{l'} C_{1(0)} \tag{2.38}$$

where υ is the stoichiometric coefficient for species 2 in the generalized reaction equation $R_1 + \upsilon_2 R_2 \rightarrow \upsilon_P P$. The initial condition for Equation 2.38 is

$$t = 0 \qquad l' = 0 . \tag{2.39}$$

Integration of Equation 2.38 gives

$$l' = \left(\frac{2\upsilon DHC_{1(0)} t}{c_{2(0)}} \right)^{1/2} \tag{2.40}$$

The lag time, when all species 2 has reacted, occurs when $l = l'$. Substituting this into Equation 2.40 and solving for the lag time gives

$$t_L = \left(\frac{l^2 c_{2(0)}}{2\upsilon DHC_{1(0)}} \right). \tag{2.41}$$

Rearrangement allows for ready comparison to previous lag time results:

$$t_L = \frac{l^2}{6D} \left(\frac{3c_{2(0)}}{\upsilon HC_{1(0)}} \right). \tag{2.42}$$

The overall concentration profile is then

$$\frac{C_1}{C_{1(0)}} = \left[\frac{DH}{l} \frac{A}{V} \right] \left[t - \frac{l^2}{6D} \left(\frac{3c_{2(0)}}{\upsilon HC_{1(0)}} \right) \right]. \tag{2.43}$$

Inspection of this equation shows a discrepancy with previous results. If no reactive species 2 is present, the lag time is expected to collapse to the homogeneous membrane result of $\frac{l^2}{6D}$. A concentration of $c_{2(0)} = 0$ in Equation 2.42 predicts a lag time of zero. This cannot be right. The error comes from the steady-state flux approximation of species 1 for $l \le l'$. Even so, Yang *et al.* (2001) show Equation 2.42 holds remarkably well for sufficiently large $c_{2(0)}$, and that it is possible design a membrane with a factor of 10 or even 100 increase in lag time. This result is encouraging for synthesizing reactive barrier membranes with significantly larger lag times.

2.3.2.5 Non-Instantaneous Reaction

The increased lag time results above are for instantaneous reactions. If a reaction cannot be considered instantaneous, barrier membrane behavior is expected to change. This change can be correlated to the Damköhler number.

Reactions with Damköhler numbers between the small and large limit lead to different membrane behavior. For a very slow reaction, the Damköhler number is much

less than one and little of diffusing species 1 is expected to react. In this limit, the barrier will behave as a homogeneous membrane. The increased lag time benefit from addition of species 2 to the membrane is not seen because it does not have time to react.

An instantaneous reaction leads to reaction immediately upon contact of species 1 with species 2. Slower reactions allow species 1 to diffuse farther into a membrane before reacting. Some molecules of species 1 may pass completely through the membrane before all of species 2 is exhausted leading to larger downstream concentrations sooner. The steady-state assumption on species 1 flux is no longer valid. Now the equations to solve are

$$\frac{\partial c_1}{\partial t} = D_1 \frac{\partial^2 c_1}{\partial z^2} - k c_1 c_2 \qquad (2.44)$$

$$\frac{\partial c_2}{\partial t} = -k c_1 c_2 \qquad (2.45)$$

the time dependent term is not set to zero. As before, D_2 is zero for immobile species 2. Instead of an analytical solution, Equations 2.44 and 2.45 are solved with finite difference methods subject to the same initial and boundary conditions in Equations 2.23 through 2.25. Concentration profiles are plotted for different values of Damköhler number, $\Phi^2 = \frac{k l^2 c_{2(0)}}{D_1}$, in Figure 2.6. Slower reactions, or lower barrier loading of species 2, lead to a faster rise in downstream concentration. Amazingly, the steady-state profile is the same for each case, thus the lag time is unchanged. The lag time equations presented above are accurate when Φ^2 is 100 or greater (Yang *et al.*, 2001).

2.3.2.6 Reactive Membrane Summary

The previous section shows how different reaction schemes affect barrier lag time. A summary of these results appears in Table 2.1. Reactions with mobile products increase the permeance of a membrane, yet may not increase lag time. These reactions are not particularly useful for barrier membranes as the key factor is increased lag time. Reversible and irreversible reactions with immobile products are prime candidates for designing barrier membranes. Both show tremendous

potential at increasing lag time and thus making better barriers for specified contaminants.

Table 2.1: Expected permeance and lag time for a variety of barrier membrane types. Larger lag times lead to more desirable barriers (adapted from Yang *et al. 2001).*

Barrier Type	Permeance	Lag Time	Reference Equation
No reaction	$\frac{DH}{l}$	$\frac{l^2}{6D}$	2.17
Reversible reaction with mobile product	$\frac{DH}{l}(1+K')$	$\frac{l^2}{6D}$	2.29
Reversible reaction with immobile product	$\frac{DH}{l}$	$\frac{l^2}{6D}(1+K')$	2.33
Irreversible Reaction with immobile product	$\frac{DH}{l}$	$\frac{l^2}{6D}\left(\frac{3c_{2(0)}}{\upsilon HC_{1(0)}}\right)$	2.43

2.4 Ion-Exchange and Sorption to Activated Carbon

One goal of this research is to incorporate an ion-exchanging material into a reactive barrier membrane to hinder transport of cesium. The previous sections show the current theory for barrier membranes and how reactions can be used to increase lag time. The following overview of ion-exchange concepts reviews the final tools necessary to tackle the work presented in chapter 3. Similar concepts are applied to the sorption of an organic compound (1,2,4-trichlorobenzene) to powdered activated carbon in chapter 4.

2.4.1 Ion-Exchange

Ion-exchange is an equilibrium process between ions in a liquid phase contacting an ion adsorbing solid phase. Ion-exchange takes place at exchange sites on the solid. Adsorption onto an exchange site leads to subsequent release of a bound ion. A visual schematic for ion exchange is shown in Figure 2.7.

Adsorbed ions may be exchanged for ions in solution via the stoichiometric reaction

$$\upsilon_A A^{z_A} + \upsilon_B \overline{B}^{z_B} \leftrightarrow \upsilon_A \overline{A}^{z_A} + \upsilon_B B^{z_B} \tag{2.46}$$

where A and B are unbound ions in the liquid phase, $\overline{A}$ and $\overline{B}$ are bound ions in the solid phase, υ_A and υ_B are stoichiometric coefficients, z_A and z_B are ionic charge numbers. A charge balance relates the stoichiometric coefficients and ionic charge numbers

$$\frac{\upsilon_A}{z_B} = \frac{\upsilon_B}{z_A} \tag{2.47}$$

preserving electroneutrality. If z_A were twice z_B, two ions of B would be released for each sorption of A. For the case of binary ion-exchange, where $z_A = z_B$, the ions would exchange in a one-to-one ratio. Binary ion-exchange is of special interest for this research because crystalline silicotitanate (CST) exchanges one sodium ion for one cesium.

Ion-exchange equilibrium can be expressed through an isotherm equation

$$q_A = f(C_A) \tag{2.48}$$

where q_A is the solid phase concentration and C_A is the liquid phase concentration of species A. The 1:1 binary ion-exchange ratio implies the total number of ions and occupied exchange sites are constant

$$q_{(0)} = z_A q_{A(0)} + z_B q_{B(0)} = z_A q_A + z_B q_B \tag{2.49}$$

$$C_{(0)} = z_A C_{A(0)} + z_B C_{B(0)} = z_A C_A + z_B C_B \tag{2.50}$$

where $q_{A(0)}$ and $q_{B(0)}$ are the initial solid phase concentrations, and $C_{A(0)}$ and $C_{B(0)}$ are the initial liquid phase concentrations of ions A and B.

An equilibrium constant for the ion-exchange equilibrium Equation 2.46 can be written

$$K_e = \frac{C_B^{\upsilon_B} q_A^{\upsilon_A}}{C_A^{\upsilon_A} q_B^{\upsilon_B}} \tag{2.51}$$

giving a relation between solid and liquid phase concentrations of ions A and B. Rearranging Equations 2.49 and 2.50 gives

$$q_B = \frac{q_{(0)} - z_A q_A}{z_B} \tag{2.52}$$

and

$$C_B = \frac{C_{(0)} - z_A C_A}{z_B} \tag{2.53}$$

which can be substituted into Equation 2.51 giving

$$K_e = \frac{\left(C_{(0)} - z_A C_A\right)^{\upsilon_B}}{C_A{}^{\upsilon_A}} \frac{q_A{}^{\upsilon_A}}{\left(q_{(0)} - z_A q_A\right)^{\upsilon_B}}. \tag{2.54}$$

This research focuses on one cesium ion replacing one sodium in CST, allowing simplification of Equation 2.54 to

$$K_e = \frac{\left(C_{(0)} - C_A\right)}{C_A} \frac{q_A}{\left(q_{(0)} - q_A\right)} \tag{2.55}$$

because $z_A = z_B = \upsilon_A = \upsilon_B = 1$. Recall, from Equation 2.48 the goal is to find a function q_A in terms of C_A. Solving Equation 2.55 for q_A gives

$$q_A = \frac{q_{(0)} K_e C_A}{C_{(0)} + \left(K_e - 1\right) C_A}. \tag{2.56}$$

Two new variables are defined

$$X_A = \frac{C_A}{C_{(0)}} \tag{2.57}$$

and

$$\overline{X}_A = \frac{q_A}{q_{(0)}} \tag{2.58}$$

where X_A is the equivalent fraction of ion A in the liquid phase and $\overline{X}_A$ is the equivalent fraction in the solid phase. Substituting Equations 2.57 and 2.58 into Equation 2.56 gives

$$\overline{X}_A = \frac{K_e X_A}{1 + \left(K_e - 1\right) X_A} \tag{2.59}$$

relating the amount of ion A in the liquid phase to the amount in the solid phase. Plots of equivalent fractions of ion A in solid phase $\overline{X}_A$ versus liquid phase X_A can have different shape depending on the value of K_e. For K_e values less than one, the reaction favors the

left hand side of Equation 2.46. When $K_e=1$, a plot of $\overline{X}_A$ versus X_A will give a 45° line. For large values of K_e, equilibrium lies to the right of Equation 2.46, the equivalent fraction of ion A in the solid phase will be larger than in the liquid phase. Sample curves for these three limits of K_e are shown in Figure 2.8.

For large values of K_e, Equation 2.59 can be simplified to

$$\overline{X}_A = \frac{K_e X_A}{1 + K_e X_A} \tag{2.60}$$

sharing the form of the more familiar Langmuir isotherm for adsorption

$$q_A = \frac{Q_{\max} K_L C_A}{1 + K_L C_A} \tag{2.61}$$

where Q_{max} is the maximum solid phase loading capacity of ion A and K_L is the Langmuir constant (Langmuir, 1916).

2.4.2 Sorption to Activated Carbon

The sorption of many organic compounds to activated carbon is also an equilibrium process. Molecules bind to activated carbon through van der Waals forces. This binding of non-charged particles to activated carbon may be mathematically modeled similarly to ion-exchange. The equilibrium for many molecules in bulk solution and the carbon will follow the same Langmuir isotherm behavior described in Equation 2.61 where K_L is the Langmuir constant, and C_A is the concentration of the molecule in solution. At low concentrations, loading on the carbon q_A will increase with increasing concentration until the maximum solid phase loading capacity, $Q_{max,}$ is reached.

A good ion-exchange or sorptive material for use in a reactive barrier membrane has a large equilibrium constant and high solid loading capacity. A reaction of the form of Equation 2.46 with a large equilibrium constant readily exchanges and binds ion A from solution. A high loading capacity leads to more ions exchanged per unit mass, increasing the total separation ability of the barrier membrane.

The above equations give the mathematical theory of ion-exchange or organic chemical sorption and allow for estimation of chemical properties such as the equilibrium constant K_e. These calculations require the concentration value in the liquid phase,

which can be measured analytically. The following section discusses one method of concentration measurement, ion-selective probes.

2.5 Ion-Selective Probes

The ability to quickly and accurately measure aqueous concentrations is the primary experimental need of this research. Downstream concentration profiles in diffusion cell experiments are essential for measuring lag time. Isotherms measuring ion-exchange equilibrium between solid and liquid phases require concentration measurements as well. The tools used for this research to make concentration measurements are ion-selective probes.

Ion-selective probes can make concentration readings without altering the composition or volume of a sample. This is possible with ion-selective probes because they use potentiometry to measure concentration. Gas chromatography (GC; used in chapter 4) and Atomic Absorption (AA) each require removal of small volumes of liquid for analysis which must be accounted for when making measurements over long periods of time. Being able to set an ion-selective probe in a solution and walk away is beneficial for experimentation.

Reference and indicator electrodes are necessary for making concentration measurements. The reference electrode has a known, constant half-cell potential that is completely insensitive to the solution being measured. The ideal reference is reversible and obeys the Nernst equation, exhibits a potential that is constant with time, returns to its original potential after being subjected to small currents and exhibits little hysteresis with temperature cycling (Skoog *et al.*, 1998).

The indicator electrode is designed to specifically detect the ion being measured. A membrane at the tip of the indicator electrode either binds, or contains a species that binds, the ion. The binding of an ion results in a potential which can be measured by an ion-selective meter. This measurement is compared to the baseline potential of the reference electrode giving the overall potential of the solution. A single potential measurement is not enough to find the concentration of a solution.

For a potential measurement to be useful, a calibration curve must be available which relates potential to concentration. To generate a calibration curve, potential measurements of standard solutions containing known ion concentrations are obtained and plotted versus concentration. An accurate calibration curve will show good correlation to the Nernst slope.

The Nernst slope is the theoretical slope of a plot of potential versus log of concentration

$$E = E^o + \frac{RT}{n\Im}\ln(Q) \qquad (2.62)$$

where E is the potential, E^o is the equilibrium potential, R is the gas constant, T is the temperature, n is the value of the ion charge, $\Im$ is Faraday's constant and Q is a ratio of concentrations. For a monovalent ion, such as cesium ion, the value of the Nernst slope is 59.2 mV per decade of concentration. This means for every factor of ten increase in concentration, the potential measurement of an ion-selective probe will increase by 59.2 mV. Ion-selective probes giving readings matching the Nernst slope are capable of making the concentration measurements necessary for this research.

2.6 Crystalline Silicotitanate (CST) and Powdered Activated Carbon (PAC)

A focus of this research is to incorporate reactive groups into barrier films. One is a cesium specific ion-exchanger, a crystalline silicotitanate. The second is powdered activated carbon for the sorption of organic compounds. The previous sections of this chapter have discussed transport through barrier films, ion-exchange and concentration measurement using ion-selective probes. This section discusses the properties of these reactive groups.

2.6.1 Crystalline Silicotitanate (CST)

CST is a hydrous crystalline sodium silicotitanate inorganic ion-exchanger with a high selectivity for Cs^+. Invented by Anthony, Dosch and Phillip, it is stable to radiation (Gu *et al.*, 1997; Anthony *et al.*, 1993). Other ion-exchangers exist for cesium, but none

can remove traces of cesium from very basic solutions with high sodium concentration as well as CST (Marsh *et al.*, 1993).

One possible application of barrier membranes made in this research is for use in containing nuclear waste such as that found at Hanford, Washington. These wastes are very basic, with over 5.0 M sodium concentrations (Zheng *et al.*, 1996). CST has a total ion-exchange capacity of 4.6 mequiv/gram, of which 0.57 mequiv/gram is for cesium, and cesium selectivity is high compared to other Group I metals: sodium, potassium and rubidium (Zheng, 1996). Gu *et al.* (1997) show CST can selectively bind cesium from solutions with Cs^+ concentrations below 10 mg/L. These properties make CST an excellent candidate for synthesis of a cesium selective reactive barrier membrane.

2.6.2 Powdered Activated Carbon (PAC)

Activated carbon is highly porous, with a large surface area for its volume, often over $500m^2$ per gram. This large surface area yields many sites for molecular adsorption. PAC and other types of black carbon have an affinity for adsorbing many chlorinated organics (Yun *et al.*, 1998), including chlorobenzenes and polychlorinated biphenyls (Bucheli and Gustafsson, 2003; Cornelissen *et al.*, 2004; Jonker and Koelmans, 2001; Jonker and Koelmans, 2002; Surdo *et al.*, 2009). Made from charcoal, activated carbon is a low cost material for remediation.

Different forms of activated carbon exist, including granular and powdered varieties. The larger granulated carbon is used in adsorption columns for water treatment, adsorbing contaminants from solution. The smaller particle size of powdered activated carbon allows for better distribution within a thin barrier film, while retaining the ability to adsorb chlorinated organics.

2.7 Summary

Lag time is a measure of how long it takes a contaminant to diffuse across a barrier and can be measured experimentally. Homogeneous barrier membranes give lag times proportional to the square of membrane thickness and inversely proportional to diffusivity. Addition of a reactive group can greatly increase the lag time of the barrier,

from 10 to 100-fold. This increase in lag for instantaneous reversible and irreversible reactions can be predicted mathematically. The steady-state flux of a barrier membrane is independent of reaction.

Ion-exchange is an equilibrium process between ions in a liquid phase contacting a solid, defined by a reaction where an ion can replace another ion at an exchange site. The ion-exchange stoichiometry is governed by electroneutrality. Equivalent ion fractions in the liquid phase can be related to those in the solid phase by an isotherm equation similar to the Langmuir adsorption isotherm. Reactions with large ion-exchange equilibrium constants are desirable for use in reactive barrier membranes.

Ion-selective probes can measure liquid phase concentrations without altering the composition of solution. Two electrodes are necessary to make a measurement: a reference and an indicator electrode. The Nernst equation describes ion-selective probe behavior and can be used to correlate concentration data.

CST is a crystalline silicotitanate with high selectivity for Cs^{+}, even in the extreme conditions found in nuclear waste at Hanford, Washington. The capacity of cesium in CST is 0.57 mequiv/gram. CST has all the properties desired to make a cesium specific barrier membrane. PAC has a capacity to adsorb chlorinated organics from solution, with a high surface area to volume.

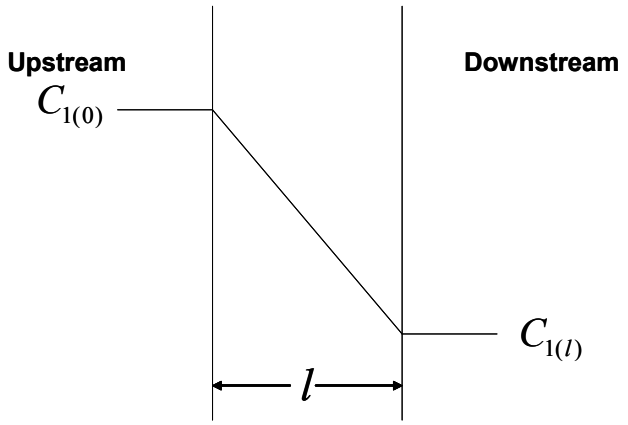

Figure 2.1: Concentration profile for a thin-film with thickness l and partition coefficient H = 1, experiencing steady-state transport.

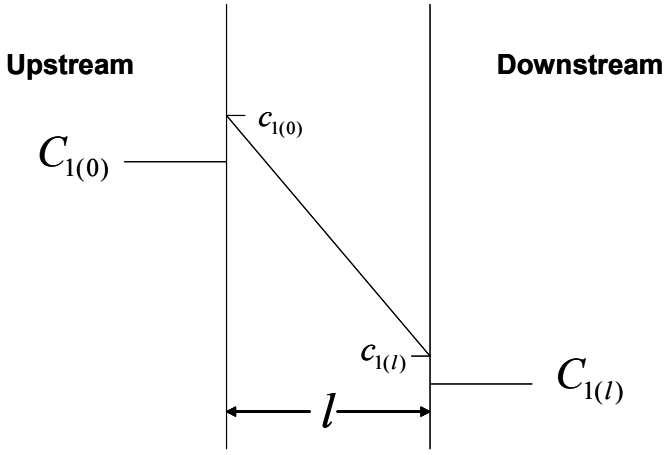

Figure 2.2: A barrier membrane with a partition coefficient H > 1 experiencing steady-state transport.

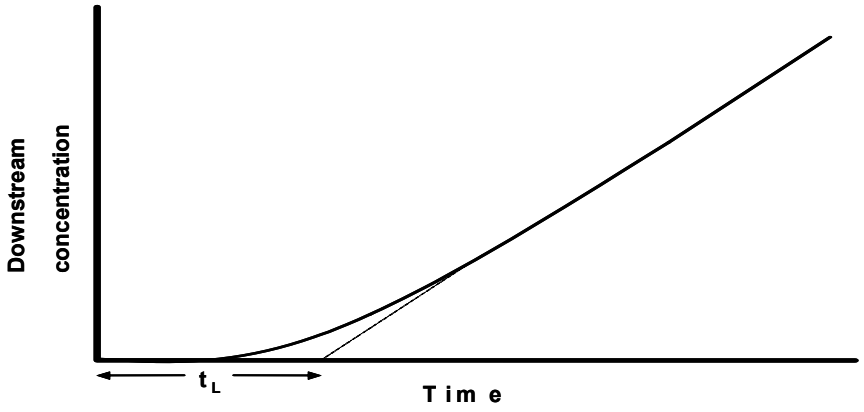

Figure 2.3: Typical curve for a diffusion cell experiment showing a linear regression of the steady-state slope and corresponding lag time, t_L.

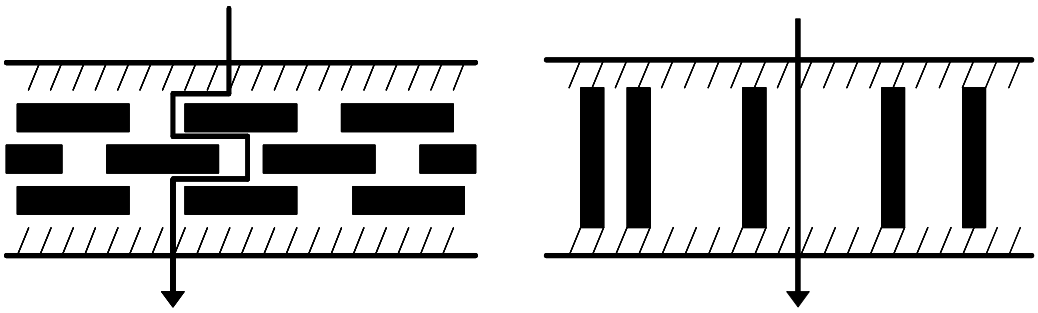

Figure 2.4: Impermeable particles aligned perpendicular to the direction of diffusion increase path length leading to a less permeable barrier.

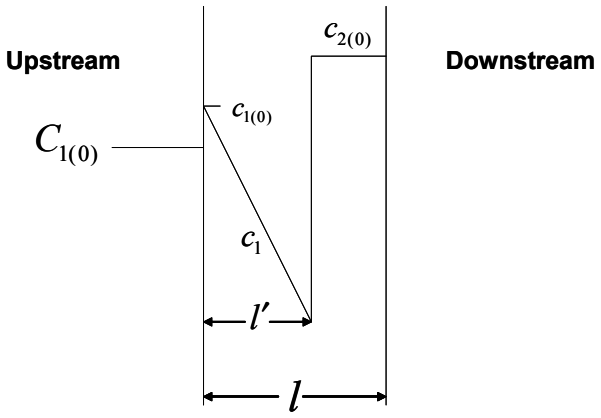

Figure 2.5: Irreversible instantaneous reaction model advancing front. Ahead of the front, species 2 has initial loading concentration, behind the front, species 1 has steady-state linear concentration profile.

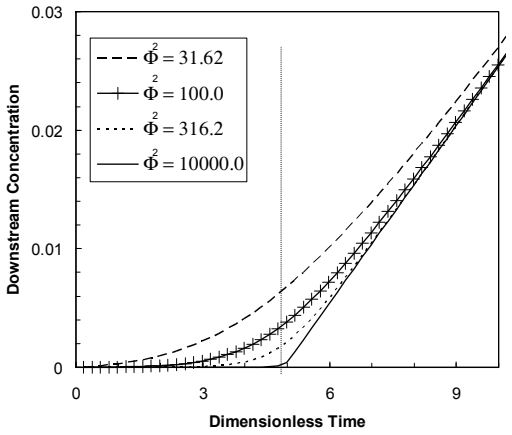

Figure 2.6: As reaction rate becomes slower compared to diffusion, downstream concentration increases faster. Φ is a Damköhler number, the ratio of rate of reaction to rate of diffusion. (From Yang *et al.*, 2001)

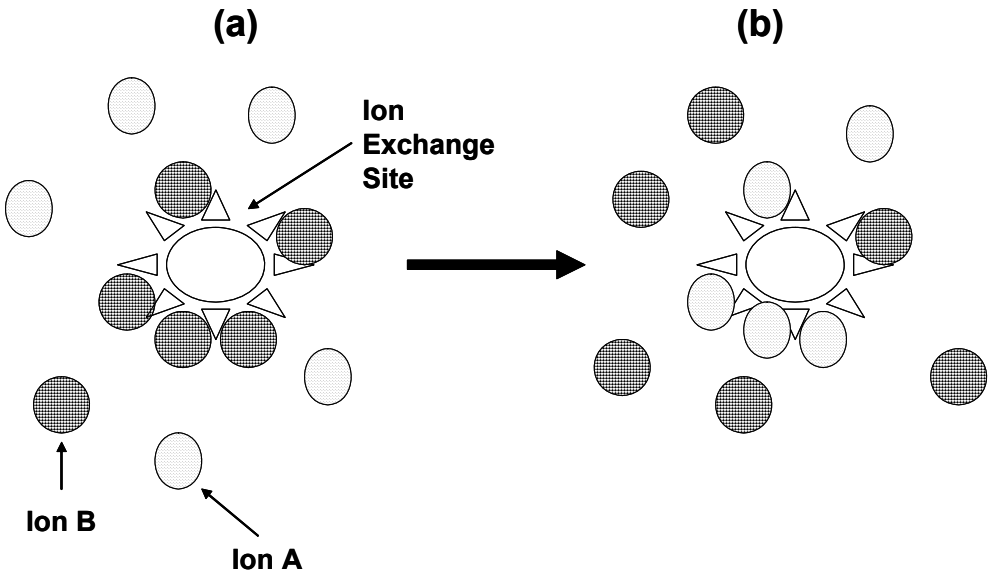

Figure 2.7: An ion-exchange solid with selectivity for Ion A over Ion B.
(a) Initially, solid loaded with Ion B.
(b) Later, Ion A has replaced Ion B at many exchange sites.

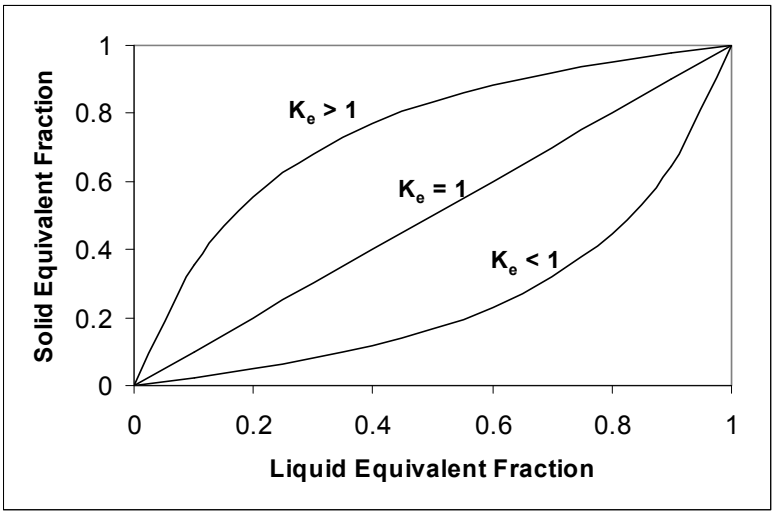

Figure 2.8: Plot of different K_e values for Equation 2.59.

Chapter 3

Permeable Membranes Containing Crystalline Silicotitanate as Model Barriers for Cesium Ion*

In diaphragm cell experiments, a permeable model reactive barrier for the containment of cesium is tested. Primary targets for cesium containment are former plutonium processing sites (*e.g.,* Hanford, WA and Savannah River, SC) which are currently contaminated with cesium-137. Adding up to 10 wt% crystalline silicotitanate (CST), a sacrificial reagent, to polyvinylalcohol (PVA) films increases the time before cesium can cross the film by a factor of thirty. The increased lag times are consistent with theories developed for this type of reactive membrane. Theory also correctly predicts the effects of cesium concentration and membrane thickness on membrane performance. Because the relative improvements of the model barrier are expected to be independent of the polymer used, these increased lags should hold for less permeable polymers which are more resistant to radiation, although these polymers have not been tested.

3.1 Introduction

Cesium-137 is one of the most dangerous isotopes produced in the manufacture of plutonium. It decays into barium-137, emitting both a β-particle and γ–rays. These rays are high energy and thus dangerous over the 30-year half-life of cesium. Such properties are shared by many of the isotopes produced in the manufacture of thermonuclear weapons (Garrick, 2003; Moore, 1993; Garten *et al.*, 2000).

The reason that cesium-137 is particularly dangerous is that it is highly water-soluble. At present, it is most frequently stored in concrete vats as a basic aqueous slurry. Because much of the cesium-137 is in vats at weapons manufacturing sites near the Savannah River or the Columbia River (Garten *et al.*, 2000; Huckman *et al.*, 2001), tank rupture either by accident or by terrorist activity is a significant risk. Efforts to convert the cesium into an insoluble form are underway (Huckman *et al.*, 2001; Hamm *et al.,* 2002), but these have been slowed by technical uncertainty and political obstruction. At the same time, the concrete vats are older than their design life and are starting to leak (Flury *et al.*, 2002). Cesium-137 poses a significant risk.

This research begins development of a barrier membrane – a "geotextile" – that would reduce this risk. Barrier membranes are often used to contain subsurface pollutant

sources (Koerner, 1998; LaGrega *et al.,* 2001). Because they are largely impermeable to water and water-soluble salts, the membranes dramatically reduce the leak rate of these solutes. Recently, barrier membranes containing sacrificial reagents have been developed to provide still more protection (Shimotori *et al., 2006*). These membranes do not change the leak rate of the pollutants, but they do increase the time before the membrane starts to leak. These increases can be large: for example, if the original membrane leaks after a decade, a membrane with sacrificial reagents may not leak for several centuries.

In this work, we begin development of a membrane that is a selective barrier for cesium. We are especially interested to discover if the sacrificial reagent in the membrane can be crystalline silicotitanate (CST), an inorganic ion exchanger which selectively adsorbs cesium (Huckman *et al.,* 2001; Gu *et al.,*1997; Zheng *et al.,* 1996). Another goal is to determine if ion exchangers as a class can be used as sacrificial reagents in this type of barrier membrane.

This work uses a model system to determine potential improvements in lag time for a practical barrier membrane. Polyvinylalcohol (PVA) is chosen as the polymer because it is highly permeable and hence allows fast experiments. Obviously, for any real barrier membrane, we would choose an impermeable polymer, but such a polymer implies impractically long experiments. In earlier studies, we showed that PVA could give good barriers for a variety of oxidized contaminants if nanoparticles of iron (Fe^0) are added as a sacrificial reagent (Shimotori *et al.*, 2004). We also showed that the fast PVA experiments gave reasonably accurate predictions of tedious experiments on polyethylene barriers loaded with the same iron nanoparticles (Shimotori *et al.*, 2006). These studies imply that the results from model systems can be extrapolated using the theory presented below to estimate the lag time for actual barrier membranes used for containment, but testing of such impermeable reactive barrier membranes is still necessary.

3.2 Theory

Before discussing the experiments involved, the results expected when the sacrificial reagent, CST, is added to a barrier membrane are summarized. In this review, we imagine the membrane between two well-mixed volumes of solution, one initially

containing cesium and the other initially without cesium. The membrane also initially contains no cesium. In this case, the cesium concentration in the initially cesium-free solution volume is given at small times by

$$c_1 = \frac{DHAc_{10}}{l}\left(\frac{1}{V_{upsream}} + \frac{1}{V_{downstream}}\right)\left(t - t_{lag}\right) \qquad (3.1)$$

where D is cesium's diffusion coefficient in the membrane; H is its partition coefficient, that is the ratio of the cesium concentration in the membrane at equilibrium with that in the adjacent aqueous solution; c_{10} is the concentration of species *1*, cesium, in the loaded "upstream" solution; c_1 is the cesium concentration in the "downstream" solution; A and l are the membrane area and thickness, respectively; $V_{upstream}$ and $V_{downstream}$ are the two volumes, and t and t_{lag} are the time and the time before any significant flux across the membrane occurs (Cussler, 1997). Equation 3.1 is an approximation, and the complex, exact solution is known. This equation, first developed in 1920 (Daynes, 2001), normally provides a good fit to the experimental results.

The key for reactive barrier membranes is the time before significant flux occurs, usually called the lag time. For a membrane without any reactive additive, the lag time is given by

$$t_{lag} = \frac{l^2}{6D} \qquad (3.2)$$

For example, in a typical non-reactive barrier film that is 10^{-3} m thick, the diffusion coefficient is around 10^{-11} m^2/sec, and so the lag time is about 5 hours. This is not a significant factor in barrier performance.

The lag for a reactive barrier will be significantly longer. How much longer depends on the details of the reaction with the sacrificial reagent within the membrane. Three special cases have been developed theoretically: that of instantaneous, irreversible reaction; that of fast, reversible reaction with a linear isotherm; and that of fast, reversible

reaction with a Langmuir isotherm. The case of instantaneous irreversible reaction is exemplified by a diffusing acid reacting with nanoparticles of a solid base (Yang *et al,* 2001). In this case, we find that

$$t_{lag} = \left(\frac{l^2}{2\nu DH} \right) \frac{c_{20}}{c_{10}} \tag{3.3}$$

where c_{20} is the initial concentration of sacrificial reagent. The molar stoichiometric coefficient ν equals one for the ion exchangers used in this work. If l and D are still 10^{-3} m and 10^{-11} m^2/sec, respectively; but H is 10^{-4}, c_{20} is 10^{-2} M, and c_{10} is 10^{-3} M, the lag is over 150 years. A minor delay in the nonreactive case becomes extremely significant in the reactive case.

Results for the other cases are similar. If the reaction is reversible with a linear isotherm,

$$t_{lag} = \frac{l^2}{6D}(1 + K) \tag{3.4}$$

where K is the equilibrium constant for the isotherm (Paul and Koros, 1976). This result is sometimes applied to reactive dyes, where K is of order 10^5; this means that t_{lag} would be over 50 years using the values for l and D above. If the reaction is reversible with a saturated Langmuir isotherm, the result is known analytically but is complicated (Paul and Koros, 1976). As shown below, however, our experiments are in the limit where the isotherm is almost flat. In other words, the reagents in the membrane quickly become saturated with cesium, and this adsorbed and immobilized cesium concentration is dramatically larger than the concentration of non-adsorbed cesium. In this limit, the complicated analytical expressions for t_{lag} simplify dramatically to give

$$t_{lag} = \left(\frac{l^2}{2DH} \right) \frac{c_{20}}{c_{10}} \tag{3.5}$$

where c_{20} is now the total number of adsorbing sites on species *2*, the CST; and c_{10} is again the upstream cesium concentration. This result is mathematically equivalent to that for an irreversible reaction given in Equation 3.3, although its physical basis is different.

We expect any favorable isotherm will give the same result if the reaction is sufficiently rapid. These equations are used in analyzing the experimental results that follow.

3.3 Experimental

3.3.1 Materials

Cesium nitrate (99%, Aldrich), sodium chloride (99.9% Mallinckrodt), crystalline silicotitanate (CST, IONSIV-910 Lot 1998000001, UOP) and PVA (Elvanol grade 71-30 lot L1A352, molecular weight 138,000-146,500 Dupont) were used as received. DOWEX® Nonosphere® 550 A (OH) anion exchange resin was ground by hand with a pestle and mortar to approximately 10 μm diameter particles. Distilled water was used unless otherwise specified.

3.3.2 Membrane Preparation

Membranes were prepared by adding 4.0 g of PVA to 36 mL of water at 90 °C and stirring at 60 rpm in a 150 mL beaker on a heated stir plate for 30-60 minutes to dissolve the PVA. The solution was removed from the stir plate and degassed under vacuum at room temperature for five minutes. For membranes containing added ion-exchangers, the degassed solution was returned to the heated stir plate, the desired amount of ion-exchanger was added and the covered solution was stirred for 2-3 more hours at 90 °C. The solution was again degassed. After degassing, the covered solution was allowed to cool to room temperature. The solution was then poured onto a Teflon block, and a doctor blade was pulled by hand across the surface at about 0.5 cm/sec. The resulting film was covered with aluminum foil to minimize air convection across the surface and dried at room temperature for three days. The film was placed in an oven at 150 °C for 135 minutes to crosslink the polymer. After the film's mass was measured, it was soaked overnight in 1 L of water. This doubled its mass. The hydrated film was cut into circular segments of radius 2 cm.

3.3.3 Membrane Permeability

Film segments were tested in the diffusion cell apparatus shown schematically in Figure 3.1. The cell consists of two well-stirred volumes of 15 cm^3 and 30 cm^3, called the "upstream" and "downstream" compartments, respectively. These volumes are separated by a barrier membrane of 5.3 cm^2 active area. Normally, a solution of solute is added to the upstream compartment to start an experiment. Solute concentration in the downstream compartment, which is initially zero, rises with time. These measured concentrations are the basic data of the experiment.

These downstream solute concentrations are measured with ion selective-electrodes. Cesium ion was measured with a model AB560 Cesium Electrode and Cl^- was measured with a model AB110 Chloride Electrode, both from Advanced Sensor Technologies (ASTI) Orange County, CA. The probes each require an external reference probe. The reference probes used were both triple-junction glass reference electrodes Model RC501, also from ASTI. The reference probe used for Cs^+ measurements contained saturated magnesium chloride while the probe used for Cl^- measurements contained saturated potassium nitrate. The saturated reference solutions were replaced weekly.

Readings from the ion-selective and respective reference probes were taken with a Hach Sension 4 meter attached to a Micron Electronics Millenia computer for data recording. A four-point calibration of each ion-selective probe was made daily. The concentration of the cesium solutions used for calibration were: 5×10^{-5}, 1×10^{-4}, 1×10^{-3} and 1×10^{-2} M cesium nitrate. Those for the chloride-selective probe were: 1×10^{-4}, 1×10^{-3}, 1×10^{-2} and 1×10^{-1} M sodium chloride. These values lie within ASTI's reported linear calibration range. To calibrate, 30 mL of each solution was placed in stirred 50 mL beakers. The ion-selective and reference probe were placed in each of the solutions, starting with the least concentrated solution stirring at 80 rpm. The cesium/CST isotherm was also measured using the ion-selective probes.

3.4 Results

This work tests a permeable barrier membrane for cesium ion. These experiments serve as the first step towards impermeable membranes which could be used to reduce the

risk of leaks of radioactive cesium waste. The development has three parts: the adsorption isotherms of the ion exchangers used, chloride breakthrough as a test system, and cesium breakthrough using the permeable model system. In the paragraphs below, these three parts are described sequentially, with the most detail for the cesium barrier.

The adsorption isotherm for cesium ion is shown in Figure 3.2. The cesium/CST data show strong adsorption reaching saturation at about 10^{-4} M solution concentration. Although a saturation value exists, the data at low concentrations do not fit a Langmuir isotherm but the data set do approximate a Freundlich isotherm, as illustrated in the inset of this figure. The Freundlich isotherm also better approximates the observed shoulder than does a Langmuir isotherm. The best fit of these data is

$$c_2^* = 0.0018 c_1^{0.0962} \qquad (3.6)$$

where c_2^* is the cesium concentration in the CST in moles per gram, and c_1 is the molar concentration of cesium in water at equilibrium. The apparent saturation value, q_{max}, for CST was found to be $0.9 \frac{mmol}{gram}$ for Cs^+. This value is larger than the value reported by Gu *et al*., (1997), and Zheng *et al.,* (1996) of $0.56 \frac{mmol}{gram}$. One possible reason for this difference is that in these previous studies the measurement was made in a solution containing 5.1 M $NaNO_3$, while our measurement was made in aqueous cesium nitrate alone (Gu *et al.,* 1997; Zheng *et al.*, 1996).

We next turn to the increases in lag time caused by ion exchangers in the barrier film. Chloride diffusion is retarded with the DOWEX exchanger, as illustrated by the data in Figure 3.3. The presence of the exchanger increases the lag about 20 times, from less than one minute to around twenty minutes. The lag times in this experiment and in those shown below are determined from the x-intercept of a regression of the linear portion of the breakthrough curve.

Cesium diffusion gives similar results. As shown in Figure 3.4, the experimental data are reproducible. In these experiments, a 0.1 M $CsNO_3$ solution was placed in the upstream volume of the cell in Figure 3.1, and the cesium concentration was measured in the downstream volume. None of the experiments show much of a lag; none has a

downstream concentration over 2 percent of the upstream; and much of the systematic difference between the experiments is due to the 10 percent variation in membrane thickness (cf. Equation 3.1).

For membranes containing CST, the effects of upstream Cs^+ concentration, barrier thickness, and CST concentration were measured. The results for different upstream concentrations at a constant CST loading are given in Figure 3.5(a). Decreasing the feed concentration increases the lag as Equations 3.3 and 3.5 predict. (Because the isotherm is not linear, Equation 3.4 is not applicable.) Note that these equations imply that the slopes after breakthrough should be the same. Those for 0.1 and 0.001 M are, but that for 0.01 M is smaller.

The effect of different membrane thickness is shown in Figure 3.5(b). As expected, the lag times increase sharply for thicker films. The slopes after breakthrough are smaller for the thicker membranes, as expected from Equation 3.1. The effect of differing CST concentrations is illustrated in Figure 3.5(c). Increases are dramatic, with lag times increasing by a factor of six when the CST concentration increases by a factor of four. This is more than the factor of four expected from Equations 3.3 and 3.5, which predict a linear variation with CST concentration. The slope of concentration versus time after breakthrough, expected to be constant, drops about four times over the loading range studied.

We were concerned that the lags and the concentration variations showed effects different than the theory. On the one hand, we are pleased that the lags are bigger than expected and that the leaks occur more slowly than expected. Thus the barriers seem even better than anticipated. On the other hand, the theory summarized above has been widely verified, both by us and by others (Shimotori, *et al.*, 2004; Yang *et al.*, 2001; Bansleben *et al.*, 2001; Schwark *et al.*, 2004). Some uncertainty in our measurements is suspected.

We have identified two sources of this uncertainty. First, it is assumed that the upstream concentration is constant during the experiment, as implied by Equation 3.1. For nonreactive membranes, it changes less than 3 percent. For some reactive membranes studied elsewhere, however, this concentration has dropped significantly

(Shimotori, 2005). Results in our case, show that that this concentration is not constant here either. If a CST laden membrane is used, the breakthrough curve shows a long lag and a small slope as shown in Figure 3.6. The long lag is expected because of cesium adsorption by the CST. If an additional breakthrough experiment is performed using the same, exhausted membrane, the breakthrough curve shows almost no lag and a larger slope. The small lag is expected because the CST is now largely saturated with cesium from the first run. The larger slope is believed to result because the upstream concentration is not depleted as much by reaction, and so the flux stays high. Thus a depleted upstream concentration may be part of the reason for the smaller slopes at higher CST concentrations shown in Figure 3.5(c).

The second source of uncertainty comes from the location of the CST in the membrane. Experiments and theories utilizing detailed numerical models which are more complete than those summarized above show that where the reaction occurs matters (Nuxoll *et al.*, 2005). If the reaction occurs on the upstream membrane face, the lag is half that when the reaction occurs on the downstream face. If the CST settles while the membrane is being made, the lag time will be different depending on the orientation of the membrane.

To test whether membrane orientation was important, experiments were made in which we deliberately changed membrane orientation. Normally, the experiments used membranes with the top surface of the membrane during fabrication oriented towards the more concentrated, "upstream" volume. This meant that the downward face, which was oriented towards the "downstream" volume, may have a higher CST concentration than the membrane's average because of CST settling during fabrication. Changing the membrane's orientation does change the lag time about 30 percent as shown in Figure 3.7, suggesting that the CST distribution within the membrane is not completely uniform. This second uncertainty is still much less than the increased lag of 3000 percent between the original membranes and those with added CST.

Finally, we turn away from studies of model solutions to a study with groundwater from the nuclear waste facility in Hanford, WA. These experiments simulate performance in the containment of cesium contaminated groundwater. This

water has an ionic strength of about 0.013 M, largely because of calcium and magnesium carbonates and sulfates, and a pH of 8.18. In these experiments samples of Hanford water were spiked with 0.001 M $CsNO_3$ and then placed in the upstream compartment of our cell. Typical results, shown in Figure 3.8, show lag times across membranes with five weight percent CST which are as much as 40 times larger than across membranes without CST. Again, adding CST improves the membrane's barrier properties. In fact, the increase with the Hanford water is about 3 times larger than in distilled water. We are unsure about the cause of this difference.

3.5 Discussion

The data above show that adding crystalline silicotitanate to polymer films makes the films much better barriers to the diffusion of cesium ion. In this section we first discuss how the results compare with earlier efforts on this type of system. Second, we explore how we could adapt our model studies to make a practical system and what its expected properties would be. Each of these topics is covered in the following paragraphs.

3.5.1 Experiment versus Theory

As shown above, the results obtained here are roughly consistent with the theoretical predictions summarized by Equations 3.1-3.5. Adding CST to a barrier membrane, making the membrane thicker, and reducing the upstream cesium concentration all delay the penetration of cesium across the barrier membranes. This delayed penetration, summarized as a lag time, can be increased by more than a factor of thirty. This large effect makes these membranes interesting.

The increases in lag times observed in our experiments roughly agree with those predicted, as shown in Figure 3.9. In this figure, the measured lag times are shown on the abscissa, and the predictions are on the ordinate. In fact, the measured lags seem somewhat longer than those predicted; i.e., our actual results are better than expected. As discussed above, we believe that part of the reason for this discrepancy may be the nonuniform distribution of CST within the membrane.

There is a second, more fundamental reason, however, why the membranes are behaving better than expected. This is the result of the nonlinear isotherm operating in this system and shown in Figure 3.2. To explore the effect of this nonlinear isotherm, we imagine first that the reaction between cesium and CST is instantaneous and irreversible, and that it occurs at some position *l'* within the membranes. The rate of this reaction is then diffusion controlled

$$j_1 = \frac{DH}{l'}(c_{10} - 0) \tag{3.7}$$

where j_1 is the diffusive flux of cesium and *l'* is the reaction location. The reaction location changes with time according to the mass balance

$$c_{20}\frac{dl'}{dt} = \frac{DH}{l'}(c_{10} - 0) \tag{3.8}$$

Because the reaction starts at the upstream surface of the membrane, *l'* is zero when *t* is zero, and Equation 3.8 is easily integrated to give

$$l' = \sqrt{2DHc_{10}t / c_{20}} \tag{3.9}$$

When the reaction location has crossed the membrane, *l'* equals the membrane thickness *l* and

$$t = t_{lag} = l^2 c_{20} / 2DHc_{10} \tag{3.10}$$

which was given without derivation as Equation 3.3.

Now we imagine that the reaction is instantaneous but stops at some equilibrium concentration c_{ie}, which is roughly the shoulder of the isotherm shown in Figure 3.2. This shoulder is an approximation, most accurate for Freundlich isotherms with an exponent much less than one. The exponent in Equation 3.6 is about 0.10. In this case, Equation 3.7 should be replaced by

$$j_1 = \frac{DH}{l'}(c_{10} - c_{ie}) \tag{3.11}$$

which leads to

$$t_{lag} = l^2 c_{20} / 2DH(c_{10} - c_{ie}) \tag{3.12}$$

This does predict that the lag times should be slightly longer than those expected from Equations 3.3 and 3.8, and hence is consistent with the data in Figure 3.9. At this point, however, it is uncertain if this argument is more significant than a nonuniform distribution of CST in these experiments.

3.5.2 Considerations for Practical Application

The increased lag caused by CST in PVA is significant, but this is certainly not a practical barrier for at least two reasons beyond the cost of CST (~$300/kg). First, PVA is much too permeable by itself. We recognized this at the beginning of the project when we deliberately chose a highly permeable polymer to ensure fast experiments. Note that the theory sketched above, however, which is supported by our experiments, predicts that the factor by which the lag is increased is independent of the polymer used. Thus our results should be general. For example, imagine that by using PVA we can increase the lag thirty times, from one day to one month. Then by using a pure, less permeable polymer with a lag of one year, we expect by loading this polymer with the same amount of CST we will get a lag of thirty years. This assumes that the instantaneous development of a concentration gradient is appropriate for the impermeable material and that the theory presented above is valid. Experiments will be necessary for verification, but the results from previous studies show the model PVA system is adequate for predicting the behavior of a less permeable polymer (Shimotori *et al.*, 2006).

The second reason that the current PVA system is impractical is that PVA will not stand the γ-radiation produced by Cs-137 decay. Because the CST concentrates the cesium, it will also concentrate this radiation. This dramatically restricts the choice of polymers. We believe that one possible polymer is polyparaphenyleneterephthalamide (Kevlar) (Lundquist and White, 1999). This material is said to be stable under radiation, but we have not documented this behavior ourselves. Another possibility would be to blend CST into a thin layer of clay, but such an inorganic layer is very different than the intact polymers used in this research.

Other factors to be considered are the effect of competing ions and temperature. As shown by the difference between our measurement of the Cs^+ uptake capacity of the

CST and those conducted in the presence of 5.1 M $NaNO_3$ (simulated tank waste), Group I cations will alter the amount of Cs^+ uptake. Decreased uptake will lead to shorter lag times. The heat generated by radioactive decay will also increase the value of *D* and thus adversely affect membrane performance.

If a polymer that can stand the radiation can be identified and the theory derived above is valid for impermeable materials, its chances as a successful barrier are excellent. As an example, we imagine that a polyethylene barrier membrane is 1 mm thick, which is typical for geotextiles. Because transport parameters for cesium through polyethylene are unavailable, those for chloride are used for calculation purposes. The reported diffusion coefficient for chloride through polyethylene is of order 10^{-14} m^2/sec (Rowe *et al*., 1995), giving an approximate permeability of 10^{-17} m^2/sec. This latter value corresponds to a transmission rate of about 0.1 mg mm/m^2 day.

We can now estimate the lags across the hypothetical barrier membranes. For the CST-free membrane, we have from Equation 3.2

$$t_{lag} = \frac{\left(10^{-3}\, m\right)^2}{6\times 10^{-14}\, m^2/sec} \equiv 4600 hrs \qquad (3.13)$$

The CST-free membrane will prevent leakage for approximately 6 months. For a membrane with 10 percent CST (by weight) and challenged with a 10^{-3} M cesium solution, we have from Equation 3.5 and Figure 3.2

$$t_{lag} = \frac{(10^{-3}\, m)^2}{2\times 10^{-17}\, m^2/sec}\left[\frac{\frac{0.1g}{cm^3}\left(\frac{10^{-3}\, mol}{g}\right)}{10^{-6}\, mol/cm^3}\right] \equiv 1.6\times 10^5\, yrs \qquad (3.14)$$

The lag is now many centuries. This dramatic increase can be seen from Equation 3.14 to result from two factors. The first is the concentration of CST versus the concentration of cesium. The second is the appearance of the permeability (*DH*) in place of the diffusivity *D*. In other words, for a reactive membrane, the fact that the solubility *H* is small makes the lag big. It is the hope of this research that the promise of these barriers can be realized in practice.

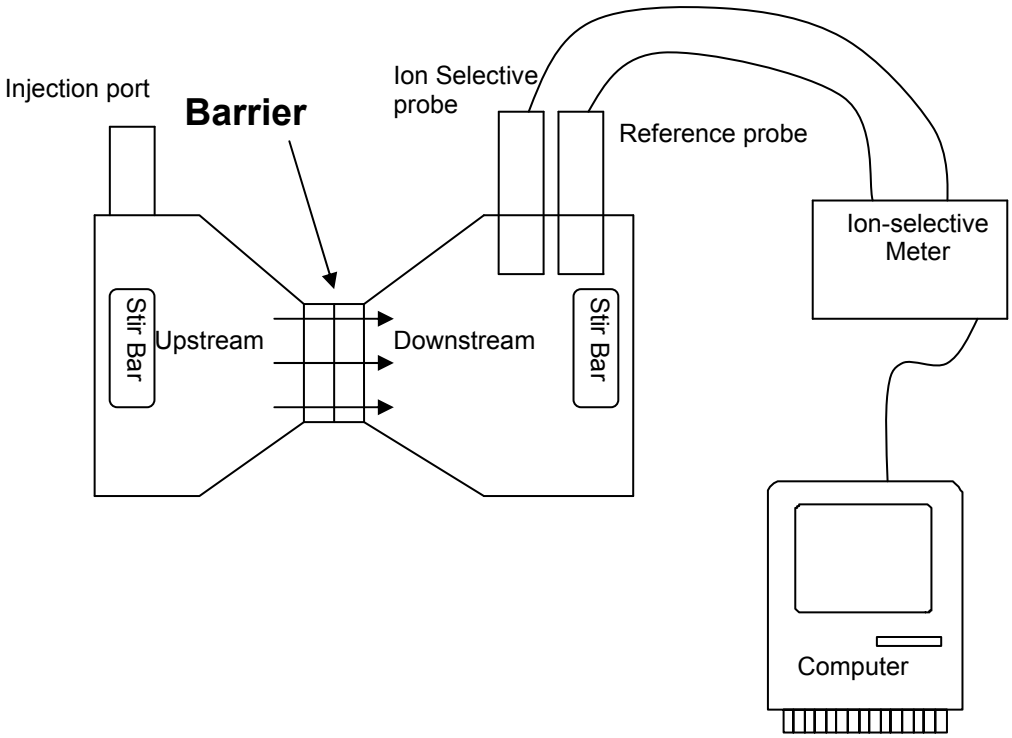

Figure 3.1: Diffusion cell apparatus used to measure downstream ion concentrations in breakthrough experiments.

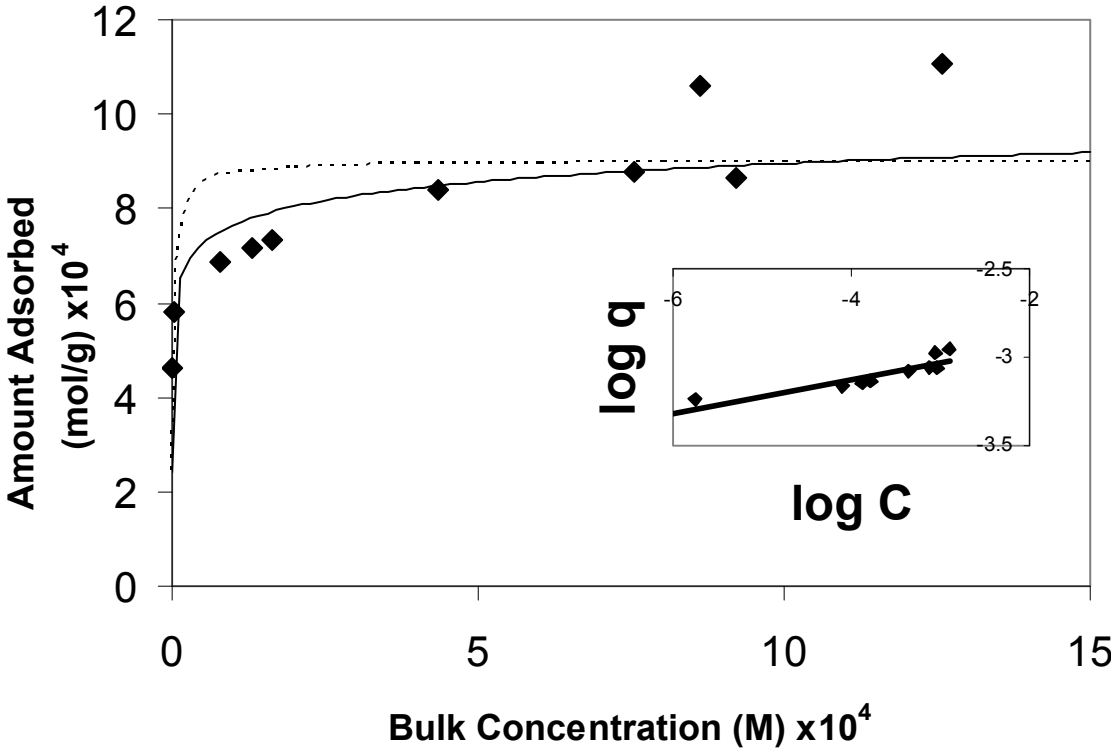

Figure 3.2: Fits of Freundlich (solid line and inset) and Langmuir (dashed line) isotherms to the cesium/CST system. The Freundlich isotherm captures the shoulder of the isotherm. Measurements were obtained at 23 °C from batch experiments using solution/adsorbent ratios between 120 and 700 mL of solution per gram of CST. The CST was added into stirring solutions with initial concentrations of 0.004-0.005 M $CsNO_3$.

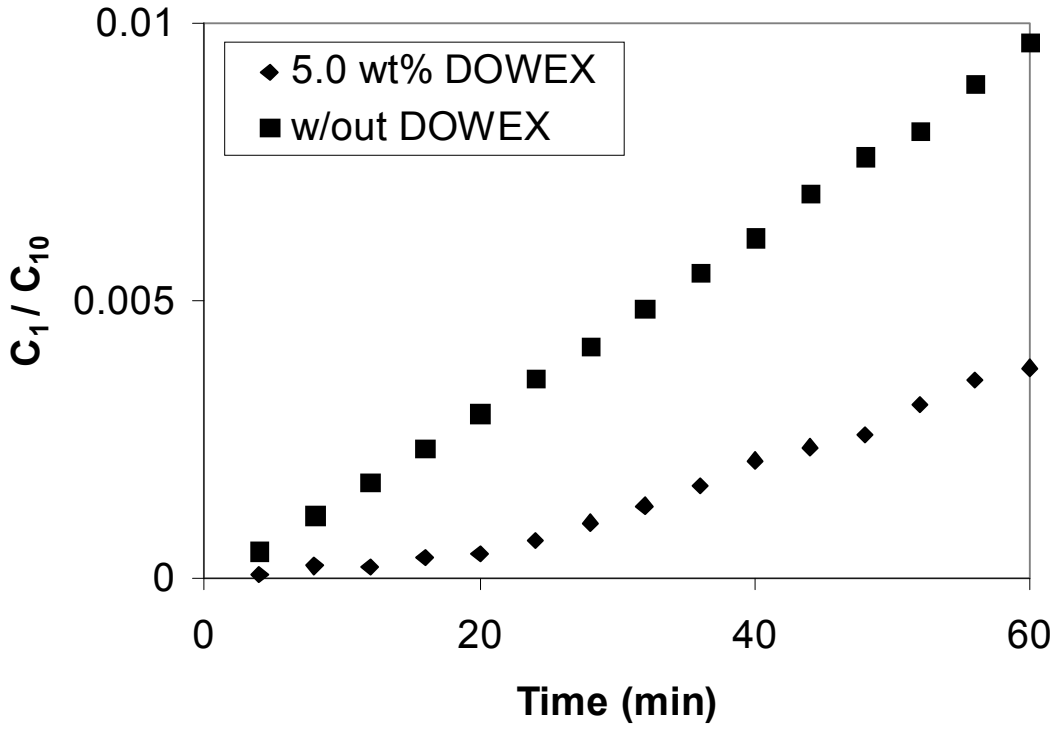

Figure 3.3: Addition of DOWEX ion-exchanger resin to a PVA barrier membrane increases the lag time for NaCl diffusion.

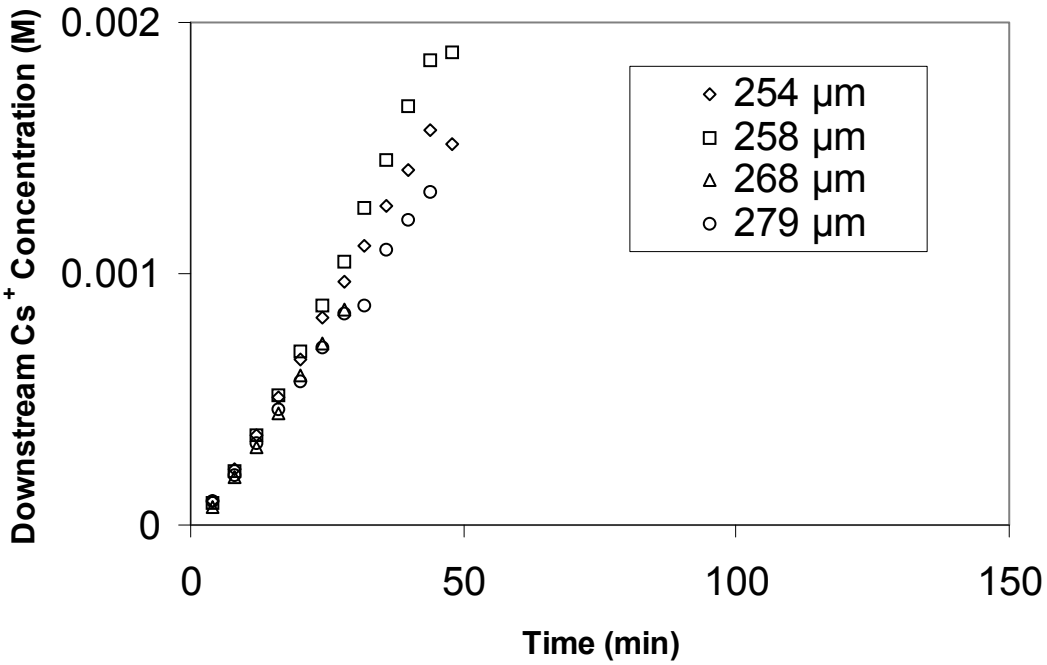

Figure 3.4: Cesium breakthrough curves for 0.1 M $CsNO_3$ through PVA barrier membranes are reproducible.

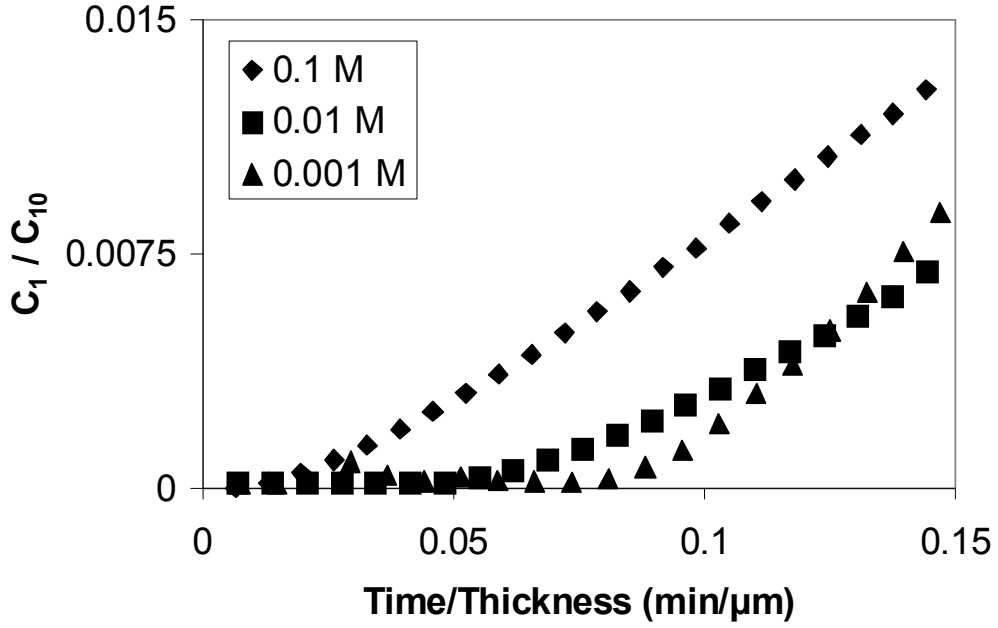

(a)

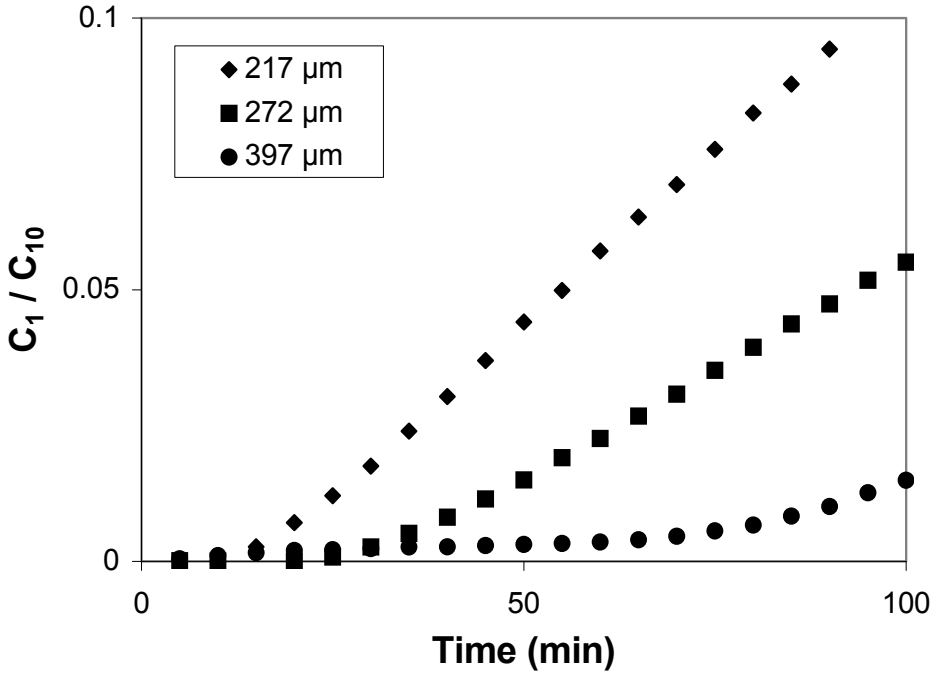

(b)

Figure 3.5: (a) A lower concentration of $CsNO_3$ in the upstream cell results in a larger lag time for barrier membranes with the same CST loading (5.0 wt%). (b) Thicker barrier membranes with the same CST loading (5.0 wt%) have longer lag times. (c) Effect of CST loading on breakthrough curves for 0.001 M $CsNO_3$.

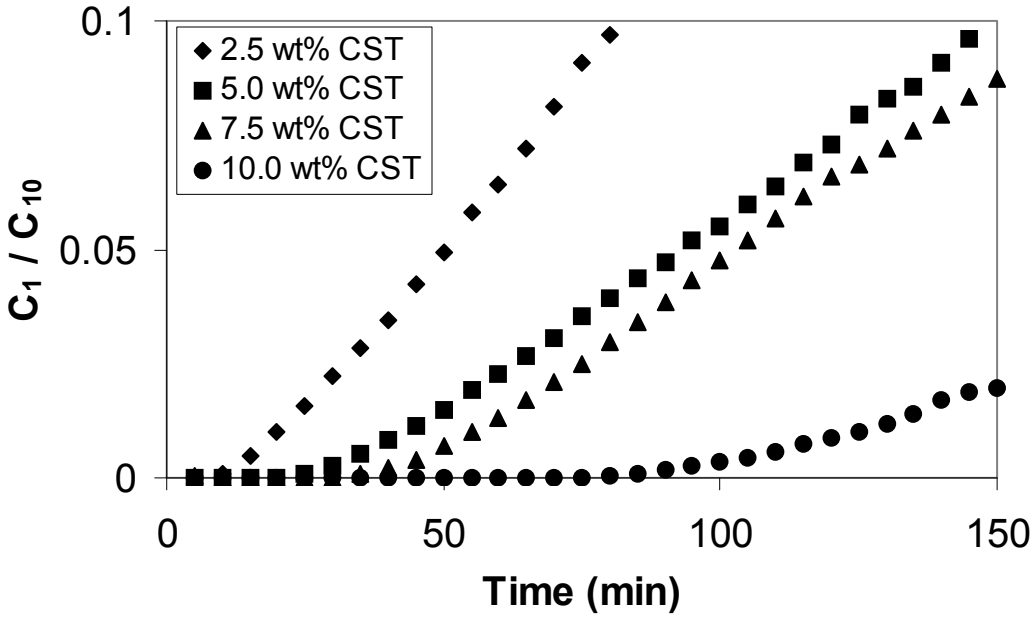

(c)

Figure 3.5 continued (page 2 of 2)

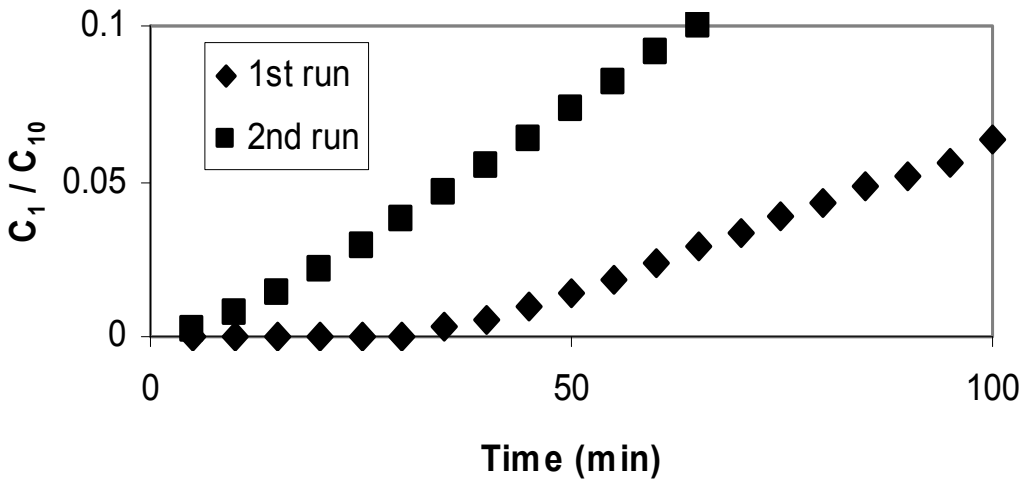

Figure 3.6: A demonstration of the effect of depletion of upstream volumes. Two consecutive breakthrough experiments performed on the same 5 wt% CST-containing membrane with 0.001M $CsNO_3$ upstream concentration C_{10}. The smaller slope for the first run is due to an effective decrease in C_{10}. C_1 is the Cs^+ concentration measured in the downstream cell.

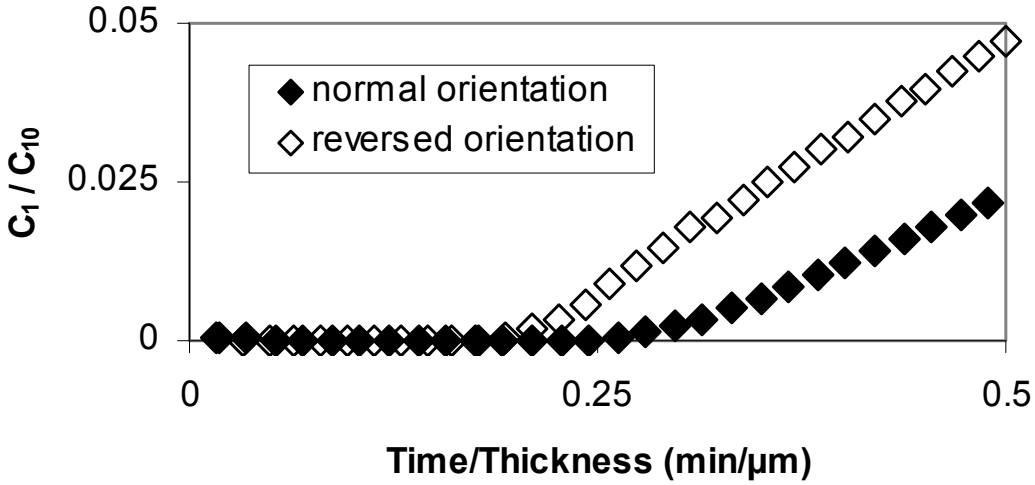

Figure 3.7: This plot shows the effect of membrane orientation. Different 7.5wt% CST-containing barrier membranes show the effect of particle settling on lag time by reversing the orientation of membrane in diffusion cell.

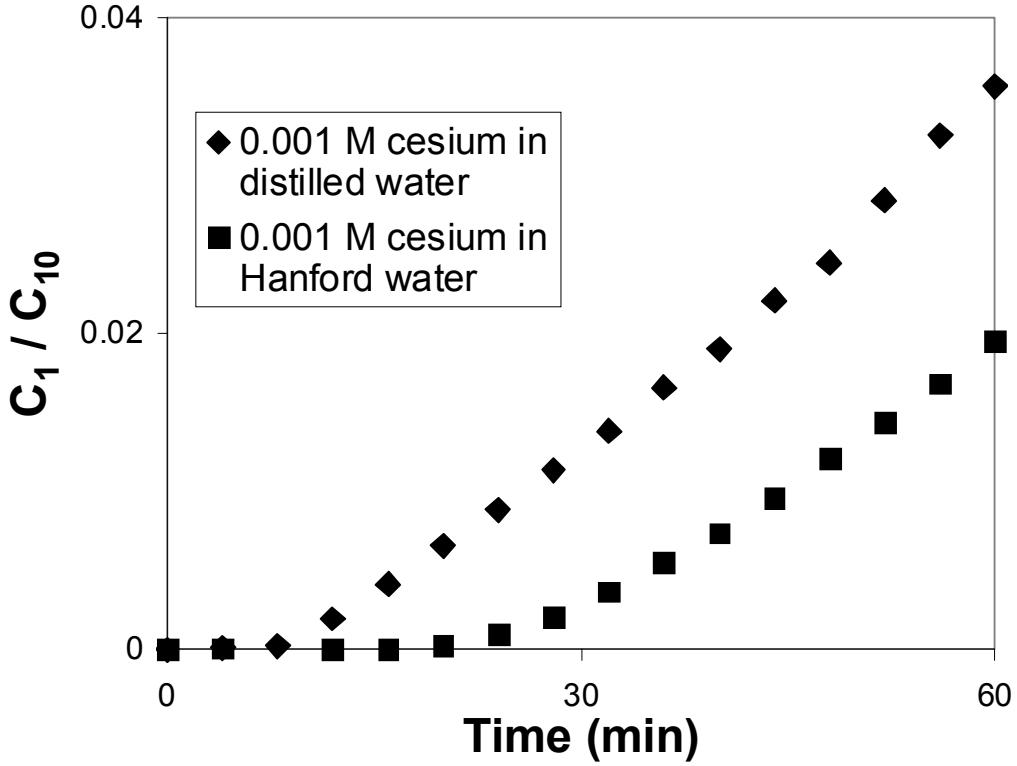

Figure 3.8: Measurement of breakthrough for cesium added to groundwater from Hanford,WA shows increased lag time when diffusing through a 5.0 wt% CST membrane. The lag time is nearly three times longer for the Hanford water trial (197μm; 28.3 min.) compared to that for distilled water (195μm; 9.6 min.).

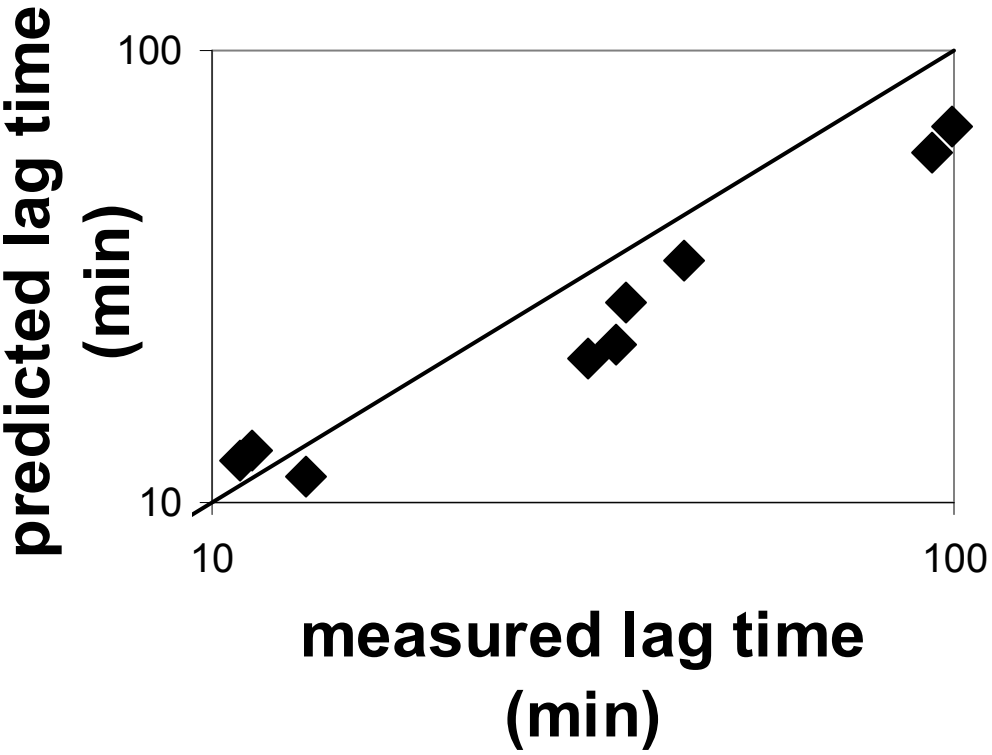

Figure 3.9: Measured lag times correlate with theoretical predictions from Equation 3.5.

Chapter 4

The Effect of Upstream Concentration Changes on the Performance of Powdered Activated Carbon Containing Barrier Membranes and Predicted Behavior of Such Membranes when Coupled to a Reactive System

The previous chapter focuses on batch breakthrough experiments of reactive barrier membranes where the upstream concentration is held constant. This chapter looks at barrier performance when the upstream concentration is allowed to vary. The first part of the chapter discusses experiments and results. The second part of the chapter develops theories to model how these barriers could be used in practice.

4.1 Introduction

Polychlorinated biphenyls (PCBs) leaked into the environment bioaccumulate (Safe *et al.*, 1987) and pose a risk to humans and wildlife, including damage to nervous systems and links to some cancers (Backlin *et al.*, 1997; Bell *et al.*, 1994; Jacobson and Jacobson, 1997; Mayes *et al.*, 1998; Tan *et al.*, 2003). PCBs are hydrophobic, strongly sorbing to sediments containing organic matter, including river beds.

A goal of this research is to build towards creating a barrier working in concert with a biologically active compartment to degrade PCBs. This compartment may contain the microorganism *Burkholderia fungorum* LB400, an aerobic bacterium capable of degrading many PCBs (Bedard *et al.*, 1986). In the environment, contaminant concentration may vary with time. Such variations may overwhelm the reactive capacity of the compartment or be toxic to the microorganism. Use of such a compartment would require means to control contaminant concentration fluctuations, and the barrier is one means to do so.

Powder activated carbon (PAC) has been shown to sorb PCBs and other chlorinated hydrocarbons (Surdo *et al.*, 2009; Yun *et al.*, 1998). The sorption of chlorinated contaminants on PAC may be modeled by a Langmuir isotherm. As the concentration of contaminant in solution increases, the loading of contaminant on PAC increases. Thus, when a plume challenges a PAC containing barrier membrane, more contaminant will be adsorbed than a barrier membrane can sorb alone. Designing a barrier membrane that incorporates PAC should aid in concentration control.

Besides being toxic, PCBs are extremely insoluble in water, making experiments measuring concentration changes and PAC uptake difficult. Surdo showed that 1,2,4-trichlorobenzene (1,2,4-TCB) is a good model for PCBs (Surdo, 2009). 1,2,4-TCB is

more soluble, making for easier detection. Both molecules include an aromatic ring with multiple chlorine atoms replacing hydrogen atoms. Importantly for this work, each follows Langmuir isotherm behavior on PAC. The experiments discussed below use 1,2,4-TCB with the expectation that experimental and modeling results may be extrapolated to use with PCBs.

4.2 Experimental Procedures

4.2.1 Materials

1,2,4 trichlorobenzene (99%+, Sigma Aldrich), methanol (99.9% Mallinckrodt), hexanes (65% n-hexane, Fisher Scientific), PVA (Elvanol grade 71-30 lot L1A352, molecular weight 138,000-146,500 Dupont) were used as received. Powdered activated carbon (J.T. Baker) was sieved with 150 mesh sieve tray. Distilled water was used unless otherwise specified.

4.2.2 Membrane Preparation

Membranes were prepared by adding 4.0 g of PVA to 36 mL of water at 90 °C and stirring at 60 rpm in a 150 mL beaker on a heated stir plate for 30-60 minutes to dissolve the PVA. The solution was removed from the stir plate and degassed under vacuum at room temperature for five minutes. For membranes containing added powdered activated carbon, the degassed solution was returned to the heated stir plate, the desired amount of powdered activated carbon was added and the covered solution was stirred for 2-3 more hours at 90 °C. The solution was again degassed. After degassing, the covered solution was allowed to cool to room temperature. The solution was then poured onto a Teflon block, and a doctor blade was pulled by hand across the surface at about 0.5 cm/sec. The resulting film was covered with aluminum foil to minimize air convection across the surface and dried at room temperature for three days. The film was placed in an oven at 150 °C for 135 minutes to crosslink the polymer. After the film's mass was measured, it was soaked overnight in 1 L of water. This doubled its mass. The hydrated film was cut into circular segments of radius 2 cm.

4.2.3 Membrane Experiments

Film segments were tested in the diffusion cell apparatus shown in Figure 4.1. The cell consists of two well-stirred volumes of 255 – 260 cm^3 each, called the "upstream" and "downstream" compartments. These compartments are separated by a barrier membrane of 5.1 cm^2 active area. The barrier membrane is sealed between the compartments with epoxy (5-Minute Quickset Loctite). Each compartment is initially filled with contaminant-free distilled water. A volume of contaminant containing solution in methanol was injected into the upstream compartment to start the experiment. Contaminant concentration in the downstream compartment is measured with time. These measured concentrations are the basic data of the experiment.

4.2.4 Flow-through Cell Experiments

Experiments utilizing a flow-through cell are conducted similarly to the membrane experiments described above, in the system shown in Figure 4.2. The upstream cell is replaced with a well-stirred 66 cm^3 compartment with an injection/sample port, 5.1 cm^2 active area for a barrier membrane, and ¼ inch outside diameter inlet and outlet ports. These ports are connected with Swagelock fittings to Teflon tubing. A ball valve separates the inlet port from a pump which draws contaminant free water from a reservoir. The outlet port tubing empties into a sealed waste reservoir.

For experiments using pure PVA barrier membranes, the barrier is sealed between the well-stirred upstream flow-through cell and a 258 cm^3 well-stirred downstream cell. For experiments using PAC containing barrier membranes, an impermeable aluminum disc is used in place of a downstream cell. To start the experiment, a solution of 1,2,4-TCB in methanol is injected into the upstream cell, and for pure PVA barrier membranes, into the downstream cell as well. After some time, the pump connected to the upstream flow-through cell is started, pumping 1,2,4-TCB-free solution at a rate of 19 mL/min. The volume of solution in the upstream flow-through cell is kept constant, with an equal flow leaving the cell as waste. The pump is then turned off. The pump may be turned on

and off multiple times over the course of the experiment. Additional 1,2,4-TCB in methanol solution may be injected to increase the concentration of the upstream flow-through cell.

4.2.5 1,2,4-TCB Concentration Measurements

1,2,4-TCB concentrations were measured after extraction in hexane. 0.1 – 1.0 mL volumes of aqueous solution were extracted with 1.0 mL of hexane (volumes determined by mass) in a capped vial. The vials were held by hand on a vortex mixer (Touch Mixer 232, Fischer Scientific) for 30 seconds. The hexane phase was hand-pipetted into a separate vial, which was then capped.

Vials were placed on an autosampler of a Hewlett Packard 5890A gas chromatograph equipped with a an electron capture detector (oven temperature at 100 °C for 2 min, 15 °C/min to 160 °C, 5 °C/min to 235 °C, hold for 3 min, 15 °C/min to 270 °C, hold for 2 min). Two-microliter samples were injected to a splitless inlet at 225 °C on an HP-5 column (30 m × 0.32 mm i.d. × 0.25 μm film thickness, J&W). . Six calibration standards of 1,2,4-TCB in hexane were used within the linear calibration range from 1×10^{-7} to 1×10^{-5} M 1,2,4-TCB in hexane.

4.2.6 Isotherm Procedure

Glass sample bottles with a volume of 160 mL were filled with distilled water and a mass of sieved PAC. A volume of 1,2,4-TCB in methanol was added. The vials were crimped sealed with no head space, and placed on a shaker table for 8 days. The final concentrations were measured using the extraction procedure described above.

4.3 Results and Discussion

This work tests a permeable barrier membrane for 1,2,4-TCB as a model for chlorinated aromatic contaminants, including PCBs. These experiments build towards the idea of using PAC containing barrier membranes in applications where contaminant concentrations vary. The development has four parts: the adsorption isotherm for 1,2,4-

TCB on PAC, 1,2,4-TCB breakthrough of barrier membranes, validation of a flow through diffusion cell, and PAC containing membrane behavior.

The adsorption isotherm for 1,2,4-TCB on PAC is shown in Figure 4.3. These data are approximated by a Langmuir isotherm, which captures the shoulder of the data and has the form given in Equation 2.61:

$$c_2^* = \frac{q_{\max} b c_1}{1 + b c_1} \tag{4.1}$$

where c_2^* is the 1,2,4-TCB concentration in mg per gram PAC, q_{max} is the apparent maximum capacity of 1,2,4-TCB on PAC, c_1 is the bulk concentration of the solution, and b is an equilibrium constant. The best fit of these data is for a maximum capacity, q_{max}, of 540 mg 1,2,4-TCB per gram PAC, and an equilibrium constant, b, of .02 L per μmol 1,2,4-TCB in water. For comparison, the maximum capacity for 1,2,4-TCB of 1 gram of PAC equals that of 15.7 L of water with a solubility of 1,2,4-TCB of 34.6 mg per L. This capacity makes PAC an ideal candidate for addition to a barrier membrane to retard breakthrough of 1,2,4-TCB.

The effect of PAC addition to PVA, a permeable model barrier membrane, was studied in the diffusion cell shown in Figure 4.1. Plots of the resulting data are shown in Figure 4.4. Lag times for 1,2,4-TCB, defined by the x-intercept of a linear regression of the slope of the downstream concentration curve at large times, increases significantly with the addition of PAC to PVA. Breakthrough of 1,2,4-TCB through pure PVA is fast enough that it cannot be calculated from the measurements of downstream concentration. Breakthrough time of 1,2,4-TCB through a PVA barrier membrane containing 2.5wt% PAC is over 85 minutes.

The preceding results show PAC can adsorb and effect the barrier membrane breakthrough behavior of 1,2,4-TCB at constant upstream concentration. The next step is to determine the behavior of a PAC containing barrier membrane when the concentration of solution in contact with the barrier is altered. This is tested by replacing the upstream compartment of a diffusion cell with the flow-through cell shown in Figure 4.2.

The flow-through cell allows for contaminant free solution to be pumped into the upstream compartment. The total volume of solution in the compartment is kept constant, with an equal volume of solution allowed to leave the system. The upstream compartment is well-stirred, causing the flow-through system to act as a continuously stirred tank. The compartment will behave as a closed, well-stirred volume when the pump is off as it is for the majority of time an experiment runs. During these times, the compartment can be thought of as acting the same as the upstream volume in Figure 4.1.

One can envision an experiment where a barrier membrane is placed in the diffusion cell shown in Figure 4.2. The upstream solution and barrier membrane are initially free of contaminant. An impermeable barrier is placed on the downstream side of the barrier membrane; no downstream volume is present and contaminant may only transfer between the upstream solution and barrier membrane. At the start of the experiment, a pulse of contaminant is introduced into the upstream volume. Contaminant will transfer from the upstream solution into the barrier membrane.

At some time, the pump connected to the flow-through cell is turned on, introducing contaminant free solution into the upstream cell. The concentration of contaminant will decrease. The longer the pump operates, the lower the upstream cell concentration will become. The experiment can be designed to turn off the pump after the concentration in the upstream cell falls below the concentration within the barrier membrane. Contaminant will begin to transfer from the membrane into the cell. Additional contaminant may also be injected into the upstream cell, increasing contaminant concentration.

Such an experiment with 1,2,4-TCB and pure PVA is difficult to achieve. The water swollen PVA barrier membrane has a partition coefficient close to one. The low solubility of 1,2,4-TCB in water would require a very thick barrier membrane to hold enough contaminant to measure an increase in the upstream concentration after the pump is turned off. Due to the casting procedure of PVA barrier membranes, such thicknesses are not achievable. One could conceive of using many PVA barrier membranes sandwiched together. This leads to problems ensuring the interfaces between the

individual barrier membranes are in complete contact with each other, as well as difficulties sealing the diffusion cell.

Instead, an experiment is designed to take advantage of the fact that the partition coefficient between a PVA barrier membrane and water solution is near one. A partition coefficient close to one means there is little difference in concentration on either side of the interface between the solution and barrier membrane. A volume of water will have a similar capacity for 1,2,4-TCB as a PVA barrier membrane. Recall that a PVA barrier membrane was shown above to have a short lag time for 1,2,4-TCB that could not be experimentally measured. These two properties imply a downstream volume of water may be used to simulate a very thick PVA barrier membrane.

The results of this experiment are shown in Figure 4.5. Initially, a solution of 1,2,4-TCB was injected into the upstream and downstream cell. The downstream cell concentration was 10 times greater than the minimum detection limit for 1,2,4-TCB. The upstream cell concentration was 10 times greater than the downstream cell concentration, thus 100 times greater than the minimum detection limit for 1,2,4-TCB. The upstream cell concentration initially decreases as the concentration gradient is towards the downstream cell. After some time, the pump is turned on, flowing contaminant free water into the upstream cell, flushing contaminant containing solution out. The pump is turned off when the concentration has decreased by two orders of magnitude. The downstream cell concentration is now higher than that in the upstream cell; 1,2,4-TCB moves from the downstream cell to the upstream cell. After some time, a solution containing 1,2,4-TCB is injected into the upstream cell, increasing the concentration above that in the downstream cell, and the procedure is repeated. The inset of Figure 4.5 more clearly shows the upstream concentration rise following the pump being turned off. The upstream cell concentration change when the pump is on is reproducible. With the proof of concept that a flow-through diffusion cell can be used to experimentally alter upstream concentration, PAC containing barrier membranes are tested next.

A PVA barrier membrane containing 2.5wt% PAC, preloaded with 1,2,4-TCB is placed in the diffusion cell with a flow-through upstream compartment shown in Figure 4.2. Initially, no contaminant is present in the upstream cell. The concentration of 1,2,4-

TCB in the upstream cell is plotted in Figure 4.6. After 4 hours, the pump is turned on, reducing the upstream cell concentration before being turned off. 1,2,4-TCB continues to transfer from the PAC containing barrier membrane to the upstream cell. It is important to note that the flux of 1,2,4-TCB from the PAC containing barrier membrane reduces with time. This result is expected as no additional 1,2,4-TCB enters the system after the experiment is started. The amount of 1,2,4-TCB adsorbed on PAC decreases over the course of the experiment, reducing the driving force for mass transfer between the barrier membrane and solution.

A PVA barrier membrane containing 1.25wt% PAC, initially free of 1,2,4-TCB, is placed in the diffusion cell with a flow-through upstream compartment shown in Figure 4.2. A high concentration of 1,2,4-TCB is injected into the cell and allowed to equilibrate with the PAC containing barrier membrane. After some time, the pump is turned on, reducing the upstream cell concentration before being turned off. The concentration of 1,2,4-TCB in the upstream cell is plotted in Figure 4.7. After 10 hours the pump is turned on, reducing the upstream cell concentration before being turned off. 1,2,4-TCB continues to transfer from the PAC containing barrier membrane to the upstream cell.

Again, the flux of 1,2,4-TCB decreases with time. For a closed system, after long times, the driving force for mass transfer between the membrane and solution will go to zero. This behavior can be seen after 400 minutes when the concentration in the upstream cell plateaus. If an experiment was run long enough before turning the pump on, this constant concentration region would always occur, though the concentration value would change based on PAC loading.

Predicting the mass transfer between a loaded PAC containing barrier membrane and a solution requires considering what occurs within the barrier membrane. As previously discussed, the effective concentration of 1,2,4-TCB within the membrane is higher than that in solution. This causes 1,2,4-TCB to desorb from PAC molecules close to the surface, transferring into the solution. Within the membrane, the concentration of 1,2,4-TCB near the surface decreases, resulting in desorption from PAC further from the surface. This may be modeled as a moving front, shown in Figure 4.8.

A mass balance is made within the membrane along the moving front. Mass transfers from the carbon in the membrane into solution:

$$c_2 \frac{dV_m}{dt} = j_1 A \tag{4.2}$$

where c_2 is the effective concentration of contaminant within the membrane, j_1 is the flux of contaminant into solution, A is the area mass transfer occurs across, and V_m is the volume of the membrane. For the moving front, the differential element of interest is the length, and the flux can be rewritten as:

$$c_2 \frac{d(Al)}{dt} = \frac{DA}{l}\left(c_1^* - c_1\right) \tag{4.3}$$

where c_1^* is the contaminant concentration in the loaded carbon and D is the diffusion coefficient of contaminant. The concentration of contaminant in solution is very low compared to that in the membrane, $c_1 << c_1^*$; thus

$$c_2 A \frac{dl}{dt} = \frac{DA}{l} c_1^* \tag{4.4}$$

The contaminant in the membrane will be in equilibrium with PAC as defined by the isotherm shown in Figure 4.3. An assumption is made that the isotherm can be modeled as linear from low concentrations to the shoulder:

$$c_1^* = Kc_2 \tag{4.5}$$

where K is an equilibrium constant between contaminant in solution and on PAC. Inserting Equation 4.5 into 4.4 and rearranging gives

$$ldl = DKdt \tag{4.6}$$

The boundary conditions for integration are:

$$t = 0 \qquad l = 0 \tag{4.7}$$

$$t = t \qquad l = l \tag{4.8}$$

Solving gives:

$$l = \sqrt{2DKt} \tag{4.9}$$

which defines how the moving front thickness varies with time.

A mass balance is now made on the solution:

$$V_s \frac{dc_1}{dt} = j_1 A = \frac{DA}{l}\left(c_1^* - c_1\right) \tag{4.10}$$

where V_s is the volume of solution. Again recalling $c_1 << c_1^*$ and inserting Equation 4.9 gives

$$V_s \frac{dc_1}{dt} = \frac{DA}{\sqrt{2DKt}} c_1^* \tag{4.11}$$

Integrating with respect to the boundary conditions

$$t = 0 \qquad c_1 = 0 \tag{4.12}$$

$$t = t \qquad c_1 = c_1 \tag{4.13}$$

gives

$$c_1 = \frac{A}{V_s}\sqrt{\frac{2Dt}{K}} c_1^* \tag{4.14}$$

which can also be written

$$c_1 = \frac{A}{V_s}\sqrt{2DKt}\, c_2 \tag{4.15}$$

This equation shows that the concentration of a solution in contact with a loaded PAC barrier membrane will increase linearly with the square root of time. This explains the concentration profiles in Figures 4.6 and 4.7 where the slope decreases as time goes on. The data in these figures are plotted according to Equations 4.14 and 4.15 in Figure 4.9. An adjusted concentration is defined, which corresponds to the concentration that would exist in solution if only the 1,2,4-TCB from the membrane were plotted. The experimental procedure includes flushing out the upstream cell, meeting the assumption $c_1 << c_1^*$. The moles of 1,2,4-TCB transferred to solution have been mathematically summed, divided by solution volume, and plotted against the square root of time.

4.4 Theory

The preceding sections discuss the experimental results and interpretations for how a barrier membrane loaded with a model reversible reactive group (in this case powdered activated carbon) responds to changes in upstream concentration. The following section proposes a theory to approximate the behavior of these barrier

membranes when coupled with a reactive system capable of degrading contaminants. An example system includes the previously mentioned LB400, a strain of *Burkholderia xenovorans* capable of degrading polychlorinated biphenyls (PCBs), under aerobic conditions. Such a system could be used to cap and treat sediments contaminated with PCBs. This system would include two volumes in series: a volume containing bacteria where degradation would occur and a volume containing carbon which would act as a barrier to contaminant release.

4.4.1 First-Order Reaction, Configuration 1

Begin by envisioning two volumes. The first volume, V_1, contains a reactive group which degrades contaminant and the second volume, V_2, represents a carbon-filled membrane with a carbon weight percent W that follows a linear isotherm with slope K. Contaminant present in the first volume is called c_1; contaminant in the second volume is called c_2. Contaminant can transfer via diffusion between the volumes and also out of the second volume.

The assumption is made that each volume is well-mixed. This assumption does not necessarily require mechanical mixing. Instead, it assumes transfer within each volume is rapid enough that resistance for reactions due to mass transfer is negligible.

The reaction in V_1 takes place when a molecule of contaminant comes in contact with the reagent (for this case, assume it is a bacterium). This implies the second-order reaction

$$\frac{dc_1}{dt} = -k[cells]c_1 \tag{4.16}$$

where k is a second-order reaction rate constant. If the concentration of cells remains constant

$$k_R = k[cells] \tag{4.17}$$

thus k_R is a pseudo first-order reaction rate constant. This would be the situation for a bacterial culture that has reached the stationary growth phase. The reaction in V_1 is then a first-order reaction

$$\frac{dc_1}{dt} = -k_R c_1 . \qquad (4.18)$$

The volume V_2 is the volume of the polymeric membrane only. The actual concentration of contaminant, c_2, this membrane contains will depend on the amount of carbon, W, in the membrane, and the capacity of the carbon. The capacity is determined by the contaminant/carbon isotherm. Previously, this chapter showed the isotherm is expected to be linear for low concentrations of contaminant. Taking into account the volume of the membrane and the additional capacity for contaminant due to carbon gives

$$V_e = V_2\left(1 + \frac{KW}{V_2}\right) \qquad (4.19)$$

where V_e is an equivalent volume.

To determine the concentrations c_1 and c_2 with time, mass balances on the system must be written. Contaminant in V_1 can leave in two ways. First, it is degraded by the first-order reaction. Second, the contaminant can diffuse from V_1 to V_2. The amount of contaminant transferred between the two volumes depends on the diffusion coefficient of the contaminant, D, a partition coefficient, H, the cross-sectional area, A, a characteristic thickness across which diffusion takes place, $l/2$, and the gradient in concentration, $(c_1 - c_2)$. As a necessary result of the well-mixed assumption, the concentration of contaminant within, and leaving, V_1, is equal. Physically, this means the concentration within V_1 does not depend on position within the membrane, only time. Consequences of this assumption are discussed later. The mass balance on compartment 1 is thus

$$V_1 \frac{dc_1}{dt} = -\frac{DHA}{l/2}(c_1 - c_2) - k_R c_1 V_1 \qquad (4.20)$$

Initially, V_1 is free of contaminant until a pulse with concentration $c_{1(0)}$ is introduced at time t=0. This initial pulse is the only time that contaminant is allowed to enter the system.

$$t < 0 \qquad c_1 = 0 \qquad (4.21)$$

$$t = 0 \qquad c_1 = c_{1(0)} \qquad (4.22)$$

Upon entering V_e, contaminant now exists in a carbon-filled membrane and its concentration is labeled c_2. The only reaction occurring in V_e is an equilibrium adsorption/desorption reaction between contaminant and carbon governed by the contaminant/carbon isotherm constant K, which is accounted for in the definition of V_e, Equation 4.19; no degradation of contaminant occurs in V_e. The mass balance for contaminant in V_e depends only on the rate of transfer between the two volumes, and the rate of transfer out of the system into a perfect sink. If the solutions on either side of V_e are the same (e.g., water) the resistances to mass transfer between the two volumes and out of the system will be the same. Thus the mass balance on compartment 2 is:

$$V_e \frac{dc_2}{dt} = \frac{DHA}{l/2}(c_1 - c_2) - \frac{DHA}{l/2}(c_2 - 0) \tag{4.23}$$

The carbon-filled membrane is initially free of contaminant, which only enters V_e from V_1:

$$t \le 0 \qquad c_2 = 0 \tag{4.24}$$

Four groups can be defined for the system as follows (see Appendix A). First,

$$k \equiv \frac{DH}{l} \tag{4.25}$$

k is the rate of mass transfer between the two volumes, and out of V_e. Second, the independent variable

$$\tau \equiv \frac{2kAt}{V_1} \tag{4.26}$$

τ is a characteristic time for the system. Third, the system characteristic

$$\nu \equiv \frac{V_1}{V_e} \tag{4.27}$$

ν is the ratio of volumes. Finally, the system characteristic

$$D_M \equiv \frac{k_R}{kA/V_1} \tag{4.28}$$

D_M is an apparent Damköhler number, the ratio of the rate of reaction to the rate of mass transfer.

Because D_M and ν will be the key parameters for this system, it is important to understand each in detail. A D_M value of 1 means the rate of reaction and the rate of mass transfer are equal. A large value of D_M, ($D_M >> 1$) means the rate of reaction is much larger than the rate of mass transfer. This can occur two ways: either the reaction rate is very fast, or the mass transfer rate is very slow. A small value of D_M ($D_M << 1$) means the rate of reaction is much smaller than the rate of mass transfer. The rate of mass transfer, k, appears in the dimensionless time definition τ. For this reason, when varying the value of D_M in the simulations below, the rate of reaction, k_R, is also being changed. For two given values of D_M, the larger value implies a larger value of k_R and thus a faster reaction.

The amount of carbon in the system is set by the value of ν. Recall from Equation 4.19 V_e varies with the amount of carbon, W, loaded in the membrane. A ν value of 1 means the volumes V_1 and V_e are equal. A large value of ν, ($\nu >> 1$) means the volume in which the degradation reaction takes place in is much larger than the equivalent volume for the carbon-filled membrane. This can occur two ways: either V_1 is large, or there is a low carbon loading in V_e. A small value of ν, ($\nu << 1$) means V_1 is much smaller than V_e. The volume V_1 appears in the definitions of D_M and τ. For these reasons, when varying the value of ν below, the amount of carbon, W, is being changed. For two given values of ν, the smaller value implies a larger value of W, and thus a larger amount of carbon.

Table 4.1: Dimensionless parameter dependence on system variables .

To **increase** D_M	**Increase** k_R (make reaction faster)
To **increase** ν	**Decrease** W (remove carbon)

Substituting Equations 4.25 through 4.28 into Equations 4.20 and 4.23 and rearranging gives

$$\frac{dc_1}{d\tau} = -\left(1 + \frac{D_M}{2}\right)c_1 + c_2 \tag{4.29}$$

$$\frac{dc_2}{d\tau} = \nu c_1 - 2\nu c_2 \tag{4.30}$$

with initial conditions

$$\tau = 0 \qquad c_1 = c_{1(0)} \tag{4.31}$$

$$\tau = 0 \qquad c_2 = 0 \tag{4.32}$$

Solving these equations gives (see Appendix A for detailed derivation)

$$c_1 = \xi_1 e^{a_1\tau} + \xi_2 e^{b_1\tau} \tag{4.33}$$

$$c_2 = \xi_1 a_1 e^{a_1\tau} + \xi_2 b_1 e^{b_1\tau} + \left(1 + \frac{D_M}{2}\right)\left[\xi_1 e^{a_1\tau} + \xi_2 e^{b_1\tau}\right] \tag{4.34}$$

where

$$a_1 = \frac{-\left(1 + \frac{D_M}{2} + 2\nu\right) + \sqrt{\left(1 + \frac{D_M}{2} + 2\nu\right)^2 - 4\left(\nu + D_M\nu\right)}}{2} \tag{4.35}$$

$$b_1 = \frac{-\left(1 + \frac{D_M}{2} + 2\nu\right) - \sqrt{\left(1 + \frac{D_M}{2} + 2\nu\right)^2 - 4\left(\nu + D_M\nu\right)}}{2} \tag{4.36}$$

and

$$\xi_1 = c_{1(0)} - \frac{\left(a_1 + \frac{D_M}{2} + 1\right)c_{1(0)}}{\left(a_1 - b_1\right)} \tag{4.37}$$

$$\xi_2 = \frac{\left(a_1 + \frac{D_M}{2} + 1\right)c_{1(0)}}{\left(a_1 - b_1\right)}. \tag{4.38}$$

The solutions for c_1 and c_2 given in Equations 4.33 and 4.34 are sums of exponentials. If the term in the exponent (a_1 or b_1 from Equations 4.35 and 4.36, respectively) is positive or imaginary, the solution may show oscillatory behavior. For

all values of D_M and ν in this research, a_1 and b_1 will be less than, or equal to, zero, and real. This results in c_1 and c_2 always going to zero as τ gets large; no oscillatory behavior of concentration occurs.

The concentration of bacteria in V_1 is assumed to be constant, following a first-order reaction. If instead the bacterial concentration depended on the concentration of contaminant, it would be possible to see oscillations in c_1 and c_2. This could correspond to a case where high concentrations of contaminant are toxic to the bacteria. In this case, an additional reaction rate would be required, modeling bacterial death, which may be proportional to the square of contaminant concentration. At high concentrations of contaminants, the bacteria begin to die. As contaminant concentration decreases, bacterial concentration may begin to increase. This has the potential to lead to contaminant/bacterial concentration oscillations, similar to the lynx and rabbit model discussed by Murray (2003). The models discussed below use the constant bacterial concentration assumption.

4.4.2 First-Order Reaction, Configuration 1 Model Results

Equations 4.33 and 4.34 show c_1 and c_2 are sums of decaying exponentials (a_1 and b_1 are negative for all values of D_M and ν discussed in this chapter). The rate of decay depends on both D_M and ν. At $\tau = 0$, c_1 and c_2 are equal to the initial conditions shown in Equations 4.31 and 4.32. As τ becomes very large, c_1 and c_2 both go to zero. Figure 4.11 shows how c_1 and c_2 are expected to vary with τ for different values of D_M and ν.

Figure 4.11 plots (a) and (b) compare the expected concentration curves when D_M is the same and ν changes. Plot (a) has ten times more carbon than plot (b). Plots (c) and (d) show a D_M ten times greater than (a) and (b), with (c) containing ten times more carbon than (d). Increasing the carbon loading (i.e., a smaller value of ν) decreases the maximum c_2 concentration for a given value of D_M. Increasing the rate of reaction (i.e., a larger value of D_M) decreases the maximum c_2 concentration and the time it takes for c_2 to approach zero. In practical terms, this means increasing the reaction rate or adding more carbon decreases the flux (mass per area per time) leaving the system. The mass of

material leaving the system and the time it takes to do so are an important part of this work.

Figure 4.11 shows that with a first-order degradation reaction some contaminant will leave the system. Comparing the effectiveness of barriers requires a measure of the mass leaving the system, which is

$$loss \equiv V_1 \int_0^\infty c_2 d\tau \tag{4.39}$$

where c_2 is given in Equation 4.34. This value can be thought of as the area under the c_2 curve. Two factors can be used to determine which of two barriers is more effective: the overall mass lost from the system, and the time it takes for mass to be lost.

Though it may not be apparent from Figure 4.11, solving Equation 4.39 for different values of ν at constant values of D_M shows the amount of carbon does not change the mass lost. For the system shown in Figure 4.10 with a first-order degradation reaction in V_1 upstream of a carbon containing volume V_e, adding more carbon does not decrease the amount of contaminant that will escape. Physically, this means that on a net basis, any quantity of contaminant that escapes the reaction in V_1 by diffusing into V_e, will eventually diffuse out of the system. This does not mean increasing the amount of carbon has no effect. While it does not change the *amount* of contaminant lost, it can greatly alter the *time* for that mass to be released. Figure 4.12 shows the time it takes for contaminant to leave the system with different values of ν for a given value of D_M. In Figure 4.12 (a), the same amount of contaminant leaves the system for each value of ν, but the time for this release increases greatly with decreasing ν. For D_M =1 and ν =1, τ for 99% of the contaminant that will be lost from the system to leave is 6.82. For ν =0.1 and 0.01, τ for the same mass release is 36.88 and 347.60 respectively. Figure 4.12 (b) shows a similar trend for D_M=10. The time for the mass that will leave to do so depends strongly on ν. The total amount of mass that will leave depends on D_M.

The total amount of contaminant initially in the system is

$$mass_{1,(0)} \equiv c_{1(0)} V_1 . \tag{4.40}$$

Where $mass_{1,(0)}$ is the mass of contaminant present at τ=0. Dividing Equation 4.37 by Equation 4.38 gives

$$\%loss_{1,total} \equiv \frac{\int_0^\infty c_2 d\tau}{c_{1(0)}} \qquad (4.41)$$

where $\%loss_{1,total}$ is the percentage of the initial mass present in the system that escapes. Figure 4.13 shows how $\%loss_{1,total}$ varies with ν, D_M, and τ. As one would expect, when there is no reaction (D_M=0) all of the contaminant initially present escapes. As D_M increases, the amount of contaminant initially present that escapes decreases. For larger values of D_M, degradation occurs more completely; more contaminant reacts before it is able to diffuse into the carbon containing volume V_e. The most important aspect of Figure 4.13 is how long it takes contaminant to escape for different values of ν. The time required for contaminant to be released increases dramatically as the carbon loading increases.

There are two key concepts for a first-order degradation reaction in the system shown in Figure 4.10. Increasing the rate of reaction (and therefore D_M) decreases the amount of contaminant that will ultimately leave the system. Increasing the carbon loading (decreasing ν) increases the time it takes for contaminant to leave.

4.4.3 First-Order Reaction, Configuration 2

The previous section shows predicted contaminant loss for a system where a first-order reaction occurs upstream of a carbon-filled membrane. Regardless of carbon loading, any quantity of contaminant escaping the reaction volume, on a net basis, will be lost. In this section, the order of the volumes is switched by positioning the carbon-filled membrane before the reaction volume.

As before, begin by envisioning two volumes. The first volume now represents the carbon-filled membrane, V_2, with a carbon weight percent W that follows a linear isotherm with slope K. The second volume, V_1, contains a reactive group that degrades contaminant. Contaminant present in V_2 is again called c_2; contaminant present in V_1 is again called c_1. Please note these definitions are consistent with the previous section, the

only change is the order position of V_2 and V_1 in relation to each other. Contaminant can again transfer via diffusion between the two volumes, and also out of V_1. The assumption is made that each volume is well-mixed. Equations 4.16 - 4.19 hold for this system as before. This section will use a similar approach to the one used above.

To determine the concentrations c_1 and c_2 with time, mass balances on the system must be written. Contaminant in V_e can leave via diffusion to V_1. The amount of contaminant transferred between the two volumes depends on the diffusion coefficient of the contaminant, D, a partition coefficient, H, the cross-sectional area, A, a characteristic thickness across which diffusion takes place, $l/2$, and the gradient in concentration, $(c_2 - c_1)$. Remember, as a necessary result of the well-mixed assumption, the concentration of contaminant within, and leaving, V_e, is equal.

$$V_e \frac{dc_2}{dt} = -\frac{DHA}{l/2}(c_2 - c_1) \qquad (4.42)$$

Initially, V_e is free of contaminant until a pulse with concentration $c_{2(0)}$ is introduced at time t=0. This initial pulse is the only time contaminant is allowed to enter the system.

$$t < 0 \qquad c_2 = 0 \qquad (4.43)$$

$$t = 0 \qquad c_2 = c_{2(0)} \qquad (4.44)$$

Physically, this means the carbon-filled membrane is loaded with contaminant.

Upon entering V_1, contaminant concentration is labeled c_1. In addition to transfer with V_e, contaminant in V_1 can leave in two ways: First, contaminant is degraded by a first-order reaction. Second, the contaminant can diffuse out of the system into a perfect sink. If the solutions on either side of V_1 are the same (e.g., water) the resistances to mass transfer between the two volumes and out of the system will be the same.

$$V_1 \frac{dc_1}{dt} = \frac{DHA}{l/2}(c_2 - c_1) - \frac{DHA}{l/2}(c_1 - 0) - k_R c_1 V_1 \qquad (4.45)$$

The reaction volume V_1 is initially free of contaminant, which only enters from V_e.

$$t \le 0 \qquad c_1 = 0 \qquad (4.46)$$

The groups, k, τ, ν, and D_M are the same as defined in Equations 4.25-4.28. Substituting these definitions into Equations 4.42 and 4.45 and rearranging gives

$$\frac{dc_2}{dt} = \nu c_1 - \nu c_2 \tag{4.47}$$

$$\frac{dc_1}{dt} = -\left(2 + \frac{D_M}{2}\right)c_1 + c_2 . \tag{4.48}$$

with initial conditions

$$\tau = 0 \qquad c_2 = c_{2(0)} \tag{4.49}$$

$$\tau = 0 \qquad c_1 = 0 \tag{4.50}$$

Solving these equations gives (see Appendix B for detailed derivation)

$$c_2 = \xi_1 e^{a_1\tau} + \xi_2 e^{b_1\tau} \tag{4.51}$$

$$c_1 = \frac{\xi_1 a_1}{\nu} e^{a_1\tau} + \frac{\xi_2 b_1}{\nu} e^{b_1\tau} + \xi_1 e^{a_1\tau} + \xi_2 e^{b_1\tau} \tag{4.52}$$

where

$$a_1 = \frac{-\left(\nu + \frac{D_M}{2} + 2\right) + \sqrt{\left(\nu + \frac{D_M}{2} + 2\right)^2 - 4\left(\frac{D_M\nu}{2} + \nu\right)}}{2} \tag{4.53}$$

$$b_1 = \frac{-\left(\nu + \frac{D_M}{2} + 2\right) - \sqrt{\left(\nu + \frac{D_M}{2} + 2\right)^2 - 4\left(\frac{D_M\nu}{2} + \nu\right)}}{2} \tag{4.54}$$

and

$$\xi_1 = \left(\frac{b_1 + \nu}{b_1 - a_1}\right)c_{2(0)} \tag{4.55}$$

$$\xi_2 = \left(1 - \frac{b_1 + \nu}{b_1 - a_1}\right)c_{2(0)} . \tag{4.56}$$

For all values of D_M and ν in this research, a_1 and b_1 will be less than, or equal to, zero, and real. This results in c_1 and c_2 always going to zero as τ gets large; no oscillatory behavior of concentration occurs.

4.4.4 First-Order Reaction, Configuration 2 Model Results

Equations 4.51 and 4.52 show c_2 and c_1 are sums of decaying exponentials (a_1 and b_1 are negative for all values of D_M and ν discussed in this chapter). The rate of decay depends on both D_M and ν. At $\tau = 0$, c_2 and c_1 are equal to the initial conditions shown in Equations 4.49 and 4.50. As τ becomes very large, c_1 and c_2 both go to zero. Figure 4.15 shows how c_1 and c_2 are expected to vary with τ for different values of D_M and ν.

Figure 4.15 plots (a) and (b) compares the expected concentration curves when D_M is the same and ν changes. Plot (a) has ten times more carbon than plot (b). Plots (c) and (d) show a D_M ten times greater than (a) and (b), with (c) containing ten times more carbon than (d). Plots (a) and (b) show the maximum in concentration leaving the system, c_1, increases with increased carbon-loading, as do plots (c) and (d). This trend is different than in Figure 4.11 for Configuration 1 where the maximum in concentration leaving the system decreases with increased carbon loading. The reason can be found in the initial conditions, Equations 4.31-4.32 and 4.49-4.50. The total mass in Configuration 1 at t=0 is based on the initial concentration $c_{1(0)}$, and the volume V_1. The total mass in Configuration 2 at t=0 is based on the initial concentration $c_{2(0)}$, and the volume V_e

$$mass_{2,(0)} = V_e c_{2(0)} . \qquad (4.57)$$

Equation 4.19 shows changing the amount of carbon in the system will change V_e, while V_1 is independent of carbon-loading. Increasing the amount of carbon in Configuration 2 therefore increases the total mass of contaminant initially present. While the maximum in concentration for contaminant leaving the system in Configuration 2 increases with increased carbon-loading, the maximum in concentration is less than for the corresponding values of D_M and ν in Configuration 1.

Placing the carbon-filled membrane upstream of the reaction volume decreases the concentration of contaminant in the reaction volume V_1. Equation 4.18 shows the rate of contaminant degradation depends on the concentration of contaminant. The lower concentration due to reduced release from the carbon-filled membrane results in less degradation.

The amount of contaminant that escapes is proportional to the area under the c_1 curve

$$loss_2 \equiv V_1 \int_0^\infty c_1 d\tau . \tag{4.58}$$

Dividing this value by the total mass initially present, Equation 4.57, gives

$$\%loss_{2,total} \equiv \nu \frac{\int_0^\infty c_1 d\tau}{c_{2(0)}} \tag{4.59}$$

where $\%loss_{2,total}$ is the percentage of the initial mass present in the system that escapes. Figure 4.16 shows how $\%loss_{2,total}$ varies with ν, D_M, and τ. Comparison of Figures 4.13 and 4.16 shows the percentage of contaminant initially present that escapes is larger for Configuration 2 than Configuration 1 for a given value of D_M. For a first-order reaction, a smaller percentage of contaminant will escape the system when the concentration of contaminant in contact with the reactant is higher. This implies changing the order of reaction in each of the configurations could give significantly different results.

4.4.5 Zero-Order Reaction, Configuration 1

Degradation of chlorinated compounds, as discussed previously in this chapter, can be performed by certain biological organisms. Reactions with biological organisms are often modeled in one of two ways: either as a first-order reaction, or a zero-order reaction. These approximations can be seen from the Michaelis-Menten kinetic model (Alberts *et al.*, 2002).

Michaelis-Menten kinetics describes a reaction between a substrate and an enzyme to produce a product. The enzyme is left unchanged by the reaction. A bacterium degrading a contaminant can be approximated as acting like an enzyme. The

reaction requires the contaminant to come in contact, or be bound by, the bacterium, and reacts irreversibly to produce a degradation product

$$E + S \underset{k_{-1}}{\overset{k_1}{\longleftrightarrow}} \overline{ES} \xrightarrow{k_{cat}} E + P \tag{4.60}$$

where E is the enzyme or bacterium, S is the substrate, or contaminant, $\overline{ES}$ is the bound contaminant with bacterium, P is the reaction product, k_1 is the forward reaction rate of the contaminant binding, k_{-1} is the reverse reaction rate of the contaminant binding, and k_{cat} is the irreversible reaction rate of the bound contaminant being converted to product. Two assumptions are made for the system shown in Equation 4.60: a quasi-steady state of $\overline{ES}$ where its concentration changes very slowly with time, and the total amount of bacteria is assumed to not change with time

$$\frac{d[\overline{ES}]}{dt} = 0 \tag{4.61}$$

$$[E]_0 = [E] + [\overline{ES}] \tag{4.62}$$

where [$\overline{ES}$] is the concentration of bound contaminant with bacteria, $[E]_0$ is the initial concentration of bacteria, and $[E]$ is the concentration of unbound bacteria. Solving for the reaction rate of product gives

$$\frac{d[P]}{dt} = \upsilon = \frac{\upsilon_{\max}[S]}{K_M + [S]} \tag{4.63}$$

where $[P]$ is the concentration of product, $[S]$ is the concentration of contaminant, υ is the reaction rate, $\upsilon_{\max}$ is the maximum reaction rate, and K_M is the Michaelis-Menten constant which is defined from the reaction rate constants in Equation 4.60

$$K_M \equiv \frac{k_{-1} + k_{cat}}{k_1}. \tag{4.64}$$

A generalization of reaction rate υ based on Michaelis-Menten kinetics is shown in Figure 4.17. The plot has a similar shape to the Langmuir isotherm. In region 1, the reaction rate can be approximated as linear, corresponding to a first-order reaction. In region 2, the reaction rate is a constant value, corresponding to a zero-order reaction.

First-order reactions, such as Equation 4.18 depend linearly with concentration. Zero-order reaction rates are independent of concentration

$$\frac{dc_1}{dt} = -k_{R,0} \quad . \tag{4.65}$$

It is unlikely biological organisms will exactly follow either type of reaction. Looking at predictions for first-order and zero-order reactions will give the two possible extremes for these organisms. Actual results would be expected to be between these extremes.

The previous sections show the effect of a first-order degradation reaction in a system with a reaction volume and a carbon-filled membrane in two different configurations. As contaminant concentration decreases, the first-order reaction becomes less efficient leading to incomplete degradation of contaminant which escapes from the system. Using a zero-order reaction model, some of the previously escaping contaminant is expected to be degraded resulting in reduced contaminant loss.

Writing a mass balance for the system in Figure 4.10 with a zero-order reaction gives

$$V_1 \frac{dc_1}{dt} = -\frac{DHA}{l/2}(c_1 - c_2) - k_{R,0} V_1 \tag{4.66}$$

Initially, V_1 is free of contaminant until a pulse with concentration $c_{1(0)}$ is introduced at time $t=0$. This initial pulse is the only time contaminant is allowed to enter the system.

$$t < 0 \qquad c_1 = 0 \tag{4.67}$$

$$t = 0 \qquad \mathrm{c}_1 = c_{1(0)} \tag{4.68}$$

Upon entering V_e, contaminant now exists in a carbon-filled membrane and its concentration is labeled c_2. The only reaction occurring in V_e is an equilibrium adsorption/desorption reaction between contaminant and carbon governed by the contaminant/carbon isotherm constant K, which is accounted for in the definition of V_e, Equation 4.19; no degradation of contaminant occurs in V_e. The mass balance for contaminant in V_e depends only on the rate of transfer between the two volumes, and the rate of transfer out of the system into a perfect sink. If the solutions on either side of V_e are the same (e.g. water) the resistances to mass transfer between the two volumes and out of the system will be the same.

$$V_e \frac{dc_2}{dt} = \frac{DHA}{l/2}(c_1 - c_2) - \frac{DHA}{l/2}(c_2 - 0) \tag{4.69}$$

The carbon-filled membrane is initially free of contaminant, which only enters V_e from V_1.

$$t \le 0 \qquad c_2 = 0 \tag{4.70}$$

The groups, k, τ, and ν are the same as defined in Equations 4.25-4.28. For D_M to be dimensionless, it must be divided by a reference concentration. The appropriate reference concentration for this system is $c_{1,0}$. Thus the Damköhler number is

$$D_M \equiv \frac{k_{R,0}}{c_{1,(0)} kA / V_1}. \tag{4.71}$$

Substituting these definitions into Equations 4.66 and 4.69 and rearranging gives

$$\frac{dc_1}{d\tau} = -c_1 + c_2 - \frac{D_M c_{1(0)}}{2} \tag{4.72}$$

$$\frac{dc_2}{d\tau} = \nu c_1 - 2\nu c_2 \tag{4.73}$$

with initial conditions

$$\tau = 0 \qquad c_1 = c_{1(0)} \tag{4.74}$$

$$\tau = 0 \qquad c_2 = 0 \tag{4.75}$$

Solving these equations gives (see Appendix C for detailed derivation)

$$c_1 = -D_M c_{1(0)} + \xi_1 e^{a_1 \tau} + \xi_2 e^{b_1 \tau} \tag{4.76}$$

$$c_2 = \xi_1 a_1 e^{a_1 \tau} + \xi_2 b_1 e^{b_1 \tau} + \xi_1 e^{a_1 \tau} + \xi_2 e^{b_1 \tau} - \frac{D_M c_{1(0)}}{2} \tag{4.77}$$

where

$$a_1 = \frac{-(1+2\nu) + \sqrt{1+4\nu^2}}{2} \tag{4.78}$$

$$b_1 = \frac{-(1+2\nu) - \sqrt{1+4\nu^2}}{2} \tag{4.79}$$

and

$$\xi_1 = c_{1(0)} - \frac{(1+a_1)c_{1(0)} + \left(\frac{1}{2}+a_1\right)D_M c_{1(0)}}{(a_1 - b_1)} + D_M c_{1(0)} \qquad (4.80)$$

$$\xi_2 = \frac{(1+a_1)c_{1(0)} + \left(\frac{1}{2}+a_1\right)D_M c_{1(0)}}{(a_1 - b_1)} \qquad . \qquad (4.81)$$

For all values of ν in this research, a_1 and b_1 will be less than, or equal to, zero, and real; no oscillatory behavior of c_1 or c_2 occurs.

Equations 4.76 and 4.77 are only accurate until the time τ^* when $c_1 = 0$. After this time, c_1 will remain zero as any additional contaminant that enters V_1 will immediately be reacted. V_1 now acts as a perfect sink. A new mass balance must be made on the system in Figure 4.10 to model the concentration of contaminant after τ^*.

For $\tau > \tau^*$ where τ^* is the time at which c_1 goes to zero

$$c_1 = 0 \qquad (4.82)$$

$$V_1 \frac{dc_1}{dt} = 0 \qquad (4.83)$$

$$V_e \frac{dc_2}{dt} = -\frac{DHA}{l/2}(c_2 - 0) - \frac{DHA}{l/2}(c_2 - 0). \qquad (4.84)$$

The initial condition for Equation 4.84 is

$$\tau = \tau^* \qquad c_2 = c_2(\tau^*) \qquad (4.85)$$

where $c_2(\tau^*)$ is the concentration of c_2 at $\tau = \tau^*$, the instant c_1 becomes zero. Solving c_2 gives (see Appendix C for detailed derivation)

$$c_2 = c_2(\tau^*)e^{-2\nu(\tau - \tau^*)} \qquad (4.86)$$

4.4.6 Zero-Order Reaction, Configuration 1 Model Results

To correctly predict how c_1 and c_2 will vary with τ for Configuration 1 with a zero-order reaction, two regions are needed. The first region is for $\tau \le \tau^*$, the second region is for $\tau \ge \tau^*$ where τ^* is the time at which c_1 goes to zero. τ^* may be found

numerically or graphically. There is no discontinuity in the c_2 curve as the value of c_2 at $\tau = \tau^*$ becomes the pre-exponential factor in Equation 4.86. Figure 4.18 shows how c_1 and c_2 are expected to vary with τ for different values of D_M and ν.

Figure 4.18 plots (a) and (b) compare the expected concentration curves when D_M is the same and ν changes. Plot (a) has ten times more carbon than plot (b). Plots (c) and (d) show a D_M ten times greater than (a) and (b), with (c) containing ten times more carbon than (d). Increasing the carbon loading (i.e. a smaller value of ν) decreases the maximum c_2 concentration for a given value of D_M. Increasing the rate of reaction (i.e. a larger value of D_M) decreases the maximum c_2 concentration and the time it takes for c_2 to approach zero. In practical terms, this means increasing the reaction rate or adding more carbon decreases the flux (mass per area per time) leaving the system. The mass of material leaving the system and the time it takes to do so are an important part of this work.

Determining the amount of contaminant escaping the system requires finding the area under the c_2 curve. This integration requires special attention to the two regions discussed above, $\tau \le \tau^*$ and $\tau \ge \tau^*$.

$$loss_{1,0} \equiv V_1 \int_{\tau}^{\tau^*} c_2 d\tau + V_1 \int_{\tau^*}^{\infty} c_2 d\tau \tag{4.87}$$

This is divided by the total mass present initially to give

$$\%loss_{1,0total} \equiv \frac{\int_{\tau}^{\tau^*} c_2 d\tau + \int_{\tau^*}^{\infty} c_2 d\tau}{c_{1(0)}} \tag{4.88}$$

where $\%loss_{1,0total}$ is the percentage of the initial mass present in the system that escapes.

The zero-order reaction reduces c_1 much faster than the first-order reaction did. When c_2 becomes larger than c_1, contaminant will be transferred from V_e back to V_1 where it can be degraded. In Configuration 1 with a first-order reaction, on a net basis, any quantity of contaminant reaching V_e would eventually escape regardless of carbon-loading. This is a major advantage of the zero-order reaction. Increasing the carbon-loading decreases the flux of contaminant from the system allowing more time for

contaminant to transfer back into V_1, which suggests increasing carbon-loading will decrease the amount of contaminant that ultimately leaves the system.

This effect is seen especially well when the reaction rate is 100 times slower than the mass transfer rate, $D_M = 0.01$ (open squares) in Figure 4.19. Plot (a), where carbon-loading is low, shows contaminant release is similar to release when there is no reaction, $D_M = 0$ (diamonds). Plots (b) – (d), where carbon-loading increases, show the overall amount of contaminant that escapes decreases dramatically as the time required for release increases. Decreases in the percentage of contaminant released are similarly observed for the larger values of D_M, and the time required for this release increases.

4.4.7 Zero-Order Reaction, Configuration 2

Predicted results for a first-order reaction in Configuration 2 show an increased leakage of contaminant for a given D_M when compared to Configuration 1. The low concentration leaving the carbon-loaded membrane leads to a low rate of degradation from the first-order reaction. A zero-order reaction rate is independent of concentration, degrading contaminant at a constant rate. The decreased flux into V_1 from V_e in Configuration 2 should lead to reduced contaminant escape.

Writing a mass balance for the system in Figure 4.14 with a zero-order reaction in V_1 gives

$$V_e \frac{dc_2}{dt} = -\frac{DHA}{l/2}(c_2 - c_1) \qquad (4.89)$$

Initially, V_e is free of contaminant until a pulse with concentration $c_{2(0)}$ is introduced at time $t=0$. This initial pulse is the only time contaminant is allowed to enter the system.

$$t < 0 \qquad c_2 = 0 \qquad (4.90)$$

$$t = 0 \qquad c_2 = c_{2(0)} \qquad (4.91)$$

Physically, this means the carbon-filled membrane is loaded with contaminant.

Upon entering V_1, contaminant concentration is labeled c_1. In addition to transfer with V_e, contaminant in V_1 can leave in two ways: First, contaminant is degraded by a zero-order reaction. Second, the contaminant can diffuse out of the system into a perfect

sink. If the solutions on either side of V_1 are the same (e.g. water) the resistances to mass transfer between the two volumes and out of the system will be the same.

$$V_1 \frac{dc_1}{dt} = \frac{DHA}{l/2}(c_2 - c_1) - \frac{DHA}{l/2}(c_1 - 0) - k_{R,0} V_1 \qquad (4.92)$$

The reaction volume V_1 is initially free of contaminant, which only enters from V_e.

$$t \le 0 \qquad c_1 = 0 \qquad (4.93)$$

The groups, k, τ, and ν are the same as defined in Equations 4.25-4.28. For D_M to be dimensionless, it must be divided by a reference concentration. The appropriate reference concentration for this system is $c_{2,0}$. Thus the Damköhler number is

$$D_M \equiv \frac{k_{R,0}}{c_{2,(0)} kA / V_1} \qquad (4.94)$$

Substituting these definitions into Equations 4.4*1 and 4.4*4 and rearranging gives

$$\frac{dc_2}{dt} = \nu c_1 - \nu c_2 \qquad (4.95)$$

$$\frac{dc_1}{dt} = -2c_1 + c_2 - \frac{D_M}{2} \qquad (4.96)$$

with initial conditions

$$\tau = 0 \qquad c_1 = 0 \qquad (4.97)$$

$$\tau = 0 \qquad c_2 = c_{2(0)} \qquad (4.98)$$

Solving these equations gives (see Appendix D for detailed derivation)

$$c_1 = -\frac{D_M c_{2(0)}}{2} + \xi_1 e^{a_1 \tau} + \xi_2 e^{b_1 \tau} \qquad (4.99)$$

$$c_2 = \xi_1 a_1 e^{a_1 \tau} + \xi_2 b_1 e^{b_1 \tau} + 2\xi_1 e^{a_1 \tau} + 2\xi_2 e^{b_1 \tau} - \frac{D_M c_{2(0)}}{2} \qquad (4.100)$$

where

$$a_1 = \frac{-(2+\nu) + \sqrt{4+\nu^2}}{2} \qquad (4.101)$$

$$b_1 = \frac{-(2+\nu) - \sqrt{4+\nu^2}}{2} \qquad (4.102)$$

and

$$\xi_1 = \frac{D_M c_{2(0)}}{2} - \frac{c_{2(0)} - \frac{D_M c_{2(0)}(a_1+1)}{2}}{(b_1 - a_1)} \tag{4.103}$$

$$\xi_2 = \frac{c_{2(0)} - \frac{D_M c_{2(0)}(a_1+1)}{2}}{(b_1 - a_1)} \tag{4.104}$$

For all values of ν in this research, a_1 and b_1 will be less than, or equal to, zero and real; no oscillatory behavior of c_1 or c_2 occurs.

Equations 4.99 and 4.100 are only accurate until the time τ^* when $c_1 = 0$. After this time, c_1 will remain zero as any additional contaminant that enters V_1 will immediately be reacted. V_1 now acts as a perfect sink. A new mass balance must be made on the system in Figure 4.14 to model the concentration of contaminant after τ^*. For $\tau > \tau^*$ where τ^* is the time at which c_1 goes to zero

$$c_1 = 0 \tag{4.105}$$

$$V_1 \frac{dc_1}{dt} = 0 \tag{4.106}$$

$$V_e \frac{dc_2}{dt} = -\frac{DHA}{l/2}(c_2 - 0) \tag{4.107}$$

The initial condition for Equation 4.107 is

$$\tau = \tau^* \qquad c_2 = c_2(\tau^*) \tag{4.108}$$

where $c_2(\tau^*)$ is the concentration of c_2 at $\tau = \tau^*$, the instant c_1 becomes zero. Solving c_2 gives (see Appendix D for detailed derivation)

$$c_2 = c_2(\tau^*) e^{-\nu(\tau - \tau^*)} \tag{4.109}$$

4.4.8 Zero-Order Reaction, Configuration 2 Model Results

To correctly predict how c_1 and c_2 will vary with τ for Configuration 2 with a zero-order reaction, two regions are needed. The first region is for $\tau \le \tau^*$, the second region is for $\tau \ge \tau^*$ where τ^* is the time at which c_1 goes to zero. τ^* may be found

numerically or graphically. There is no discontinuity in the c_2 curve as the value of c_2 at $\tau = \tau^*$ becomes the pre-exponential factor in Equation 4.109. Figure 4.20 shows how c_1 and c_2 are expected to vary with τ for different values of D_M and ν. Plots (a) and (b) compare the expected concentration curves when D_M is the same and ν changes. Plot (a) has ten times more carbon than plot (b). Plots (c) and (d) show a D_M 100 times greater than (a) and (b), with (c) containing ten times more carbon than (d).

Configuration 2 with a first-order reaction (Figure 4.15) has an increase in maximum c_1 concentration for a given D_M when ν increases. This effect is also seen in Figure 4.20 and is due to there being more contaminant in the system when ν is larger. When the carbon-loaded membrane was downstream of the reaction volume, this allowed a higher percentage of contaminant to escape than when the two volumes were flipped.

The zero-order reaction in Configuration 2 shows an advantage over a first-order reaction which results in little degradation when c_1 is small. The zero-order reaction is able to degrade a constant amount of contaminant independent of the value of c_1. When c_1 is small for the zero-order reaction case, much of the contaminant will react before it is able to escape from the system.

The total amount of contaminant for Configuration 2 is given by

$$mass_{2,(0)} = V_e c_{2(0)} . \qquad (4.110)$$

Equation 4.19 shows changing the amount of carbon in the system will change V_e, while V_1 is independent of carbon-loading. Increasing the amount of carbon in Configuration 2 therefore increases the total mass of contaminant initially present. Decreasing ν increases $mass_{2,(0)}$.

The amount of contaminant lost from the system is proportional to the area under the c_1 curve given by Equation 4.99

$$loss_{2,0} \equiv V_1 \int_0^{\tau^*} c_1 d\tau \qquad (4.111)$$

Dividing this value by the total mass initially present, Equation 4.110, gives

$$\%loss_{2,0,total} \equiv \nu \frac{\int_0^{\tau^*} c_1 d\tau}{c_{2(0)}} \qquad (4.112)$$

Where $\%loss_{2,0,total}$ gives the percentage of contaminant initially present that will escape from the system. The upper limit of integration for Equations 4.111 and 4.112 is τ^* because c_1 is always zero when $\tau \geq \tau^*$. Physically, this means contaminant escapes the system only when $\tau < \tau^*$, leading to much lower percentages of initial contaminant that escapes, shown in Figure 4.21.

4.5 Summary

Using 1,2,4-TCB as a surrogate for PCBs, experiments show that loading a PVA barrier membrane with PAC will significantly increase contaminant time to breakthrough. Flow-through cell testing shows the Langmuir behavior of the contaminant/PAC system allows for variations in upstream concentration. PAC loaded barrier membranes can adsorb contaminant when solution concentrations are high, and desorb contaminant when solution concentrations are low.

Release of contaminant from a PAC loaded barrier membrane can be modeled as a moving reactive front. The concentration rise in an adjacent volume of solution will go with the square root of time, and has been demonstrated for different PAC loadings. For long rise times, the solution concentration will plateau as it equilibrates with the PAC in the barrier.

Modeling of a volume containing a microorganism capable of degrading contaminant can be approximated as a first-order or zero-order reaction. When paired with a well-mixed carbon containing volume, the amount of contaminant escaping the system can be calculated. Two key parameters determine the quantity of contaminant that escapes and how quickly it does so: an apparent Damköhler number D_M which depends on the rate of reaction and mass transfer, and the volume ratio ν which depends on the amount of carbon. A larger value of D_M results in more contaminant degradation due to the reaction occurring more readily than mass transfer out of the compartment.

A reactive volume described by a first-order reaction will degrade more contaminant when the reaction occurs upstream of a carbon loaded barrier. This is due to the reaction rate being higher at high concentrations. When a loaded carbon containing barrier is upstream of the reaction, the resulting lower concentration of contaminant leads to less degradation. Any contaminant escaping the reactive volume will eventually leach out of the system. The flux of this release is greatly diminished by increasing the amount of carbon present in the barrier. When designing a reactive system along with a barrier membrane, the reactive volume should be placed upstream of the barrier to minimize the quantity and rate of leakage.

A zero-order reaction is independent of contaminant concentration. As the reaction rate increases, or mass transfer slows, contaminant concentration in the reactive volume falls faster than for a first-order reaction, eventually going to zero. Contaminant that has already escaped to the carbon containing barrier may now transfer back to the reactive volume, resulting in a decreased quantity of contaminant ultimately leaving the system. A loaded carbon containing barrier upstream of the reaction will lead to a further decreases in contaminant escape.

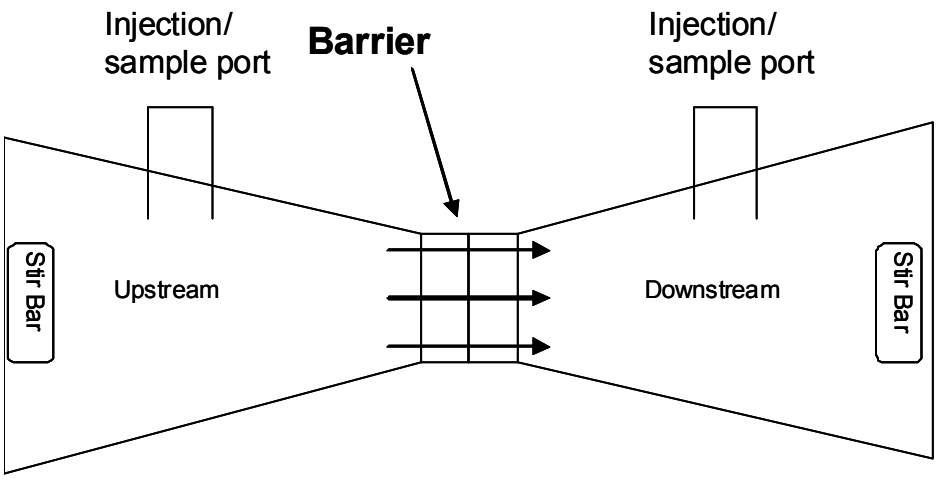

Figure 4.1: Diffusion cell apparatus used to measure contaminant concentrations in breakthrough experiments. Both volumes are well-stirred with a barrier membrane placed between.

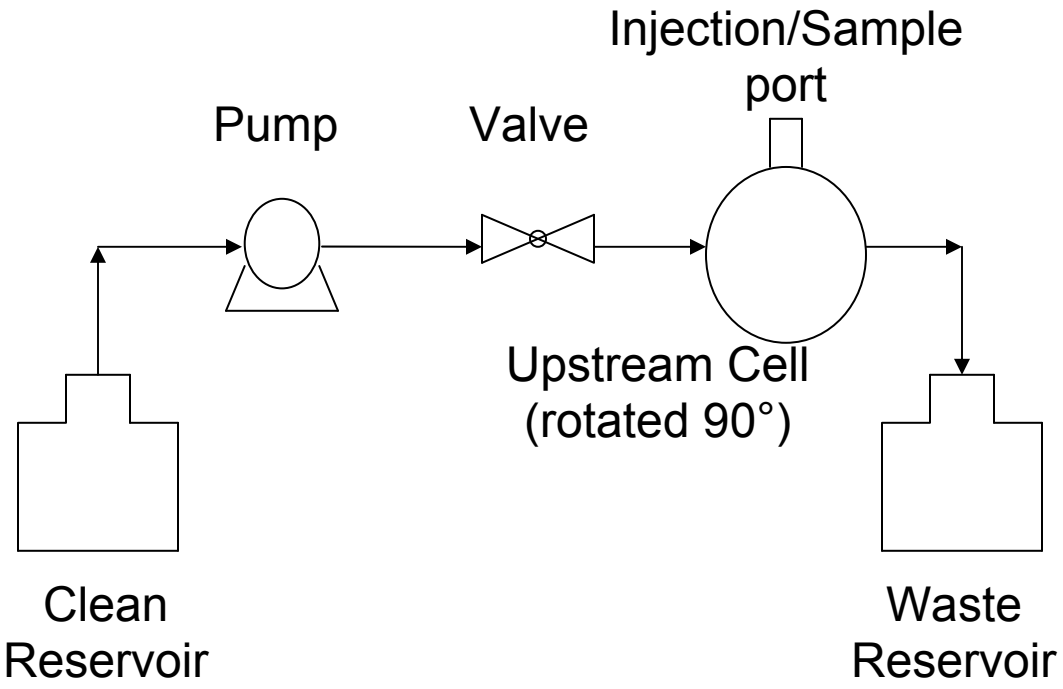

Figure 4.2: Diffusion cell setup for flow-through experiments. The direction of fluid flow is shown by the arrows. The diffusion cell, shown rotated by 90° is setup similarly to that shown in Figure 4.1.

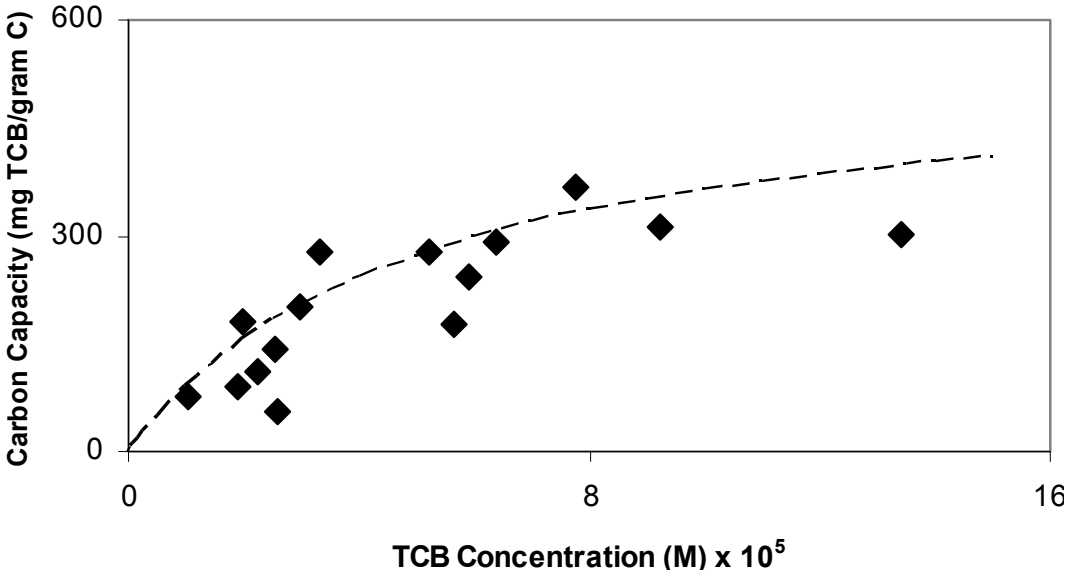

Figure 4.3: Fit of Langmuir isotherm (dashed line) for 1,2,4-TCB/PAC system. The Langmuir isotherm captures the shoulder of the isotherm. Maximum 1,2,4-TCB capacity of PAC is 540 mg 1,2,4-TCB/gram PAC.

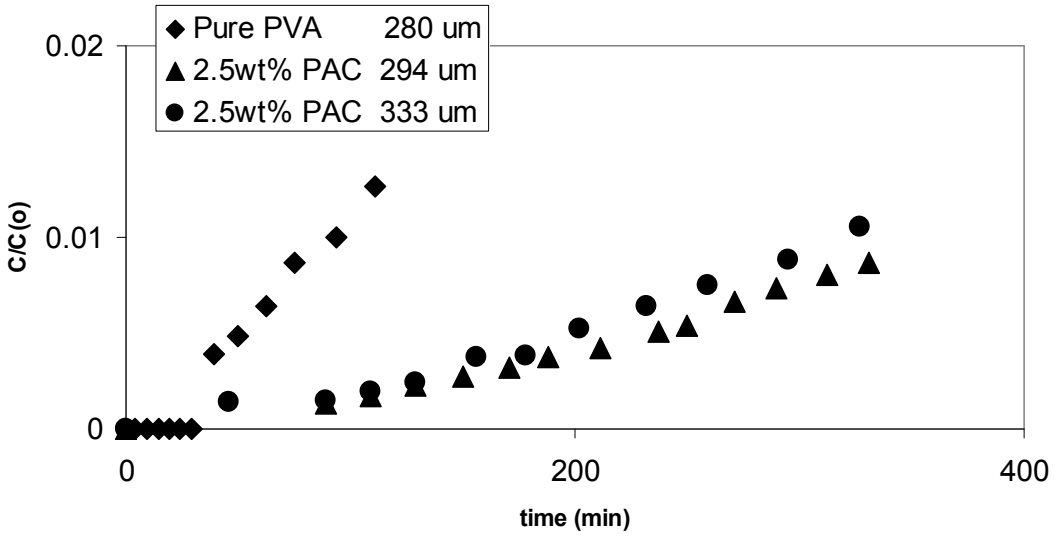

Figure 4.4: Addition of PAC to PVA barrier membranes increases the breakthrough time for 1,2,4-TCB. Lag times for 2.5wt% PAC in PVA are over 85 minutes; pure PVA lag times are too fast to measure.

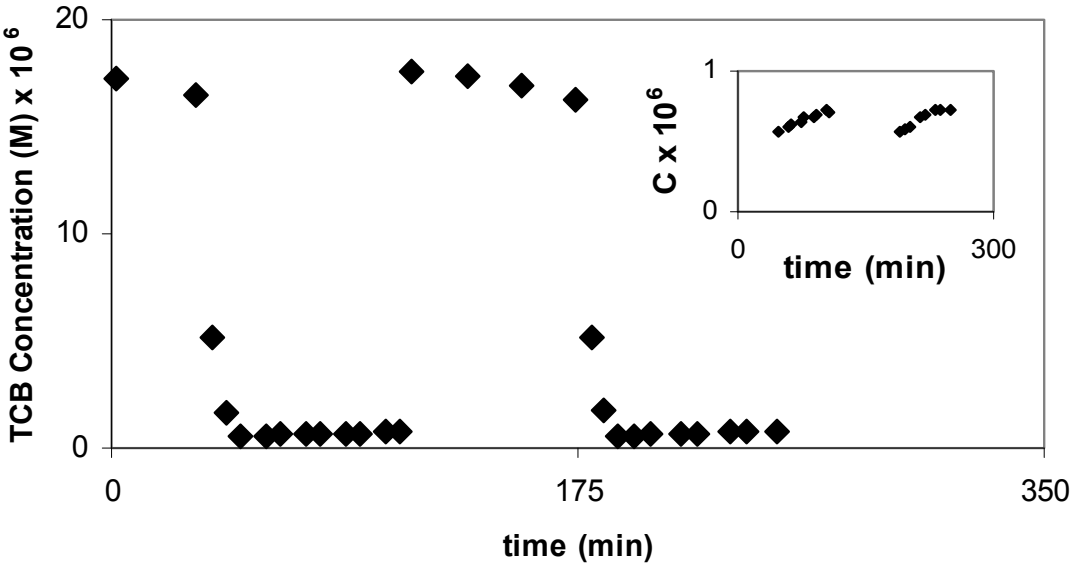

Figure 4.5: Upstream concentration of 1,2,4-TCB in a flow-through cell. Initially, the upstream concentration is 10 times greater than that in the downstream cell; contaminant moves from upstream to downstream. After flowing contaminant free water into the cell, the upstream concentration falls below that in the downstream. Contaminant moves from the downstream cell to the upstream cell. Additional contaminant is injected, and the procedure is repeated. The inset expands the regions of concentration rise after the pump has been turned off.

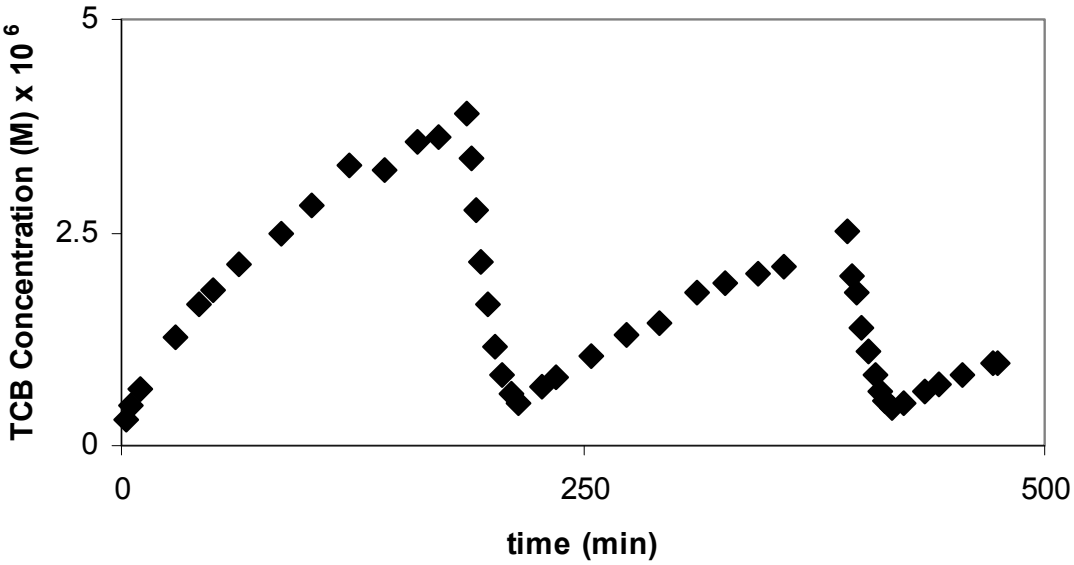

Figure 4.6: 1,2,4-TCB concentration profile in a flow-through diffusion cell from a preloaded barrier membrane containing 2.5wt% PAC. After some time, a pump flows contaminant free solution into the cell, flushing out existing solution, reducing 1,2,4-TCB concentration. The flux of 1,2,4-TCB from the barrier membrane reduces with time.

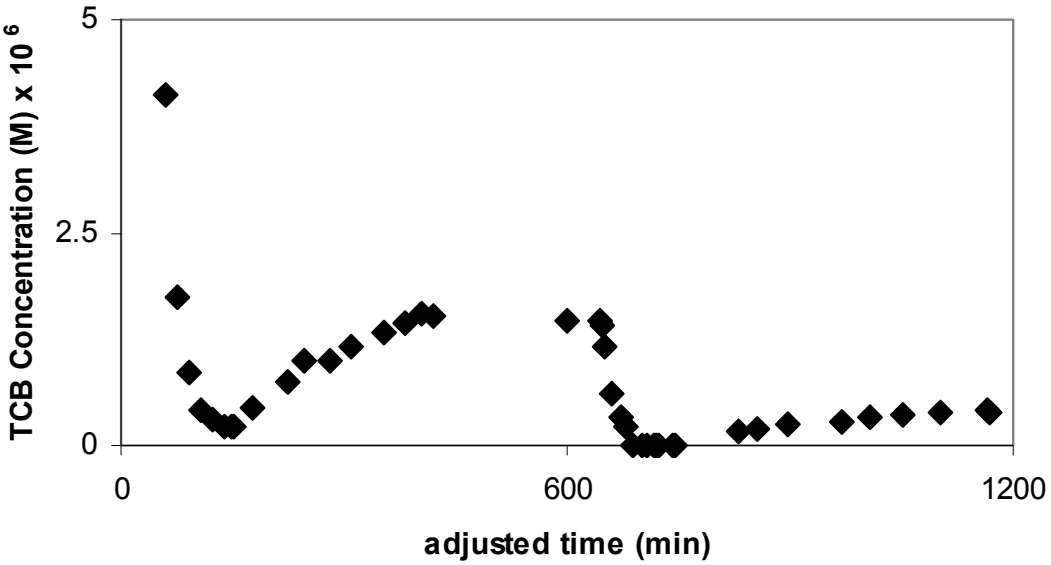

Figure 4.7: 1,2,4-TCB concentration profile in a flow-through diffusion cell from a barrier membrane containing 1.25wt% PAC. Initially, there is no 1,2,4-TCB in the barrier membrane, it is loaded within the cell. After loading, a pump flows contaminant free solution into the cell, flushing out existing solution, reducing 1,2,4-TCB concentration. After ~7.5 hours, the membrane and solution are in equilibrium. The flux of 1,2,4-TCB from the barrier membrane reduces with time.

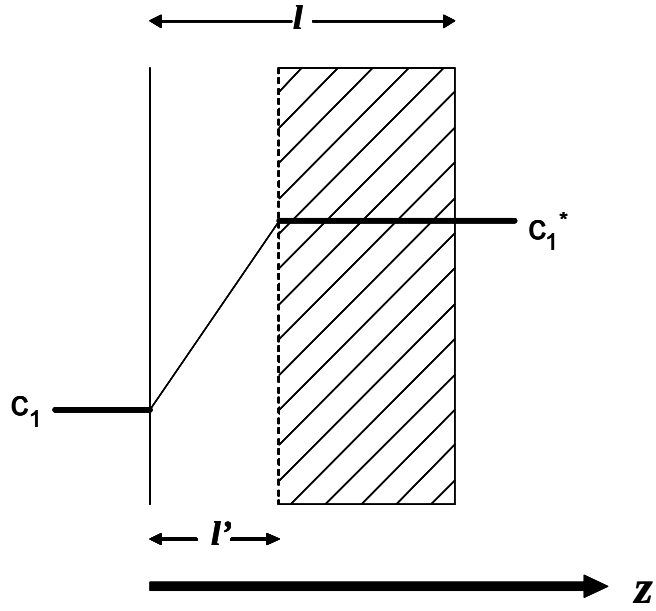

Figure 4.8: Concentration profile for a moving front of a barrier membrane with thickness *l*. The shaded region represents a region with loaded PAC, while the region of thickness *l'* is unloaded. c_1^* represents the effective concentration on PAC, c_1 is the concentration in solution. For this analysis, the partition coefficient, *H*, is assumed to be 1.

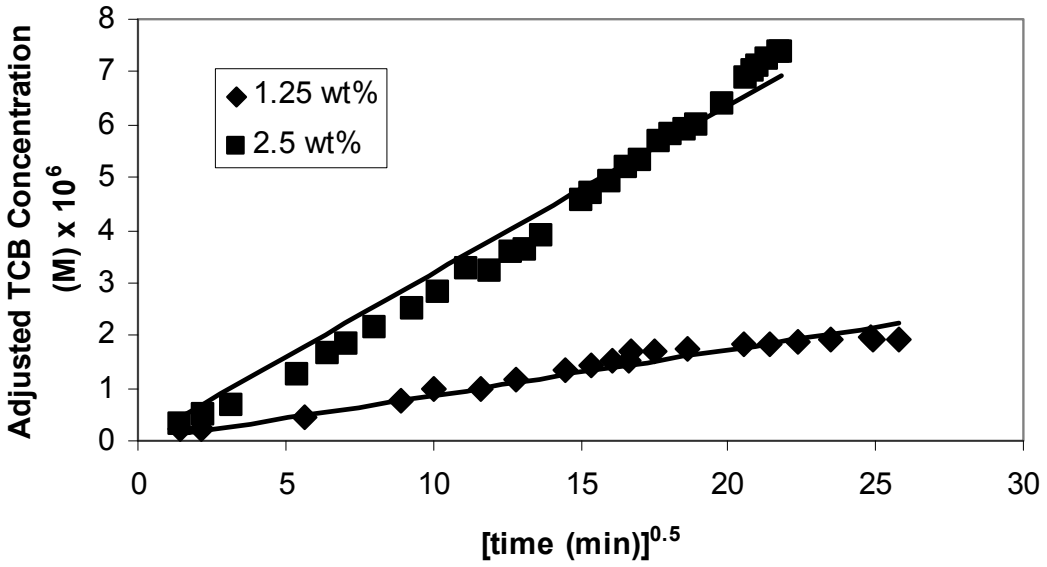

Figure 4.9: Adjusted 1,2,4-TCB concentration increases linearly with the square root of time, as described by Equation 4.14. The data result from the summation of all contaminant desorbed over multiple cycles from the experiments shown in Figures 4.6 and 4.7.

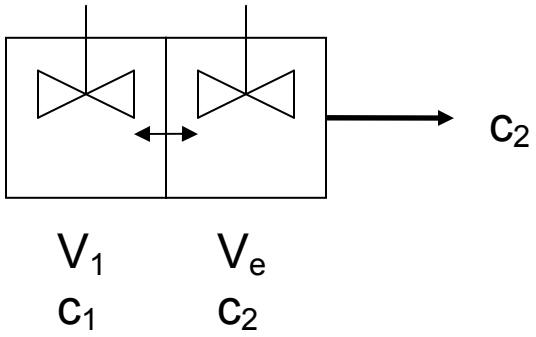

Figure 4.10: Configuration 1. Model system where a first-order reaction takes place in V_1 and carbon is contained in V_e. Both volumes are assumed to be well-mixed.

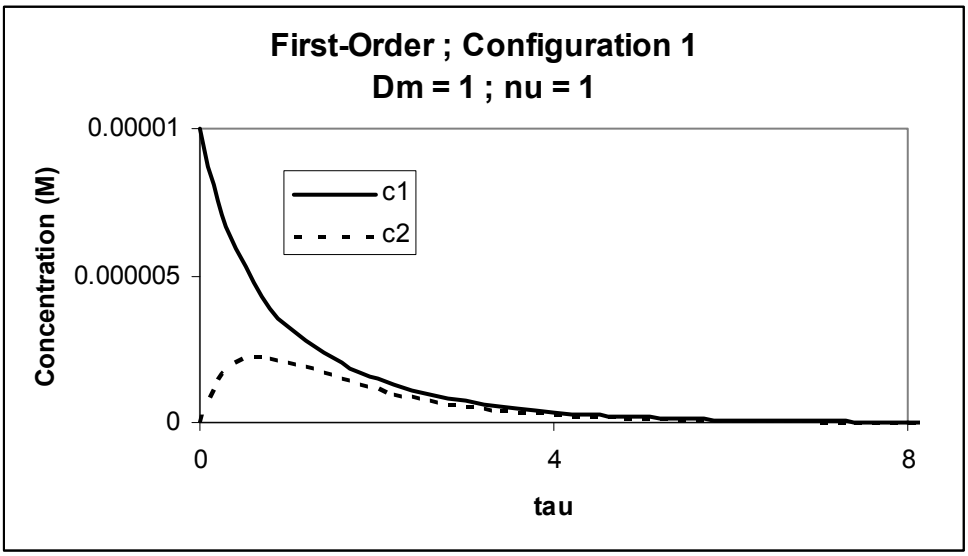

(a)

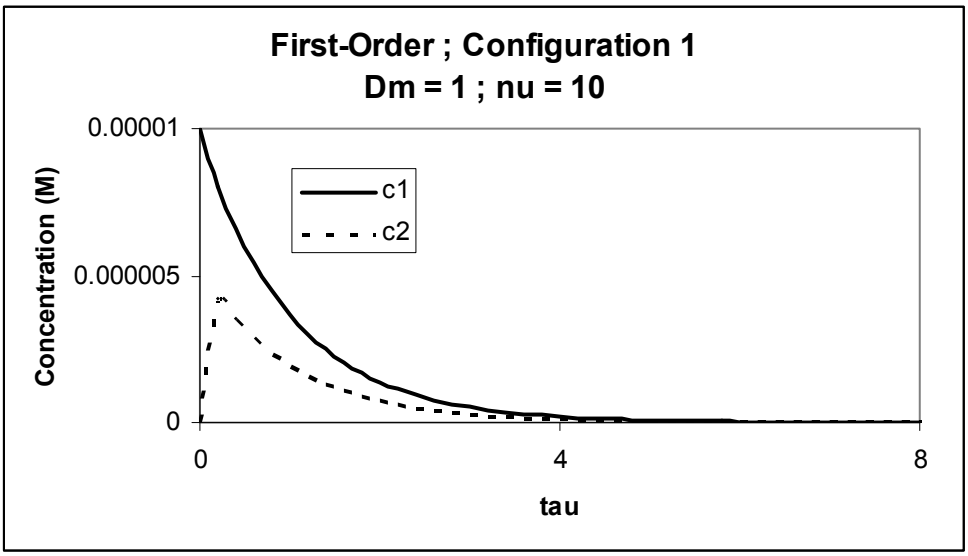

(b)

Figure 4.11: Plots of expected concentrations vs. dimensionless time for the system in Figure 4.10 with a first-order reaction. c_1 is shown with a solid line, c_2 is shown with a dashed line. There is ten times more carbon in (a) and (c) than (b) and (d). The reaction is ten times faster in (c) and (d) than (a) and (b). For a given value of D_M, the area under the c_2 curve, which is proportional to the mass released from the system, is constant regardless of ν, but the time for release increases as more carbon is added.

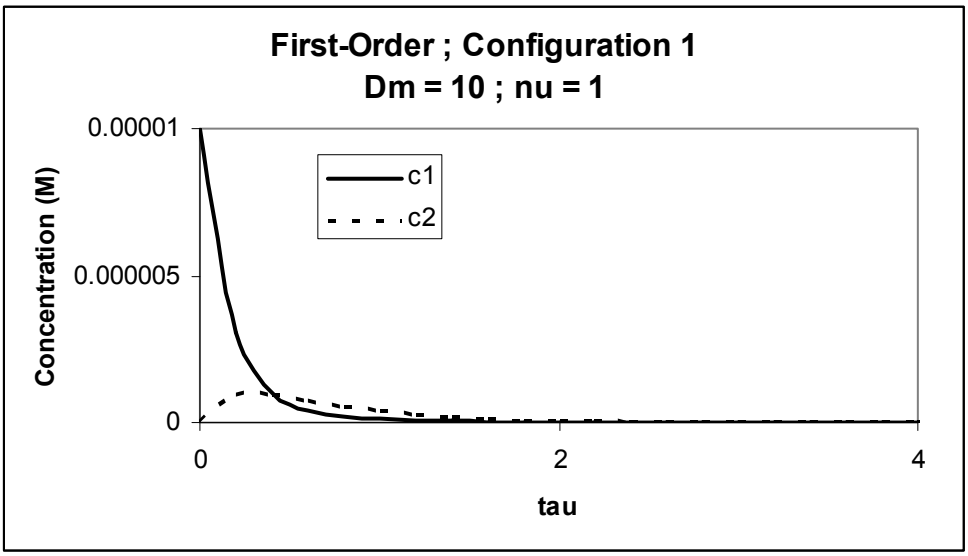

(c)

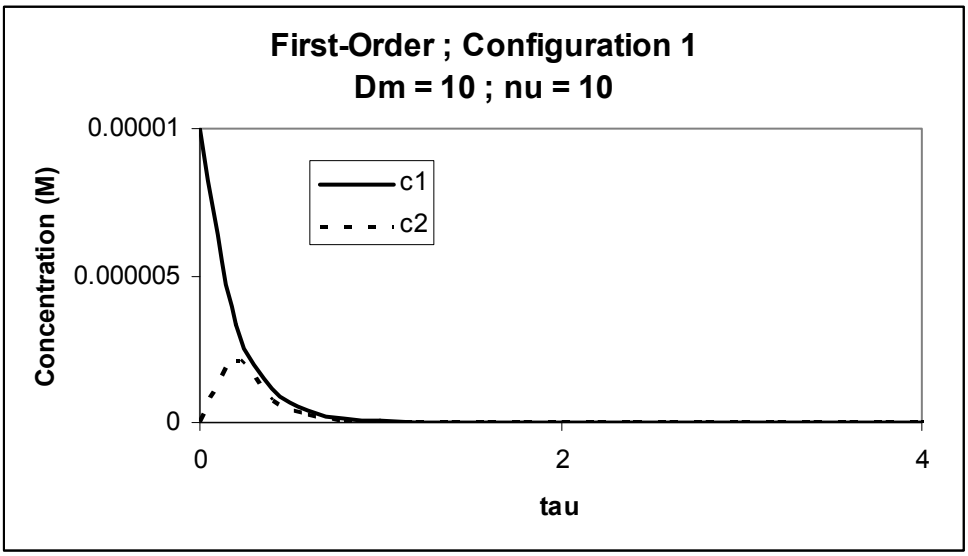

(d)

Figure 4.11 continued (page 2 of 2)

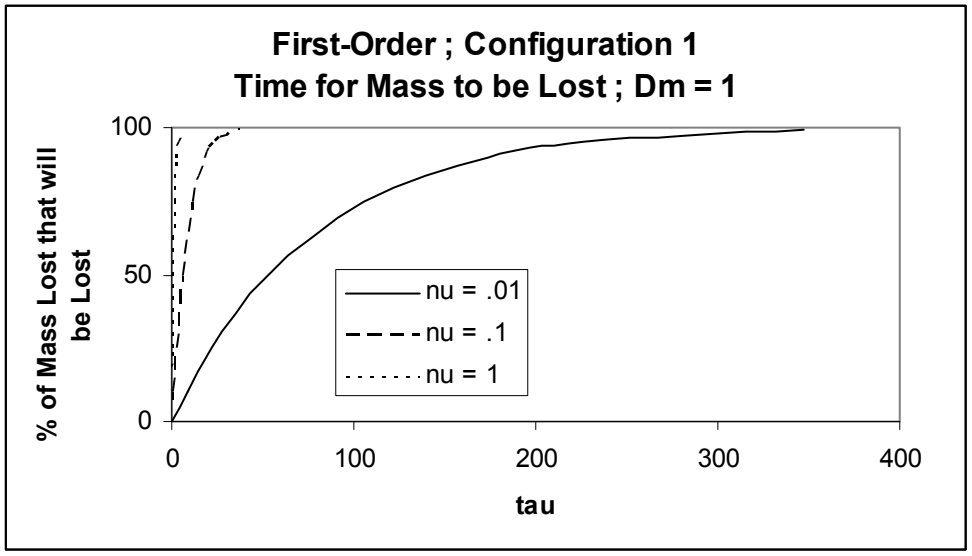

(a)

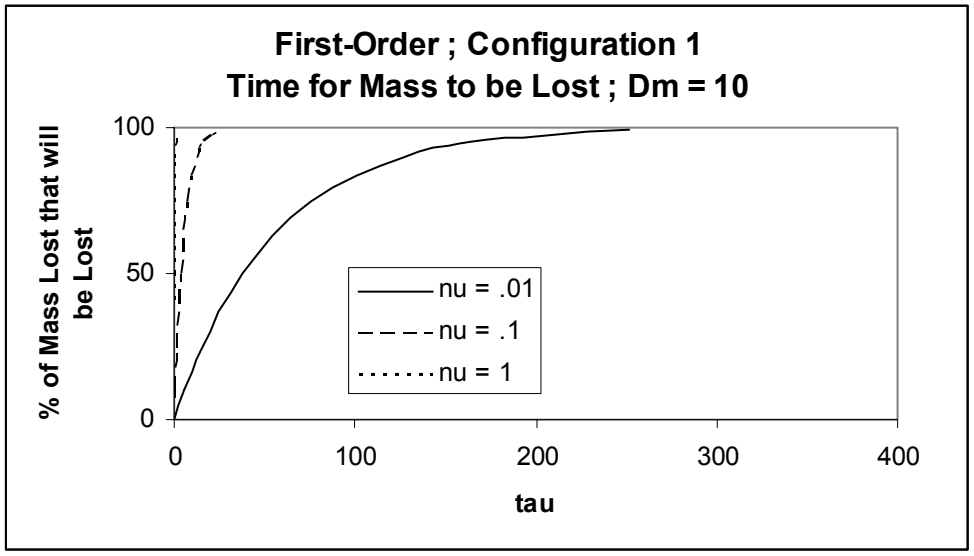

(b)

Figure 4.12: Plots showing the characteristic time it takes for mass to be lost from the system shown in Figure 4.10 with a first-order degradation reaction. For a given value of D_M, the amount of mass lost is the same regardless of ν, but the time for release increases with increased carbon loading. The reaction rate is ten times faster in (b) than (a). The mass lost in (a) is more than five times that lost in (b).

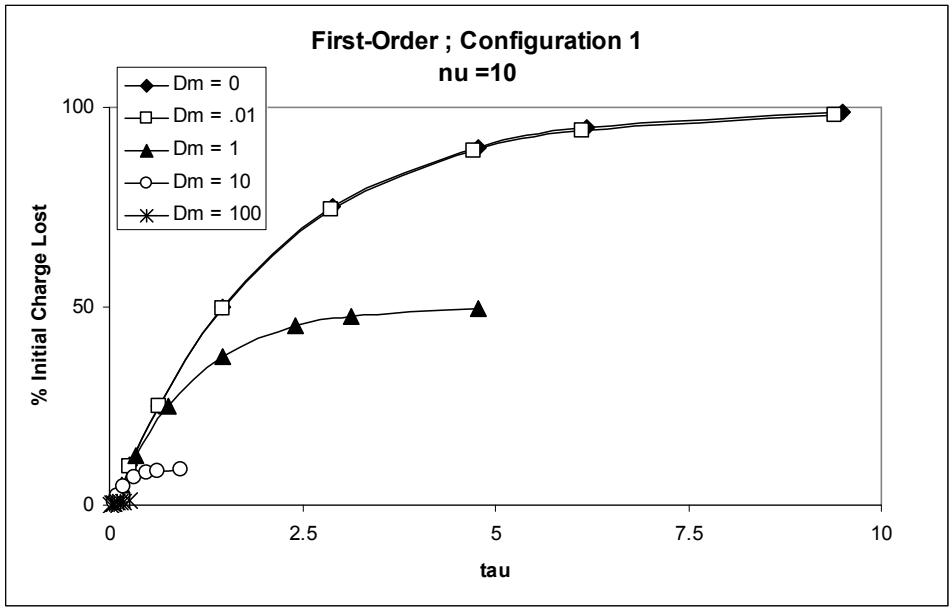

(a)

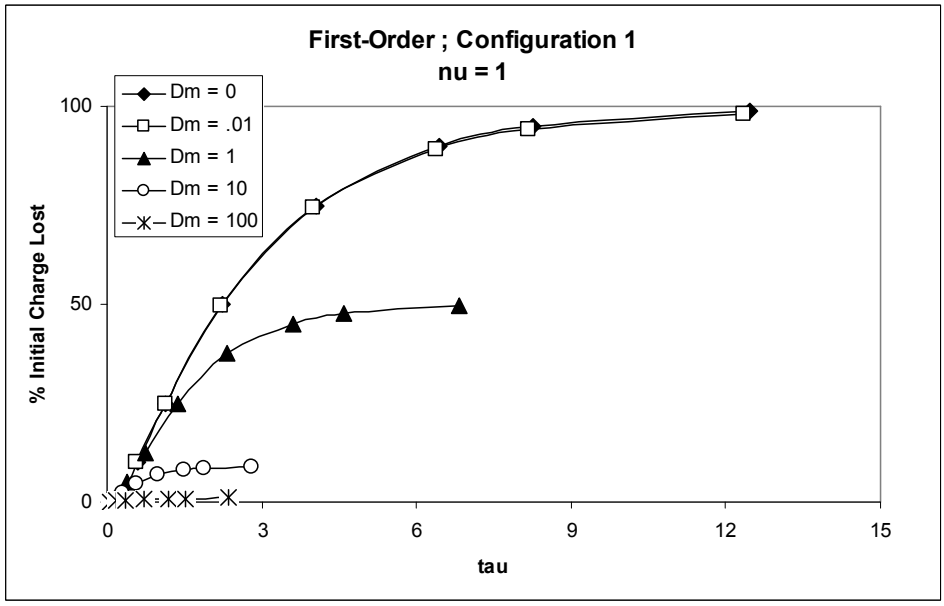

(b)

Figure 4.13: Plots of predicted amount of contaminant lost from the system. Symbols (diamonds, squares, etc) indicate a percentage of mass lost, not experimental data. Each curve has a symbol denoting 10, 25, 50, 75, 90, 95, and 99% of the amount that will escape has escaped. Increasing D_M decreases the amount of contaminant that will escape. Decreasing ν increases the amount of time required for contaminant escape.

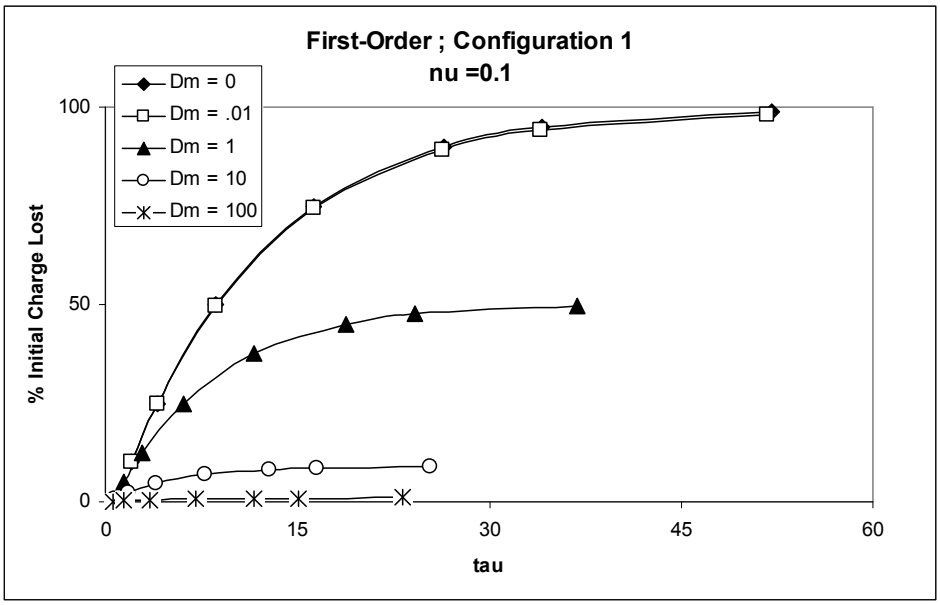

(c)

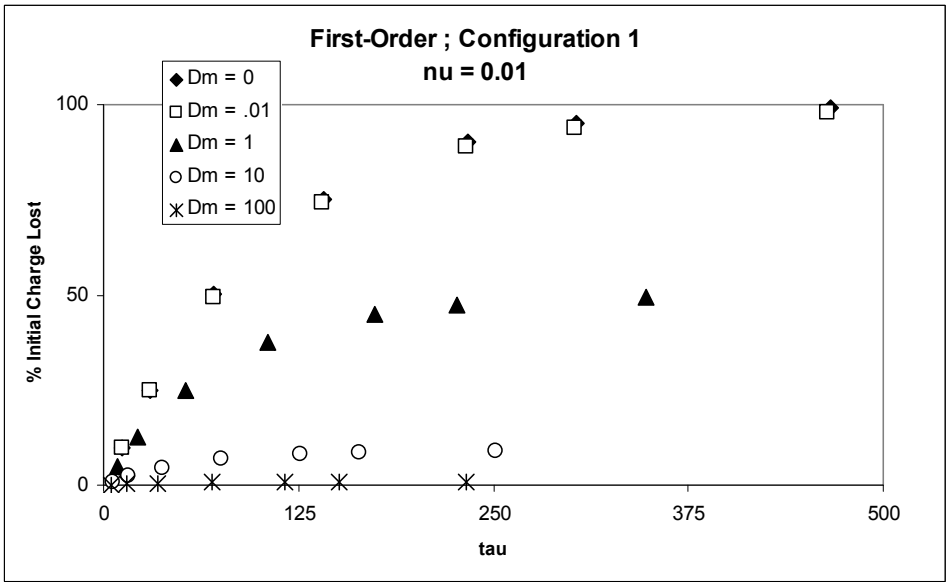

(d)

Figure 4.13 continued (page 2 of 2)

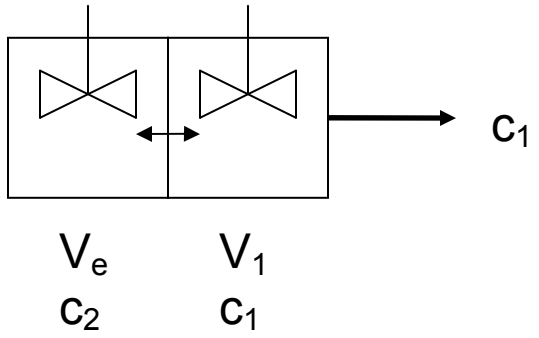

Figure 4.14: Configuration 2. Model system where carbon is contained in V_e, and a first-order reaction takes place in V_1. Both volumes are assumed to be well-mixed.

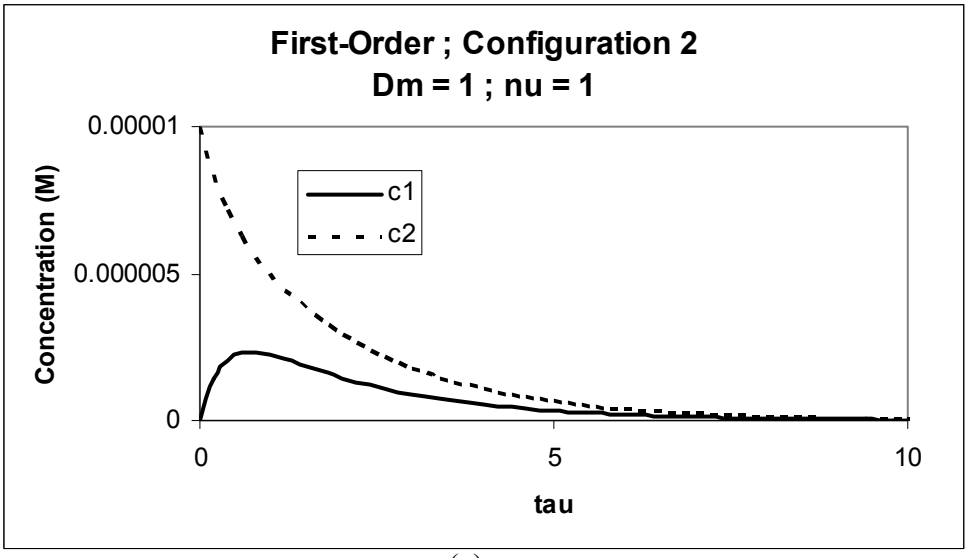

(a)

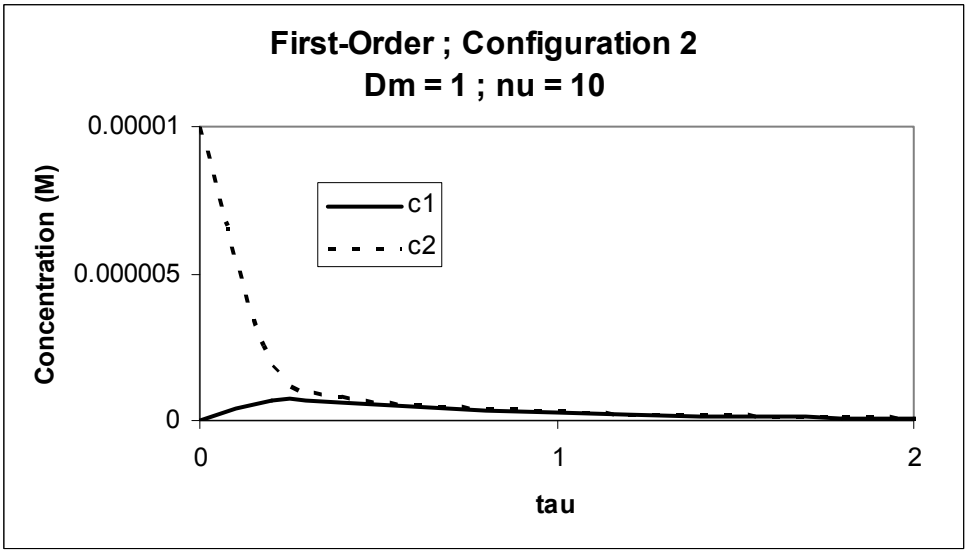

(b)

Figure 4.15: Plots of expected concentrations vs. dimensionless time for the system in Figure 4.14 with a first-order reaction. c_1 is shown with a solid line, c_2 is shown with a dashed line. There is ten times more carbon in (a) and (c) than (b) and (d). The reaction is ten times faster in (c) and (d) than (a) and (b). For a given value of D_M, the area under the c_2 curve, which is proportional to the mass released from the system, is constant regardless of ν, but the time for release increases as more carbon is added.

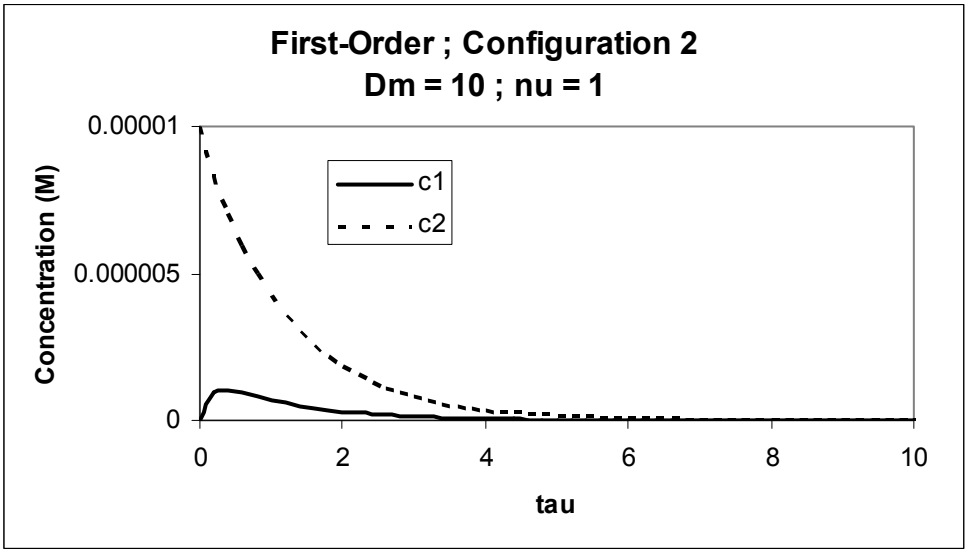

(c)

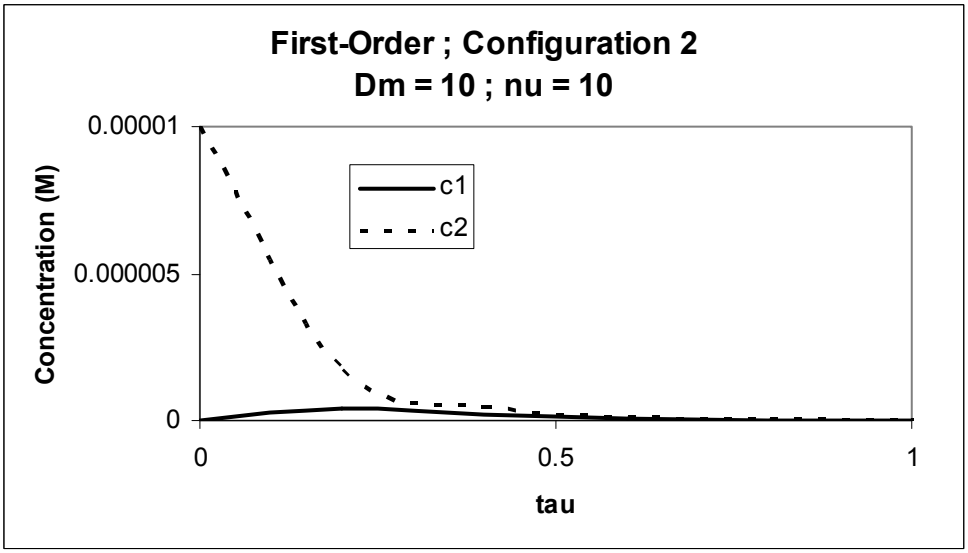

(d)

Figure 4.15 continued (page 2 of 2)

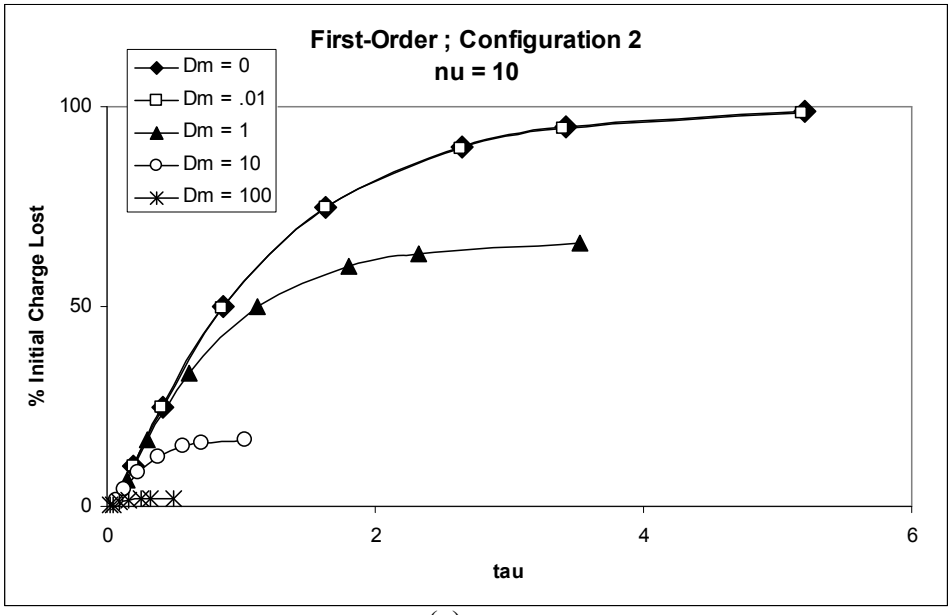

(a)

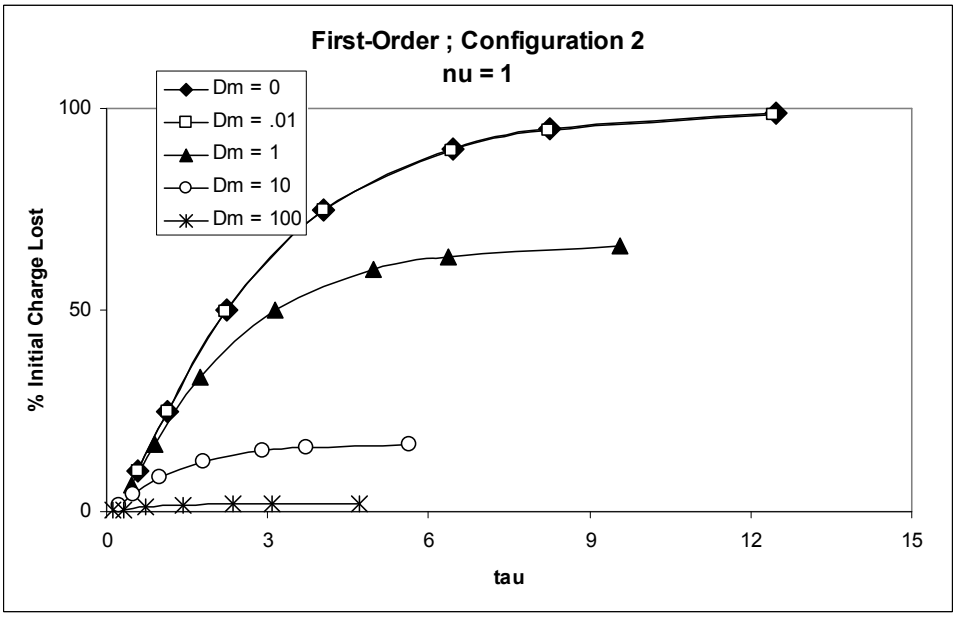

(b)

Figure 4.16: Plots of predicted amount of contaminant lost from the system. Symbols (diamonds, squares, etc) indicate a percentage of mass lost, not experimental data. Each curve has a symbol denoting 10, 25, 50, 75, 90, 95, and 99% of the amount that will escape has escaped. Increasing D_M decreases the amount of contaminant that will escape. For a given D_M the same percentage of initial contaminant will escape for each value of ν. A larger percentage of initial contaminant escapes in Configuration 2 than in Configuration 1 for the same D_M.

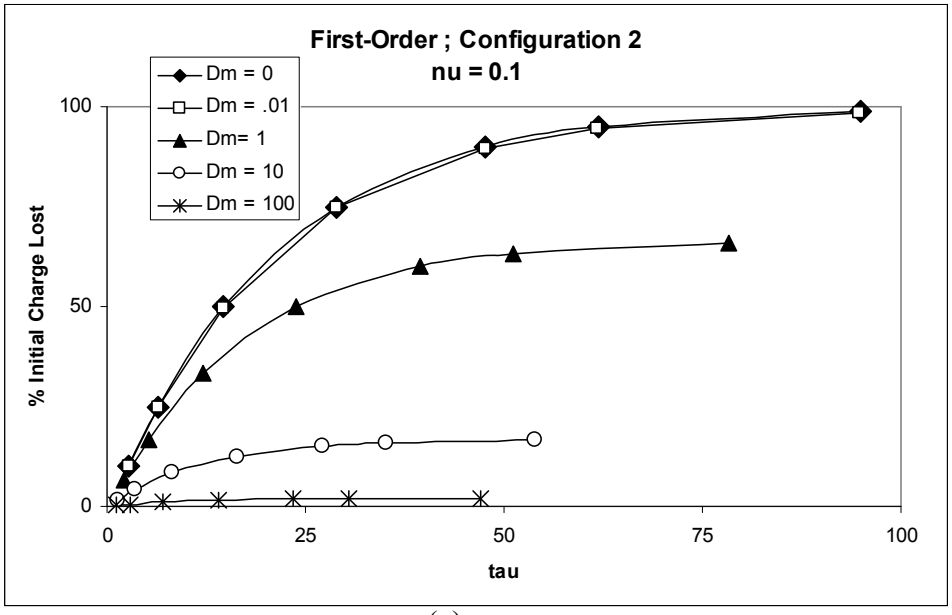

(c)

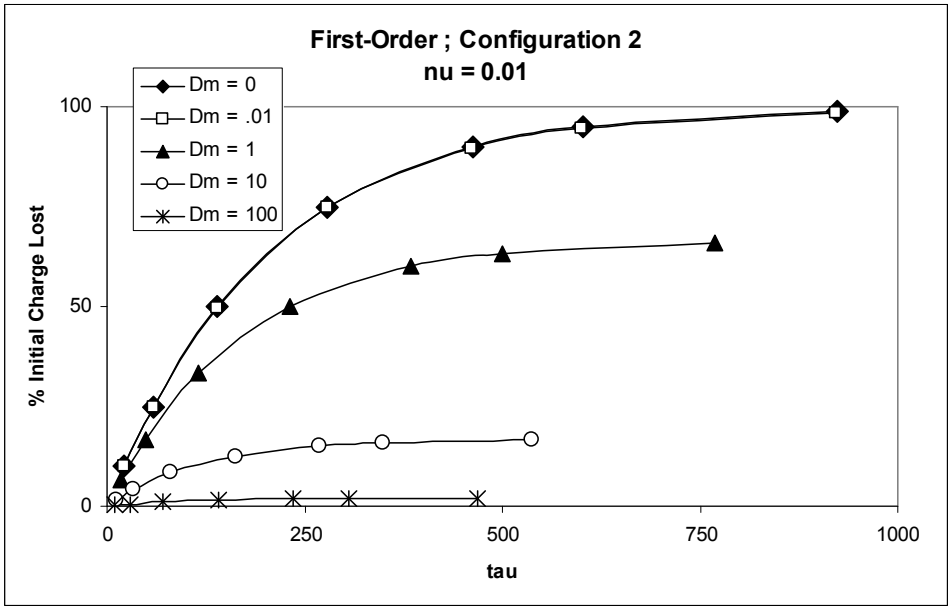

(d)

Figure 4.16 continued (page 2 of 2)

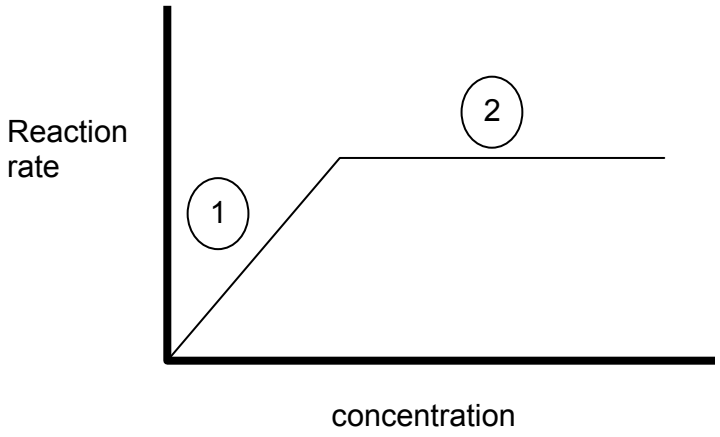

Figure 4.17: Generalized drawing showing the dependence of reaction rate on concentration. In region 1, reaction rate is proportional to concentration (first-order). In region 2, reaction rate is independent of concentration (zero-order).

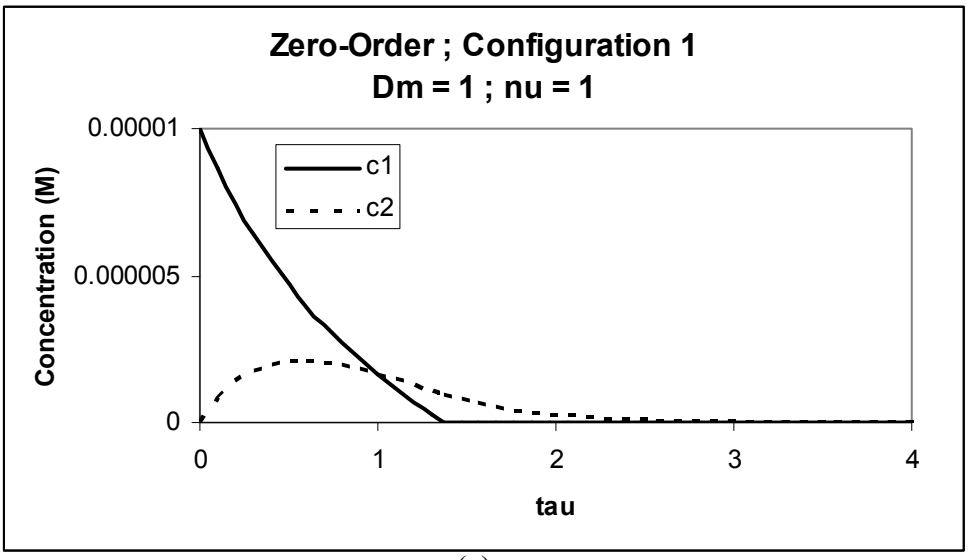

(a)

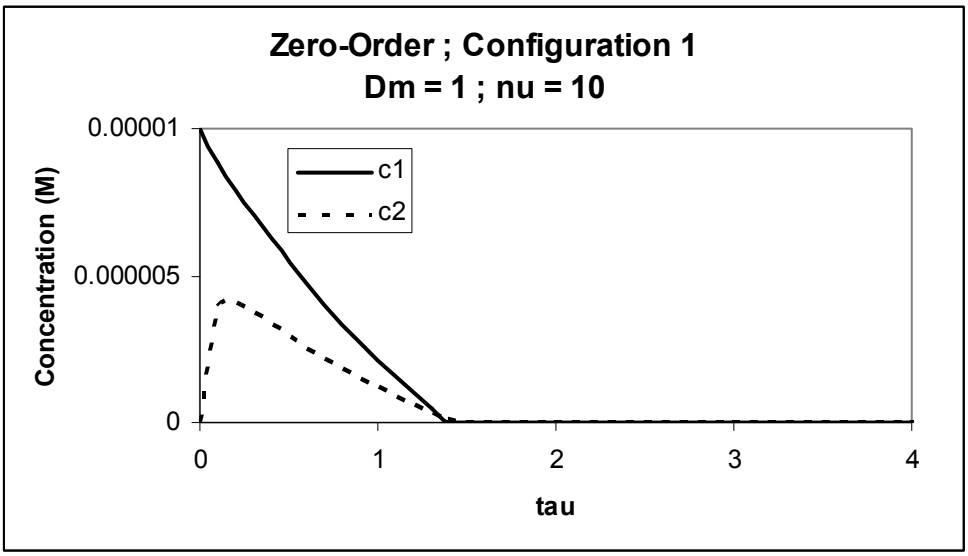

(b)

Figure 4.18: Plots of expected concentrations vs. dimensionless time for the system in Figure 4.10 with a zero-order reaction. c_1 is shown with a solid line, c_2 is shown with a dashed line. There is ten times more carbon in (a) and (c) than (b) and (d). The reaction is ten times faster in (c) and (d) than (a) and (b). Increasing the carbon-loading results in a decrease in the maximum c_2 concentration for a given value of D_M, and increases the amount of time required for all contaminant that will escape to do so.

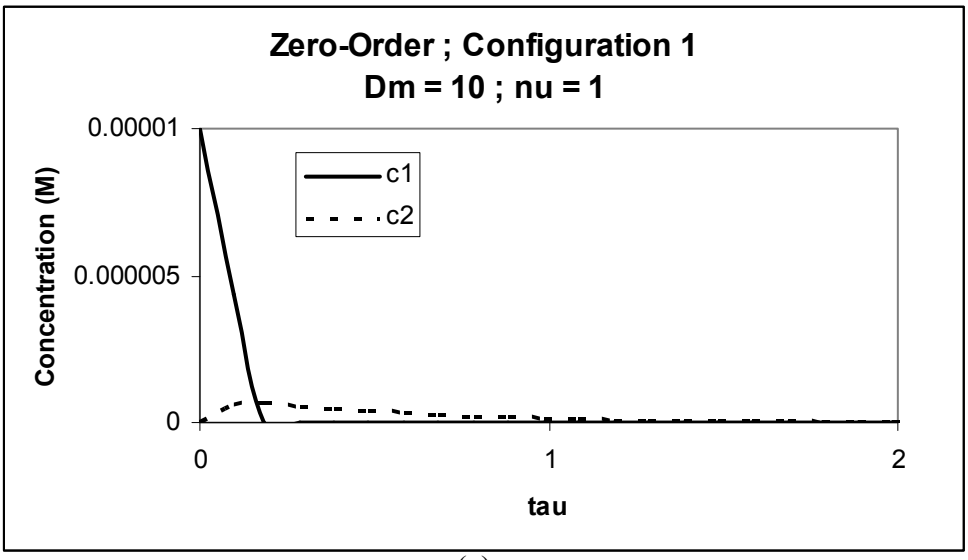

(c)

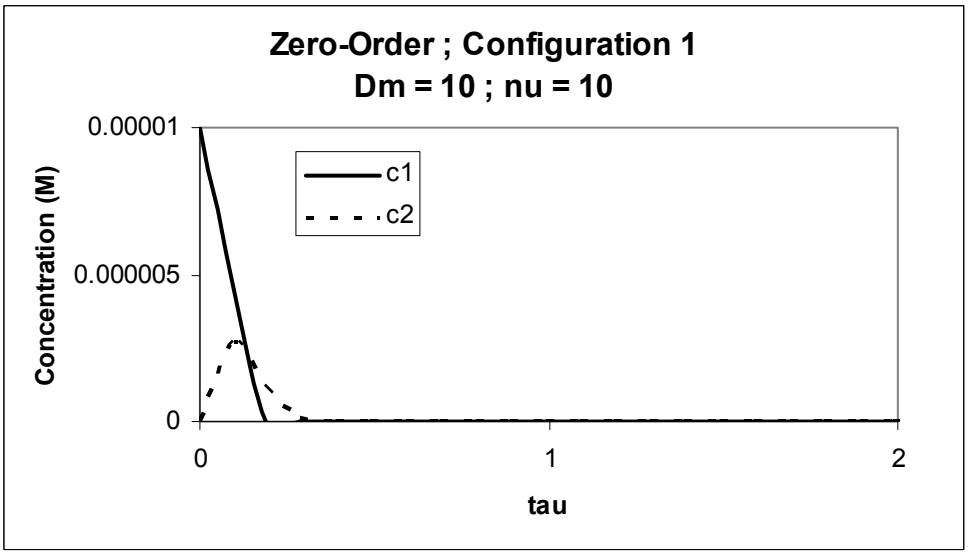

(d)

Figure 4.18 continued (page 2 of 2)

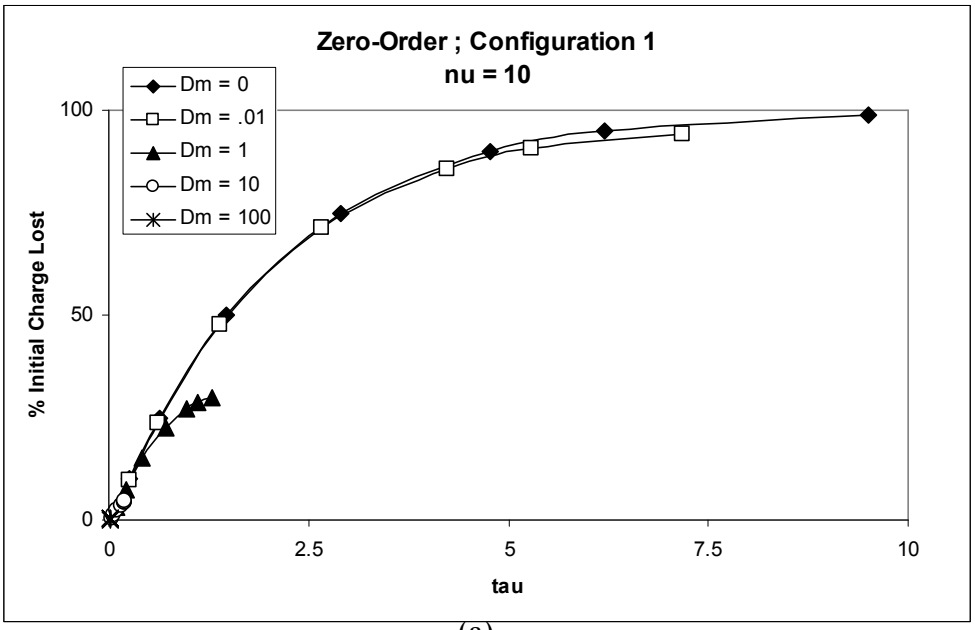

(a)

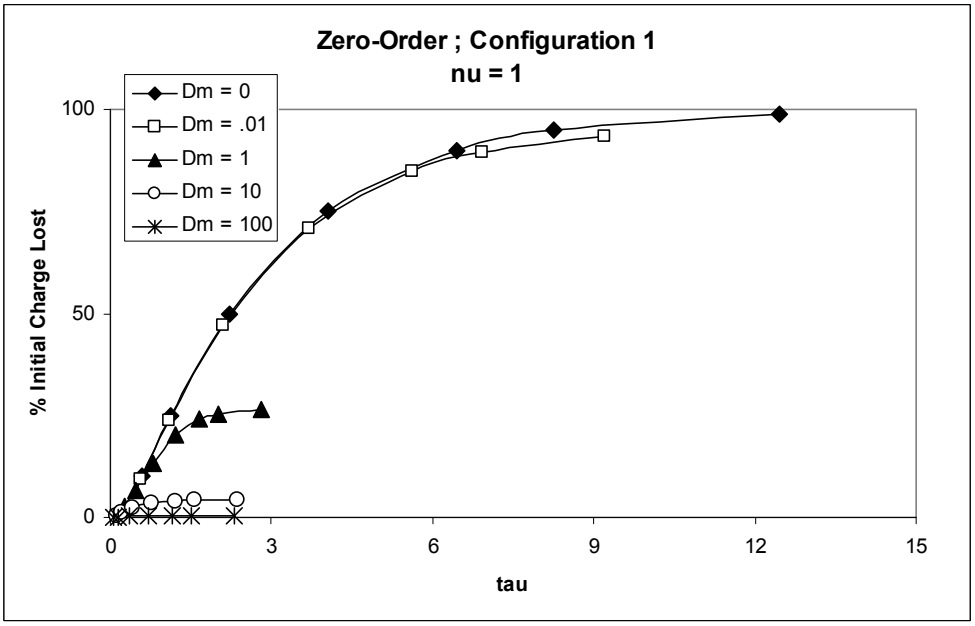

(b)

Figure 4.19: Plots of predicted amount of contaminant lost from the system. Symbols (diamonds, squares, etc) indicate a percentage of mass lost, not experimental data. Each curve has a symbol denoting 10, 25, 50, 75, 90, 95, and 99% of the amount that will escape has escaped. Increasing D_M decreases the amount of contaminant that will escape. For a given D_M, the percentage of initial contaminant that will escape decreases when ν is decreased. Decreasing ν decreases the flux from the system, increasing the time required for release.

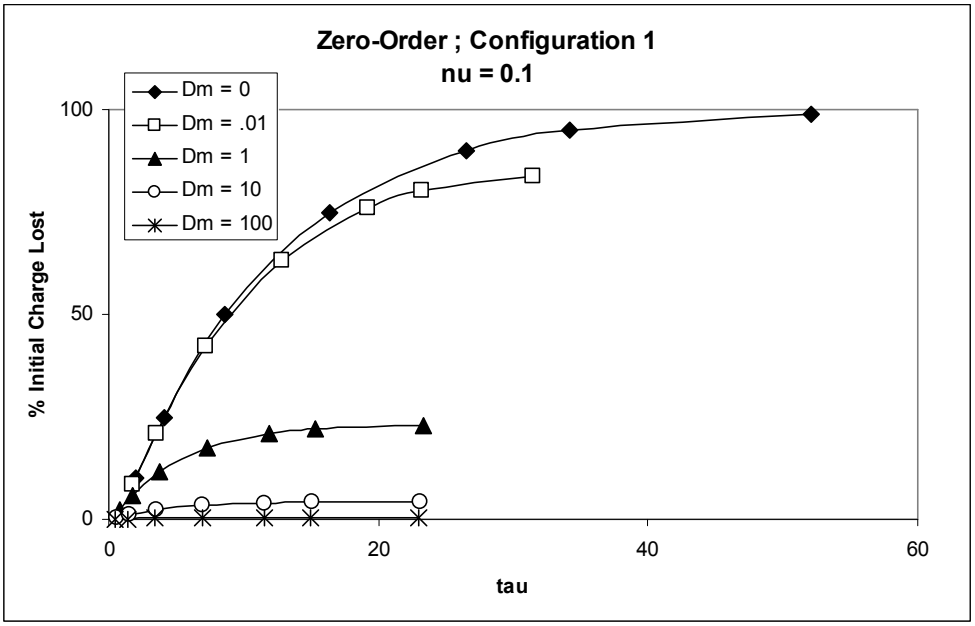

(c)

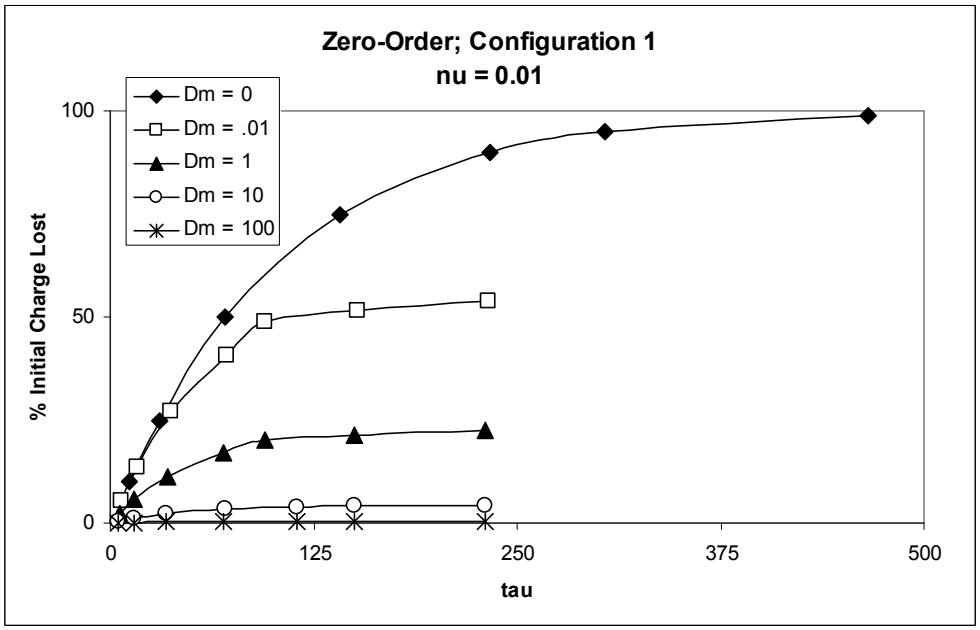

(d)

Figure 4.19 continued (page 2 of 2)

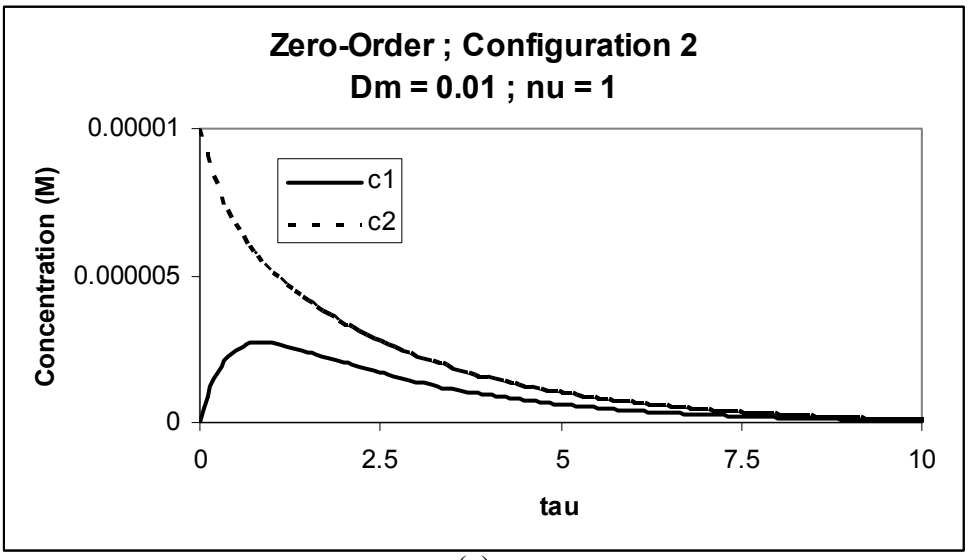

(a)

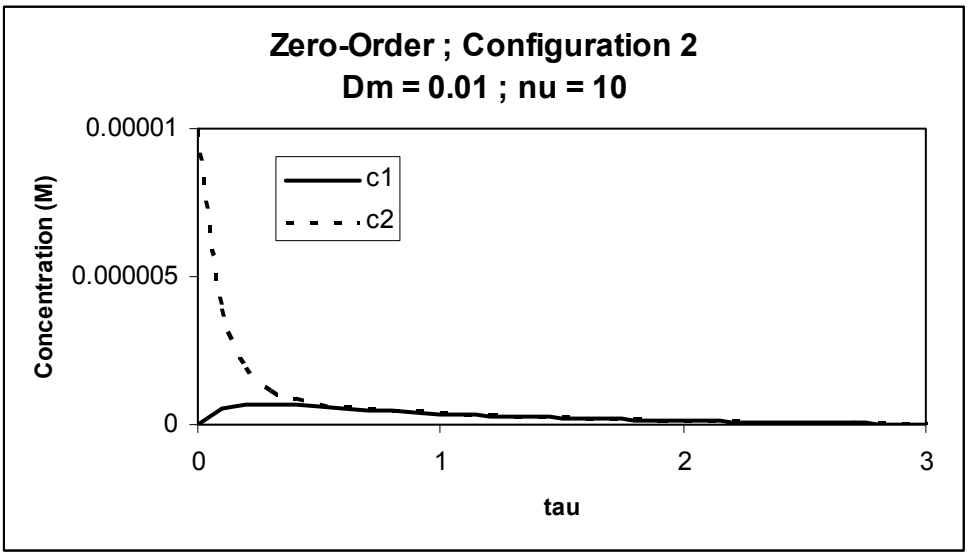

(b)

Figure 4.20: Plots of expected concentrations vs. dimensionless time for the system in Figure 4.14 with a zero-order reaction. c_1 is shown with a solid line, c_2 is shown with a dashed line. There is ten times more carbon in (a) and (c) than (b) and (d). The reaction is 100 times faster in (c) and (d) than (a) and (b). D_M values shown are less than those in previous concentration plots. As $D_M > 1$, the zero-order reaction degrades almost all contaminant entering V_1; c_1 is non-zero for only very small values of τ.

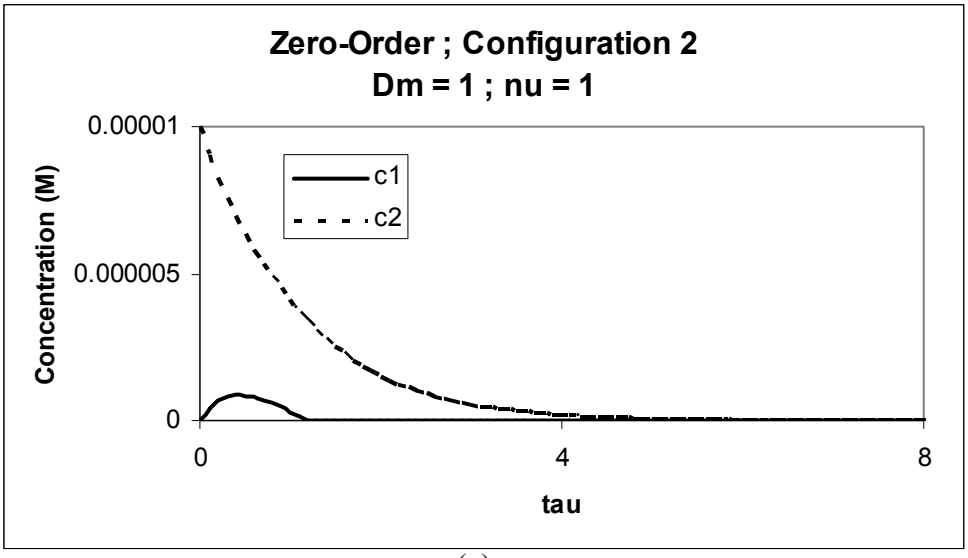

(c)

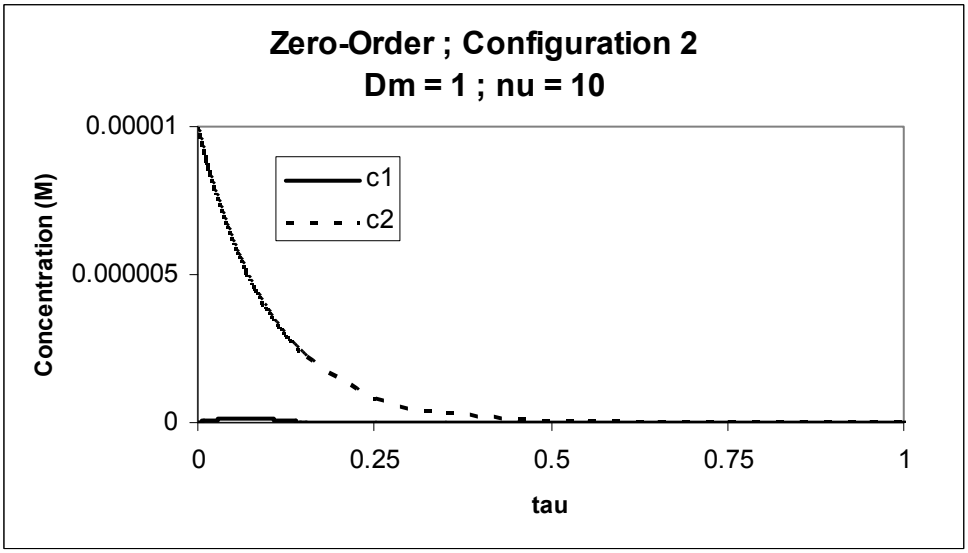

(d)

Figure 4.20 continued (page 2 of 2)

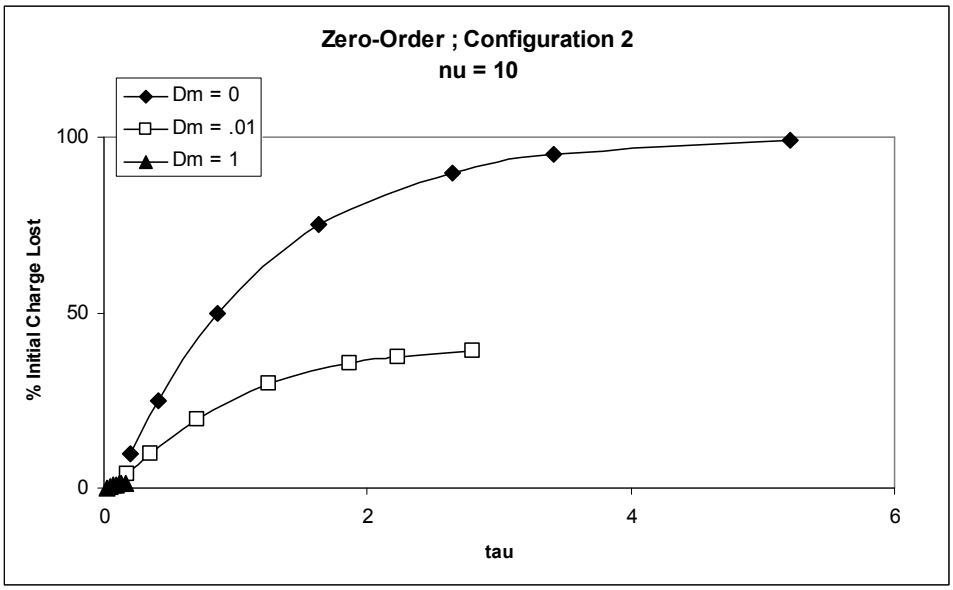

(a)

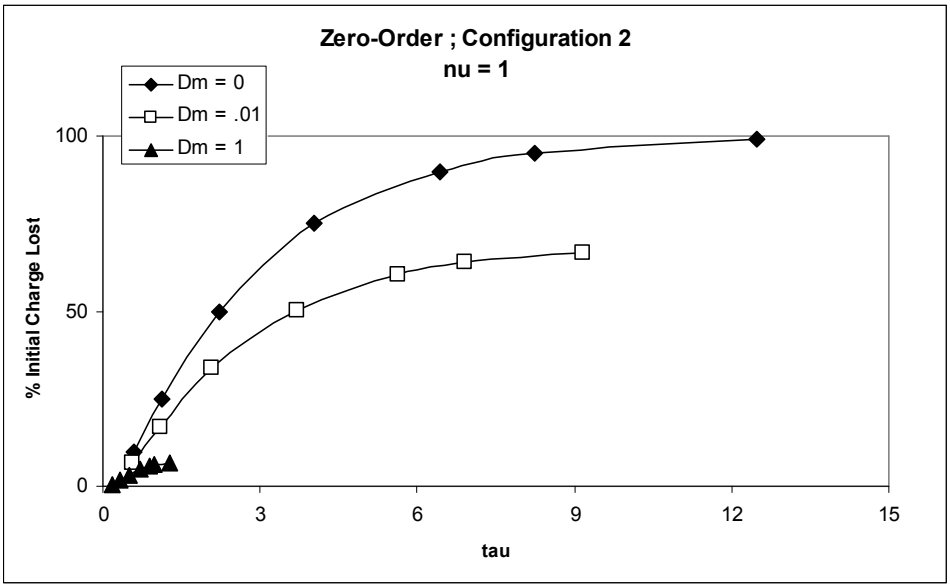

(b)

Figure 4.21: Plots of predicted amount of contaminant lost from the system. Symbols (diamonds, squares, etc) indicate a percentage of mass lost, not experimental data. Each curve has a symbol denoting 10, 25, 50, 75, 90, 95, and 99% of the amount that will escape has escaped. Increasing D_M decreases the amount of contaminant that will escape. For a given D_M, the percentage of initial contaminant that will escape increases when ν is decreased as there is more contaminant in the system. A smaller percentage of contaminant leaves than for any of the other three cases. Dm = 10 and 100 are not shown as no mass leaves the system for the values of ν. The time for release (flux) increases as ν decreases.

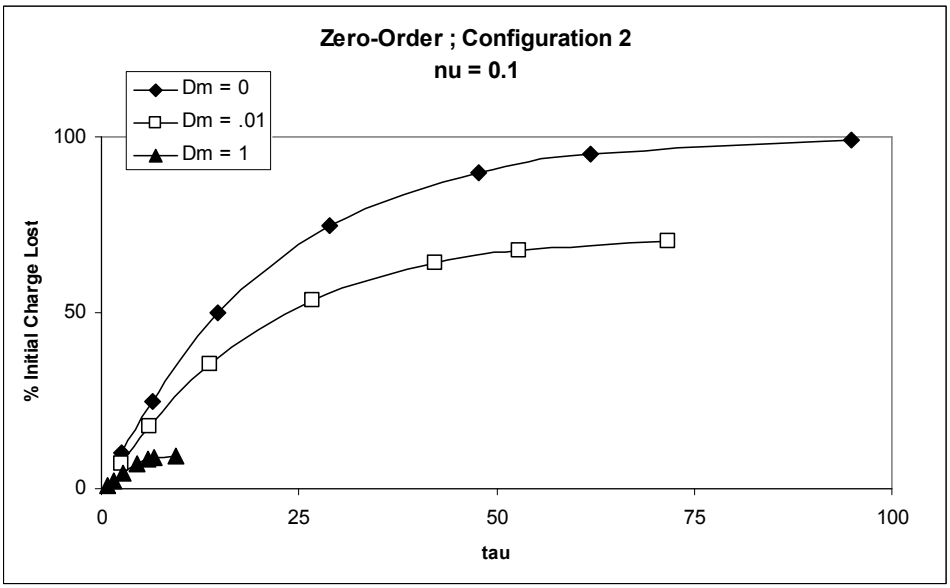

(c)

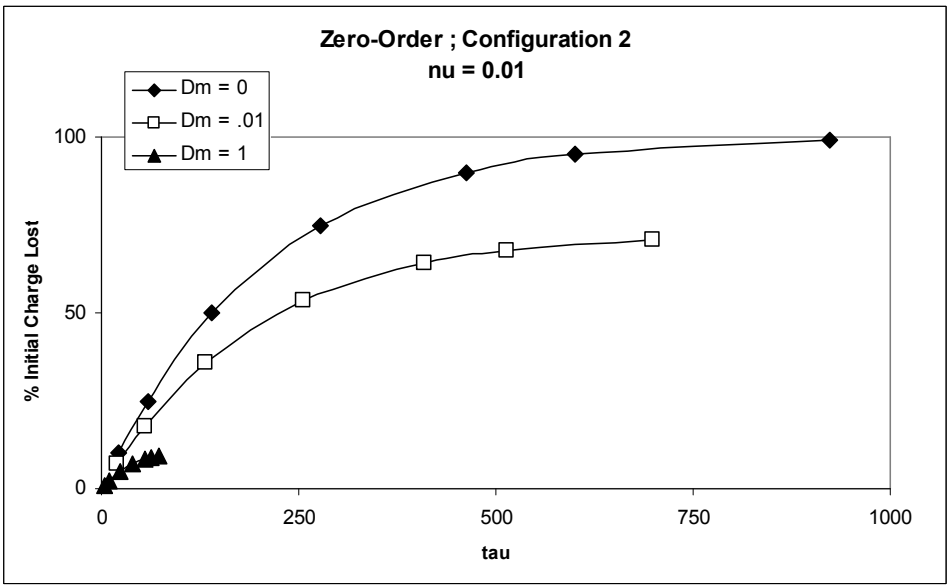

(d)

Figure 4.21 continued (page 2 of 2)

Chapter 5

Conclusions

5.1 Addition of Reactive Groups to Barrier Membranes

The results in the previous chapters have shown the addition of reactive groups to barrier membranes can greatly reduce breakthrough of specific contaminants. Adsorbents that show selectivity for contaminants are good candidates for addition to barrier membranes. The reactive capacity of a barrier membrane will depend on the loading and contaminant capacity of the adsorbent.

Crystalline silicotitanate (CST) has a high selectivity for cesium, and its sorption follows a very sharp isotherm. High selectivity and the sharp isotherm cause CST to act similarly to an instantaneous irreversible reaction. The lag time for cesium ion is increased beyond that predicted by an instantaneous irreversible reaction due to the flat portion of the isotherm. As cesium diffuses across the CST loaded barrier membrane, it adsorbs until it reaches the maximum capacity. The effective concentration of free cesium ion in the barrier is lower than in the upstream compartment. This lower concentration different leads to longer lag times.

The strong affinity for cesium will make it difficult to reuse a CST loaded barrier membrane once it has been fully loaded. Challenging such a barrier with additional cesium ion will show similar behavior to a non-reactive barrier. The high affinity for cesium would make it difficult to desorb the cesium to allow for further use. That said, the high capacity and selectivity of the CST loaded membrane indicate it will be an effective barrier for cesium containment.

Powdered activated carbon (PAC) does not show as sharp of an isotherm with chlorinated contaminants such as 1,2,4-trichlorobenzene (1,2,4-TCB) or polychlorinated biphenyls (PCBs). A barrier membrane loaded with PAC will be more sensitive to changes to concentration changes in the solution surrounding it. A lower concentration results in desorption from the barrier, while a higher concentration results in a higher contaminant loading. If a barrier were fully loaded with contaminant, it should be easier to desorb chlorinated contaminants from the PAC than cesium from CST, for reuse.

5.2 Future Reactive Barrier Applications

This research takes a major stop towards the ultimate goal of designing reactive barrier membranes for environmental applications. Model permeable barriers of water-swollen polyvinylalchol (PVA) were used to model barrier behavior, while allowing relatively fast experiments. In actual environmental applications, barrier membranes will require considerably larger lag times and contaminant capacities to be viable solutions. Barrier membranes also need to withstand forces in the environment that are not experienced in a laboratory setting, including temperature extremes, radiation, currents, debris, sharp objects, and wildlife. More robust polymeric matrices will be required. Some examples could be polyparaphenyleneterephthalamide (Kevlar) for cesium remediation, and high density polyethylene (HDPE) for organics.

5.2.1 Potential Options for CST Loaded Barriers

Care must be taken in the eventual form and application of a reactive barrier membrane. It is unlikely a real-world application will include two well mixed volumes separated by a thin film. One may envision acres of land contaminated with leaked radioactive cesium. Two options could be considered. First, designing a CST loaded barrier in the form of a landfill liner. Contaminated soil may then be dug up and landfilled within the barrier. Aqueous cesium would then be contained within the landfill zone while secondary remediation (*e.g.*, pump-and-treat) was completed. Dangers of this method include radiation exposure to workers performing the digging, and the potential of additional leakage during transport.

A second option would be to dig out trenches around the contaminated zone, and install sheets of CST containing reactive barrier membranes, preventing transfer of contamination horizontally. A pump-and-treat method of the contaminated soil could again be used, without the need of relocation. The barrier would decrease the chance of groundwater contamination near the contaminated site, and allow additional time for treatment. Either option would require care in sealing the edges of the barrier films. Contaminated zones are too large for a single sheet of material. Leakage around the edges will likely exceed that through the barriers.

5.2.2 Potential Options for PAC Loaded Barriers

Similar uses as above can be envisioned for PAC loaded barrier membranes. Sediment from rivers and waterways may be dredged up and landfilled in PAC loaded barriers. Many of the same concerns for CST loaded barriers would exist, including exposure to toxic substances. When dredging, sediment may be mobilized, further spreading the contaminant to be contained.

Another option is use in sediment capping, where a PAC loaded barrier may be placed over a contaminated area, acting as a barrier between contaminated sediment and overlaying water. Generally, sediment caps are made from sand, clay, and soil and may serve as effective barriers (Hagerty and Trotman, 2001; Moo-Young *et al.*, 2001; Talbert *et al.*, 2001; Thoma *et al.*, 1993, Wang *et al.*, 1991). Sediment capping can only contain, not degrade contaminants.

Incorporating a PAC loaded barrier membrane along with *Burkholderia fungorum* LB400, a bacterium capable of degrading PCBs, is a possibility. Models in Chapter 4 show a reactive compartment containing bacteria could work in concert with a PAC containing barrier membrane to degrade contaminants, improving upon existing sediment caps. Such caps would both reduce the quantity of contaminant and decrease transfer out of contaminated zones. The ability for PAC loaded barrier membranes to adsorb and desorb contaminant depending on solution concentration can work as a buffer for bacteria. When concentrations of PCBs are high, which may be toxic, the PAC has a higher loading, sorbing larger quantities of contaminant. As concentrations fall, contaminant will desorb, becoming available for degradation.

5.3 Critical Parameters for Reactive Barrier Membranes

Extending the findings of this research into real-world applications will depend on determining optimum barrier design, requiring attention to critical parameters. These parameters have been discussed in previous chapters, and are summarized below.

One experimental benefit of water-swollen PVA is the partition coefficient between the barrier and solution is near one. Coupled with thin barrier membranes, the partitioning of contaminant in the membrane can generally be ignored. Partition

coefficients of real-world polymers will be important for overall performance. Smaller partition coefficients lead to longer lag times. A polymer which limits diffusion of a contaminant will enhance the effects of reactive group addition.

The loading and size of reactive group within the polymer is important. The reactive capacity of the barrier depends on this loading; the amount of contaminant that can be adsorbed is directly proportional to the amount of reactant. Increasing the amount of adsorbent increases the number of active sites, increasing the probability a diffusing molecule will react. Smaller particles give better dispersion within the polymer and a higher surface area to volume ratio. There will be an optimum loading; as the amount of adsorbent increases, the properties of the polymer matrix will be impacted. Addition of reactants to a polymer matrix may cause some active sites to be inaccessible, decreasing the reactive capacity.

The location of reactive groups within a barrier can affect performance. Results for CST loaded barrier membranes in Chapter 3 showed concentrating reactant on the downstream face increases the lag time. This is due to the concentration profile of contaminant diffusing through a barrier; the concentration is high on the upstream face, and decreases towards the downstream face. A barrier may take advantage of this effect by intentionally loading the reactant towards the downstream face. Alternatively, a reactive and non-reactive barrier may be layered, with the reactive barrier placed as the downstream face.

Lag times increase with the square of membrane thickness. Increasing the thickness also allows for additional adsorbent, increasing reactive capacity. Optimum thickness will be heavily impacted by the membrane manufacturing method. As a membrane becomes thicker, it will become less flexible, which may limit installation and ease of use.

Barrier membranes coupled with biologically active organisms will pose additional difficulties. CST and PAC loaded barrier membranes require no additional reactants and may be installed and left in the environment. Aerobic bacterial colonies require a steady supply of nutrients and oxygen. It is likely these nutrients will not be present in adequate quantities where the barrier is installed, requiring addition. This

added cost must be taken into account when designing barriers. Channels within a barrier may be designed to allow transport of these nutrients to the biologically active zone.

The kinetics of the biologically active volume were assumed to be either first-order or zero-order. While it is expected the microorganisms will follow the Michaelis-Menten kinetics model, a detailed understanding of the reaction behavior would be vital for success of such a system. The amount of contaminant leaving the reactive compartment depends on the Damköhler number, D_M, which is the ratio of the rate of reaction to the rate of mass transfer. A high reaction rate relative to mass transfer is preferred for all cases studied. The value of D_M is an important parameter that must be known before designing this system. Similarly, the quantity and maximum loading of carbon (or other reactive group) is necessary to calculate ν, the ratio of the reactive volume to the apparent carbon volume. Smaller values of ν (greater amounts of carbon) decrease the rate of release of contaminant. The optimum amount of carbon will depend on the size of the system.

5.4 Potential Future Work

This research has shown reactive barrier membranes can be designed for specific contaminants. This was accomplished by loading barrier membranes with materials having a known affinity for the given contaminant. This approach can be extended to any number of applications. While this method can be generalized, care must be taken when selecting a polymer to pair with a reactant. The high reactivity of potassium permanganate ($KMnO_4$) with a large range of contaminants, including chlorinated organics, would be a good fit. For this system to work in practice, a polymer which itself does not react with $KMnO_4$ would be required. PVA, used in this research, would not be a candidate as it would be oxidized by $KMnO_4$ addition.

The structure of the reactive groups used in this research does not change when reaction occurs. One could envision a system where a reaction product is a solid. In addition to reacting away contaminant, a physical barrier is produced to further hinder contaminant diffusion. If the solid product has a flake-like structure, an impermeable wall may be setup perpendicular to the direction of diffusion. Should this structure

become cracked or scratched, contaminant diffusing through this gap will meet reactant deeper in the membrane, forming additional solid. This could be the basis of a self-healing barrier. $KMnO_4$ may be a candidate for such work. A candidate solution would require a polymer that does not react with MnO_4^-. The problem of a flake-like structure forming without being constrained by the polymer matrix would also need to be overcome. An alternative solution may aim to form the flake-like structure on the surface of barrier. Small amounts of aqueous MnO_4^- could be added downstream to react with any contaminant breaking through to reseal the barrier.

Model results of a biologically active compartment combined with a carbon containing barrier could be experimentally verified. The validity of the reaction following either first-order or zero-order kinetics could be explored. The result for a first-order reaction that all contaminant that escapes the reactive volume will eventually leach out of the system would be particularly interesting to study. The assumption of a well-stirred carbon containing volume is likely too simple and could be tested.

One aspect of PAC loaded barrier membranes not studied in this research was how downstream concentration would vary if the upstream concentration changed. Model results in Chapter 4 show increased carbon loading results in a reduced flux from the carbon containing barrier. These models assumed contaminant escaped the system into a perfect sink. Practically, this approximates a sediment cap at the bottom of a river where a convective flow is present, washing leaked contaminant away.

An alternative model could be envisioned. A biologically active volume in series with a carbon containing volume exists as before. Instead of a single pulse of contaminant entering the system at time equals zero, contaminant diffuses into the system through the carbon containing barrier. The concentration gradient driving this diffusion may be constant, or may have an oscillatory variation. Practically, this may approximate plumes of contaminant in a river washing over a sediment cap. Experimental results for PAC loaded barrier films showed concentration rise due to desorption within the barrier went with the square root of time. One could test whether this behavior could result in a dampening effect of concentration changes outside the system. A barrier capable of a dampening effect could have applications for microorganisms that react with a given

substrate, but cannot survive if the substrate concentration grows too high, or falls too low. The ability to dampen a concentration change could result in better control of the system, reducing the likelihood of a concentration spike killing the bacteria.

Finally, completion of CST containing barrier membranes for cesium remediation, and PAC containing membranes for PCB remediation should be pursued. The groundwork for these barriers is laid out in the preceding chapters. Practical, real-world deployment of these reactive barrier membranes into environmental applications should be achievable with a moderate amount of work, and should be a priority. Locations of contaminated areas are known; barriers such as those discussed in this work should be employed to contain and help ensure the contamination does not spread while secondary remediation is performed.

References

Abramowicz, D.A.; Olson, D.R. Accelerated biodegradation of PCBs. *Chemtech* **1995**, *25*, 36-41.

Alberts, B.; Johnson, A.; Lewis, J.; Raff, M.; Roberts, K.; Walter, P. *Molecular Biology of the Cell*; 4th ed.; Garland Science: New York, 2002.

Anthony, R.G.; Dosch, R.G.; Philip, C.V. *Silico-titanates and their methods of making and using*; U.S. Patent 6,479,427 B1. Published Nov. 12, 2002.

Backlin, B.M.; Madej, Forsberg, M. Histology of ovaries and uteri and levels of plasma progesterone, oestradiol-17beta and oestrone sulphate during the implantation period in mated and gonadotrophin-releasing hormone-treated mink (Mustela vison) exposed to polychlorinated biphenyls. *Journal of Applied Toxicology* **1997**, *17*, 297-306.

Bansleben, D.A.; Opuszko, S.; Speer, D.V. *Oxygen scavenging composition with improved properties and method of using same*; U.S. Patent 6,255,248 B1. Published Jul. 3, 2001.

Bedard, D.L.; Unterman, R.; Bopp, L.H.; Brennan, M.J.; Haberl, M.L; Johnson, C. Rapid assay for screening and characterizing microorganisms for the ability to degrade polychlorinated biphenyls. *Applied and Environmental Microbiology* **1986**, *51*, 761-768.

Bell, F.P.; Iverson, F.; Arnold, D.; Vidmar, T.J. Long-term effects of Aroclor 1254 (PCBs) on plasma lipid and carnitine concentrations in rhesus monkey. *Toxicology* **1994**, *89*, 39-153.

Bucheli, T.D.; Gustafsson, Ö. Soot sorption of non-ortho and ortho substituted PCBs. *Chemosphere* **2003**, *53*, 515-522.

Buckley, E.H. Accumulation of airborne polychlorinated biphenyls in foliage. *Science* **1982**, *216*, 520-522.

Brydges, W.T.; Gulati, S.T.; Baum, G. Permeability of glass ribbon-reinforced Composites. *Journal of Materials Science* **1975**, *10*, 2044-2049.

Chao, W.Y.; Hsu, C.C.; Guo, Y.L. Middle-ear disease in children exposed prenatally to polychlorinated biphenyls and polychlorinated dibenzofurans. *Archives of Environmental Health* **1997**, *52*, 257-262.

Chen, Y.C.J.; Guo, Y.L.; Hsu, C.C. Cognitive development of Yu-Cheng ("oil-disease") children prenatally exposed to heat degraded PCBs. *Journal of the American Medical Association* **1992**, *268*, 3213-3218.

Cornelissen, G.; Elmquist, M.; Groth, I.; Gustafsson, Ö. Effect of sorbate planarity on environmental black carbon sorption. *Environmental Science and Technology* **2004**, *38*, 3574-3580.

Crank, J. *The mathematics of diffusion*; 2nd ed.; Clarendon Press: Oxford, U.K., 1975.

Cussler, E.L. *Diffusion: Mass transfer in fluid systems*; 2nd ed.; Cambridge University Press: Cambridge, U.K., 1997.

Cussler E.L.; Hughes, S.E.; Ward, W.J.; Aris, R. Barrier membranes. *Journal of Membrane Science* **1988**, *38*, 161-174.

Daynes H.A. The process of diffusion through a rubber membrane. *Proceedings of the Royal Society of London A* **1920**, *97*, 286-307.

Drinker, C.K.; Warren, M.F.; Bennet, G.A. The problem of possible systemic effects from certain chlorinated hydrocarbons. *Journal of Industrial Hygiene and Toxicology* **1937**, *19*, 283-311.

Eitzman, D.M.; Melkote, R.R.; Cussler, E.L. Barrier membranes with tipped impermeable flakes. *AIChE Journal* **1996**, *42*, 2-9.

Falla, W.R.; Mulski, M.; Cussler, E.L. Estimating diffusion through flake-filled membranes. *Journal of Membrane Science* **1996**, *119,* 129-138.

Fick, A. On liquid diffusion. *Philosophical Magazine* **1855**, *10*, 30-39.

Flury, M.; Mathison, J.B.; Harsh, J.B. In situ mobilization of colloids and transport of cesium in Hanford sediments. *Environmental Science and Technology* **2002**, *36*, 5335-5341.

Garrick, B.J. The current status, safety, and transportation of spent nuclear fuel. *The Bridge* **2003**, *33*, 11-17.

Garten Jr, C.T.; Hambry, D.M.; Schreckhise, R.G. Radiocesium discharges and subsequent environmental transport at the major US weapons production facilities. *The Science of the Total Environment* **2000**, *255*, 55-73.

Gephart, R.E.; Lundgren, R.E.; *Hanford tank cleanup: a guide to understanding the technical issues*; 4th ed.; Battelle Press: Columbus, OH., 1998.

Gu, D.; Nguyen, L.; Philip, C.V.; Huckman, M.E.; Anthony, R.G. Cs^+ ion exchange knetics in complex electrolyte solutions using hydrous crystalline silicotitanates. *Industrial and Engineering Chemistry Research* **1997**, *36*, 5377-5383.

Guo, Y.L.; Lin, C.J.; Yao, W.J. Musculoskeletal changes in children prenatally exposed to polychlorinated biphenyls and related compounds (Yu-Cheng children). *Journal of Toxicology and Environmental Health* **1994**, *41*, 83-93.

Hagerty, P.A.; Trotman, T.D. In situ contaminated sediment management: unique case studies. *Contaminated Soils* **2001**, *6*, 403-410.

Hamm, L.L.; Hang, T.; McCabe, D.J.; King, W.D. An optimal ion exchange design for removal of cesium from Hanford waste. *SCS Advanced Simulation Technologies Conference*, April 2002.

Huckman, M.E.; Latheef, I.M.; Anthony, R.G.; Designing a commercial ion-exchange carousel to treat DOE wastes using CST granules. *AIChE Journal* **2001**, *47*, 1425-1431.

Jacobson, J.L.; Jacobson, S.W. Teratogen update: polychlorinated biphenyls. *Teratology* **1997**, *55*, 338-347.

Jonker, M.T.O.; Koelmans, A.A. Polyoxymethylene solid phase extraction as a partitioning method for hydrophobic organic chemicals in sediment and soot. *Environmental Science and Technology* **2001**, *35*, 3742-3748.

Jonker, M.T.O.; Koelmans, A.A. Sorption of polycyclic aromatic hydrocarbons and polychlorinated biphenyls to soot and soot-like materials in the aqueous environment: mechanistic considerations. *Environmental Science and Technology* **2002**, *36*, 3725-3734.

Kimbrough, R.D.; Jensen, A.A. *Halogenated biphenyls, tetraphenyls, naphthalenes, dibenzodioxins and related products; 2nd ed.*; Elsevier, Amsterdam, 1989.

Koerner, R.M. *Designing with Geosynthetics*; Upper Saddle River, NJ., 1998.

Kuratsune, M.; Yoshimura, T.; Matsuzaka, J.; Yamaguchi, A. Epidemiologic study on Yusho, a poisoning caused by ingestion of rice oil contaminated with a commercial brand of polychlorinated biphenyls. *Environmental Health Perspectives* **1972**, *1*, 119-128.

Kuratsune, M. An abstract of results of laboratory examinations of patients with Yusho and of animal experiments. *Environmental Health Perspectives* **1972**, *1*, 129-136.

LaGrega, M.D.; Buckingham, P.L.; Evans, J.C. Environmental resources management. *Hazardous Waste Management*; McGraw-Hill: New York, 2001.

Langmuir, I. The constitution and fundamental properties of solids and liquids. *Journal of the American Chemical Society* **1916**, *38*, 2221-2295.

Lape, N.K.; Nuxoll, E.E.; Cussler, E.L. Polydisperse flakes in barrier films. *Journal of Membrane Science* **2004**, *236*, 29-37.

Lundquist, S.H.; White, L.R. *Method for removing metal ions from solution with titanate sorbents*. U.S. Patent 5,989,434 A. Published Nov. 23, 1999.

Marsh, S.F.; Svitra, Z.V.; Bowen, S.M. *Los Alamos Report.* LA-12654(UC-940). October 1993.

Mayes, B.A.; McConnell, E.E.; Neal, B.H.; Brunner, M.J.; Hamilton, S.B.; Sullivan, T.M.; Peters, A.C.; Ryan, M.J.; Toft, J.D.; Singer, A.W.; Brown Jr, J.F.; Menton, R.G.; Moore, J.A. Comparative carcinogenicity in Sprague-Dawley rats of the polychlorinated biphenyl mixtures aroclors 1016, 1242, 1254, and 1260. *Toxicological Sciences* **1998**, *41*, 62-76.

Maxwell, JC. *Treatise on Electricity and Magnetism*; Clarendon Press: Oxford, U.K., 1881.

McKinley, J.P.; Zeissler, C.J.; Zachara, J.M.; Serne, R.J.; Lindstrom, R.M.; Schaef, H.T.; Orr, R.D. Distribution and retention of 137Cs in sediments at the Hanford site, Washington. *Environmental Science and Technology* **2001**, *35*, 3433-3441.

Michaels, A.S.; Chandrasekaran, S.K.; Shaw, J.E. Drug permeation through human skin. *AIChE Journal* **1975**, *21*, 985-996.

Moo-Young, H.; Myers, T.; Tardy, B.; Ledbetter, R.; Vanadit-Ellis, W.; Sellasie, K. Determination of the environmental impact of consolication induced convective transport through capped sediment. *Journal of Hazardous Materials* **2001**, *85*, 53-72.

Moore, M. First, puzzlement; then action. *Bulletin of the Atomic Scientist* **1993**, *2*, 24-29.

Murray, J.D. *Mathematical biology volume II: Spatial models and biomedical applications*; 3rd ed.; Springer-Verlag: New York, NY, 2003.

Nuxoll, E.E.; Siegel, R.A.; Cussler, E.L. Layered reactive barrier films, *Journal of Membrane Science* **2005**, *252*, 29-36.

Paul, D.R.; Koros, W.J. Effect of partially immobilizing sorption on permeability and the diffusion lag time. *Journal of Polymer Science: Polymer Physics Edition* **1976**, *4*, 675-685.

Perry, D.; Ward, W.J.; Cussler, E.L.; Unsteady diffusion in barrier membranes. *Journal of Membrane Science* **1989**, *44*, 305-311.

Rowe, R.K.; Hrapovic, L.; Kosaric, N. Diffusion of chloride and dichloromethane through an HDPE geomembrane. *Geosynthetics International* **1995**, *2*, 507-536.

Safe, S.; Safe, L.; Mullin, M. Polychlorinated biphenyls: environmental occurrence and analysis. *Environmental Toxin Series* **1987**, *1*, 1-13.

Schwark, D.W.; Speer, D.V.; McAllister, L.B. *Oxygen scavenging film with high slip properties*. U.S. Patent Application 2004/0151934. Published Aug. 5, 2004.

Shimotori, T. Ph.D. Thesis, University of Minnesota, Minneapolis, MN, 2005.

Shimotori, T.; Cussler, E.L.; Arnold, W.A. High density polyethylene membrane containing Fe^0 as a contaminant barrier. *Journal of Environmental Engineering* **2006**, *132*, 803-809.

Shimotori, T.; Nuxoll, E.E.; Cussler, E.L.; Arnold, W.A. A polymer containing Fe^0 as a contaminant carrier. *Environmental Science and Technology* **2004**, *38*, 2264-2270.

Skoog, D.A.; Holler, F.J.; Nieman, T.A. *Principles of instrumental analysis*; 5th ed.; Brooks Cole Publishing: Pacific Grove, CA, 1997.

Strutt W, Lord Rayleigh. On the influence of obstacles arranged in rectangular order upon the properties of a medium. *Philosophical Magazine* **1892**, *34*, 481-502.

Surdo, E.M.; Cussler. E.L.; Novak, P.J.; Arnold, W.A. Geomembranes containing powdered activated carbon have the potential to improve containment of chlorinated aromatic contaminants. *Environmental Science and Technology* **2009**, *43*, 8916-8922.

Surdo, E.M. Ph.D. Thesis, University of Minnesota, Minneapolis, MN, 2009.

Talbert, B.; Thibodeaux, L.J.; Valsaraj, K.T. Effectiveness of very thin soil layers in chemical release from bed sediment. *Environmental Progress* **2001**, *20*, 103-107.

Tan, Y.; Li, D.; Song, R.; Lawrence, D.; Carpenter, D.O. Ortho-substituted PCBs kill thymocytes. *Toxicological Sciences* **2003**, *76*, 328-337.

Thoma, G.J.; Reible, D.D.; Valsaraj, K.T.; Thibodeaux, L.J. Efficiency of capping contaminated sediments in situ. 2: mathematics of diffusion-adsorption in the capping layer. *Environmental Science and Technology* **1993**, *27*, 2412-2419.

Wakeman, W.A.; Mason, E.A.; Diffusion in multiperforate laminae. *Industrial and Engineering Chemistry Fundamentals* **1979**, *18*, 301-305.

Wang, X.Q.; Thibodeaux, L.J.; Valsaraj, K.T.; Reible, D.D. Efficiency of capping contaminated bed sediments in situ. 1: laboratory-scale experiments on diffusion-adsorption in the capping layer. *Environmental Science and Technology* **1991**, *25*, 1578-1584.

Ward III, W.J. Analytical and experimental studies of facilitated transport. *AIChE Journal* **1970**, *16*, 405-410.

Wiegel, J.; Wu, Q. Microbial reductive dehalogenation of polychlorinated biphenyls. *FEMS Microbiology Ecology* **2000**, *32*, 1-15.

Yang, C.; Nuxoll, E.E.; Cussler, E.L. Reactive barrier films. *AIChE Journal* **2001**, *47*, 295-302.

Yang, C.; Smyrl, W.H.; Cussler, E.L. Aligning flakes in barrier coatings. *Journal of Membrane Science* **2004**, *231*, 1-12.

Yun, J.H.; Choi, D.K.; Kim, S.H. Adsorption equilibria of chlorinated organic solvents onto activated carbon. *Industrial and Engineering Chemistry Research* **1998**, *37*, 1422-1427.

Zheng, C.V.; Philip, C.V.; Anthony, R.G. Ion exchange of group I metals by hydrous crystalline silicotitanates. *Industrial and Engineering Chemistry Research* **1996**, *35*, 4246-4256.

Appendix A

First-Order Reaction, Configuration 1 Derivation

The results discussed previously show how a barrier membrane loaded with a model reversible reactive group responds to changes in upstream concentration. Following is a theory demonstrating how these results can be used in a real-world situation. We begin by envisioning two well-stirred volumes. The first volume, V_1, contains a reactive group which degrades contaminant with a first-order reaction rate constant k_R. The second volume represents a carbon-filled membrane. The membrane has a volume, V_2, with a carbon weight percent W that follows a linear isotherm with slope K. Contaminant can transfer via diffusion between the volumes and out of the second volume. Contaminant present in the first volume is called c_1; contaminant in the second volume is called c_2.

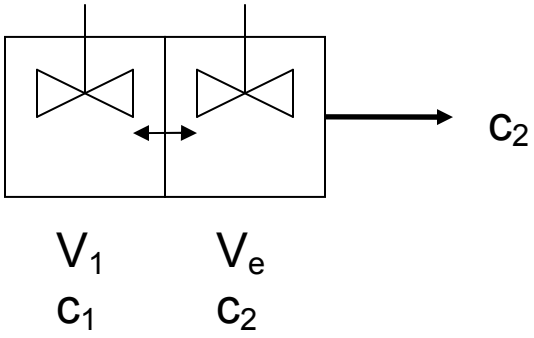

Figure A.1: Model system where a first-order reaction takes place in V_1 and carbon is contained in V_e. Both volumes are assumed to be well-mixed.

Writing a mass balance on each volume gives

$$V_1 \frac{dc_1}{dt} = -\frac{DHA}{l/2}(c_1 - c_2) - k_R c_1 V_1 \qquad \text{(A.1)}$$

$$V_e \frac{dc_2}{dt} = \frac{DHA}{l/2}(c_1 - c_2) - \frac{DHA}{l/2}(c_2 - 0) \qquad \text{(A.2)}$$

with initial conditions

$$t = 0 \qquad c_1 = c_{1(0)} \qquad \text{(A.3)}$$

$$t = 0 \qquad c_2 = 0 \qquad \text{(A.4)}$$

where the diffusion coefficient for the contaminant is D, the partition coefficient is H, the area diffusion occurs across is A, and the length diffusion occurs across is $l/2$. Equation A.2 uses an equivalent volume V_e which takes into account the capacity of the carbon

$$V_e = V_2\left(1+\frac{KW}{V_2}\right). \tag{A.5}$$

Dividing both sides of Equations A.1 and A.2 by their respective volumes and rearranging gives

$$\frac{dc_1}{dt} = -\frac{2DHA}{V_1 l}c_1 - k_R c_1 + 2\frac{DHA}{V_1 l}c_2 \tag{A.6}$$

$$\frac{dc_2}{dt} = \frac{2DHA}{V_e l}c_1 - \frac{4DHA}{V_e l}c_2. \tag{A.7}$$

Defining groups

$$k \equiv \frac{DH}{l} \tag{A.8}$$

$$\tau \equiv \frac{2kAt}{V_1} \tag{A.9}$$

$$\nu \equiv \frac{V_1}{V_e} \tag{A.10}$$

$$D_M \equiv \frac{k_R}{kA/V_1} \tag{A.11}$$

and rearranging Equations A.6 and A.7 gives

$$\frac{dc_1}{d\tau} = -\left(1+\frac{D_M}{2}\right)c_1 + c_2 \tag{A.12}$$

$$\frac{dc_2}{d\tau} = \nu c_1 - 2\nu c_2 \tag{A.13}$$

Equations A.12 and A.13 are a set of coupled, linear, ordinary differential equations depending on the concentrations of contaminants in the two volumes, the ratio of volumes, ν, and an apparent Damköhler number, D_M, which is the ratio of the rate of

reaction, k_R, and the rate of mass transfer, $\frac{kA}{V_1}$. Solving for c_1 and c_2 allows one to predict how the volumes in Figure A.1 are affected by changes in the amount of carbon (achieved by varying ν) and increasing or decreasing the reaction rate (achieved by varying D_M).

Coupled, linear, ordinary differential equations can be transformed into a single higher order equation and solved. A second order differential equation can be found by solving Equation A.12 for c_2

$$c_2 = c_1' + \left(1 + \frac{D_M}{2}\right)c_1 \tag{A.14}$$

and substituting into Equation A.13

$$c_1'' + \left(1 + \frac{D_M}{2}\right)c_1' = \nu c_1 - 2\nu c_1' - 2\nu\left(1 + \frac{D_M}{2}\right)c_1 \tag{A.15}$$

where a prime denotes a derivative with respect to τ (i.e. $c_1' = \frac{dc_1}{d\tau}$ and $c_1'' = \frac{d^2c_1}{d\tau^2}$). Grouping like terms gives

$$c_1'' + \left(1 + \frac{D_M}{2} + 2\nu\right)c_1' - (\nu + D_M\nu)c_1 = 0. \tag{A.16}$$

This equation is of the form

$$Ax_1'' + Bx_1' + Cx_1 = 0 \tag{A.17}$$

which has the solution

$$x_1 = \xi_1 e^{a_1 t} + \xi_2 e^{b_1 t} \tag{A.18}$$

where

$$a_1 = \frac{-B + \sqrt{B^2 - 4AC}}{2A} \tag{A.19}$$

and

$$b_1 = \frac{-B - \sqrt{B^2 - 4AC}}{2A}. \tag{A.20}$$

ξ_1 and ξ_2 are constants determined by the initial conditions.

Solving Equation A.16 then gives

$$c_1 = \xi_1 e^{a_1 \tau} + \xi_2 e^{b_1 \tau} \tag{A.21}$$

with

$$a_1 = \frac{-\left(1 + \frac{D_M}{2} + 2\nu\right) + \sqrt{\left(1 + \frac{D_M}{2} + 2\nu\right)^2 - 4\left(\nu + D_M \nu\right)}}{2} \tag{A.22}$$

and

$$b_1 = \frac{-\left(1 + \frac{D_M}{2} + 2\nu\right) - \sqrt{\left(1 + \frac{D_M}{2} + 2\nu\right)^2 - 4\left(\nu + D_M \nu\right)}}{2}. \tag{A.23}$$

a_1 *and* b_1 depend on the ratio of volumes, ν, and the apparent Damköhler number, D_M. Neither depend on the dimensionless time, τ.

c_2 is solved for by substituting Equation A.21 into Equation A.14

$$c_2 = \xi_1 a_1 e^{a_1 \tau} + \xi_2 b_1 e^{b_1 \tau} + \left(1 + \frac{D_M}{2}\right)\left[\xi_1 e^{a_1 \tau} + \xi_2 e^{b_1 \tau}\right]. \tag{A.24}$$

To find the constants ξ_1 and ξ_2, apply the initial conditions from Equations A.3 and A.4 to Equations A.21 and A.24

$$c_1\left(t = \tau = 0\right) = c_{1(0)} = \xi_1 + \xi_2 \tag{A.25}$$

$$c_2\left(t = \tau = 0\right) = 0 = \xi_1 a_1 + \xi_2 b_1 + \left(1 + \frac{D_M}{2}\right)\left[\xi_1 + \xi_2\right] \tag{A.26}$$

From Equation A.25

$$\xi_1 = c_{1(0)} - \xi_2 . \tag{A.27}$$

Substituting in to Equation A.26

$$0 = \left(c_{1(0)} - \xi_2\right) a_1 + \xi_2 b_1 + \left(1 + \frac{D_M}{2}\right)\left[\left(c_{1(0)} - \xi_2\right) + \xi_2\right] \tag{A.28}$$

and rearranging

$$0 = a_1 c_{1(0)} - a_1 \xi_2 + \xi_2 b_1 + c_{1(0)} + \frac{D_M c_{1(0)}}{2} \tag{A.29}$$

then solving for ξ_2 gives

$$\xi_2 = \frac{\left(a_1 + \frac{D_M}{2} + 1\right)c_{1(0)}}{(a_1 - b_1)}. \tag{A.30}$$

Substituting into Equation A.27 gives

$$\xi_1 = c_{1(0)} - \frac{\left(a_1 + \frac{D_M}{2} + 1\right)c_{1(0)}}{(a_1 - b_1)}. \tag{A.31}$$

In summary, for the system shown in Figure A.1

$$c_1 = \xi_1 e^{a_1\tau} + \xi_2 e^{b_1\tau}$$

$$c_2 = \xi_1 a_1 e^{a_1\tau} + \xi_2 b_1 e^{b_1\tau} + \left(1 + \frac{D_M}{2}\right)\left[\xi_1 e^{a_1\tau} + \xi_2 e^{b_1\tau}\right]$$

$$a_1 = \frac{-\left(1 + \frac{D_M}{2} + 2\nu\right) + \sqrt{\left(1 + \frac{D_M}{2} + 2\nu\right)^2 - 4\left(\nu + D_M\nu\right)}}{2}$$

$$b_1 = \frac{-\left(1 + \frac{D_M}{2} + 2\nu\right) - \sqrt{\left(1 + \frac{D_M}{2} + 2\nu\right)^2 - 4\left(\nu + D_M\nu\right)}}{2}$$

$$\xi_1 = c_{1(0)} - \frac{\left(a_1 + \frac{D_M}{2} + 1\right)c_{1(0)}}{(a_1 - b_1)}$$

$$\xi_2 = \frac{\left(a_1 + \frac{D_M}{2} + 1\right)c_{1(0)}}{(a_1 - b_1)}.$$

Appendix B

First-Order Reaction, Configuration 2 Derivation

The results discussed previously show how a barrier membrane loaded with a model reversible reactive group responds to changes in upstream concentration. Following is a theory demonstrating how these results can be used in a real-world situation. We begin by envisioning two well-stirred volumes. The upstream volume represents a carbon-filled membrane. The membrane has a volume, V_2, with a carbon weight percent W that follows a linear isotherm with slope K. Downstream of V_2 is a volume, V_1, containing a reactive group which degrades contaminant with a first-order reaction rate constant k_R. Contaminant can transfer via diffusion between the volumes and also out of V_1. Contaminant present in V_e is called c_2; contaminant present in V_1 is called c_1.

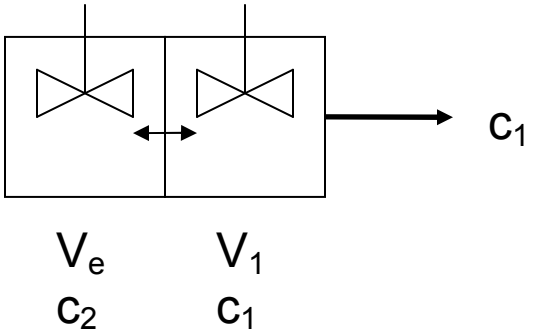

Figure B.1: Model system where carbon is contained in V_e and a first-order reaction takes place in V_1. Both volumes are assumed to be well-mixed.

Writing a mass balance on each volume gives

$$V_e \frac{dc_2}{dt} = -\frac{DHA}{l/2}(c_2 - c_1) \qquad \text{(B.1)}$$

$$V_1 \frac{dc_1}{dt} = \frac{DHA}{l/2}(c_2 - c_1) - \frac{DHA}{l/2}(c_1 - 0) - k_R c_1 V_1 \qquad \text{(B.2)}$$

with initial conditions

$$t = 0 \qquad c_2 = c_{2(0)} \qquad \text{(B.3)}$$

$$t = 0 \qquad c_1 = 0 \qquad \text{(B.4)}$$

where the diffusion coefficient for the contaminant is D, the partition coefficient is H, the area diffusion occurs across is A, and the length diffusion occurs across is $l/2$. Equation B.1 uses an equivalent volume V_e which takes into account the capacity of the carbon

$$V_e = V_2\left(1+\frac{KW}{V_2}\right). \tag{B.5}$$

Dividing both sides of Equations B.1 and B.2 by their respective volumes and rearranging gives

$$\frac{dc_2}{dt} = \frac{2DHA}{V_e l}c_1 - \frac{2DHA}{V_e l}c_2 \tag{B.6}$$

$$\frac{dc_1}{dt} = -\frac{4DHA}{V_1 l}c_1 + \frac{2DHA}{V_1 l}c_2 - k_R c_1 \tag{B.7}$$

Defining groups

$$k \equiv \frac{DH}{l} \tag{B.8}$$

$$\tau \equiv \frac{2kAt}{V_1} \tag{B.9}$$

$$\nu \equiv \frac{V_1}{V_e} \tag{B.10}$$

$$D_M \equiv \frac{k_R}{kA/V_1} \tag{B.11}$$

and rearranging Equations B.6 and B.7 gives

$$\frac{dc_2}{dt} = \nu c_1 - \nu c_2 \tag{B.12}$$

$$\frac{dc_1}{dt} = -\left(2+\frac{D_M}{2}\right)c_1 + c_2 \tag{B.13}$$

Equations B.12 and B.13 are a set of coupled, linear, ordinary differential equations depending on the concentrations of contaminants in the two volumes, the ratio of volumes, ν, and an apparent Damköhler number, D_M, which is the ratio of the rate of

reaction, k_R, and the rate of mass transfer, $\frac{kA}{V_1}$. Solving for c_1 and c_2 allows one to predict how the volumes in Figure B.1 are affected by changes in the amount of carbon (achieved by varying ν) and increasing or decreasing the reaction rate (achieved by varying D_M).

Coupled, linear, ordinary differential equations can be transformed into a single higher order equation and solved. A second order differential equation can be found by solving Equation B.13 for c_1

$$c_1 = \frac{c_2'}{\nu} + c_2 \tag{B.14}$$

and substituting into Equation B.12

$$\frac{c_2''}{\nu} + c_2' = c_2 - \left(\frac{D_M}{2} + 2\right)\left(\frac{c_2'}{\nu} + c_2\right) \tag{B.15}$$

where a prime denotes a derivative with respect to τ (i.e. $c_2' = \frac{dc_2}{d\tau}$ and $c_2'' = \frac{d^2c_2}{d\tau^2}$).

Grouping like terms and multiplying through by ν gives

$$c_2'' + \left(\nu + \frac{D_M}{2} + 2\right)c_2' + \left(\frac{D_M\nu}{2} + \nu\right)c_2 = 0. \tag{B.16}$$

This equation is of the form

$$Ax_2'' + Bx_2' + Cx_2 = 0 \tag{B.17}$$

which has the solution

$$x_2 = \xi_1 e^{a_1 t} + \xi_2 e^{b_1 t} \tag{B.18}$$

where

$$a_1 = \frac{-B + \sqrt{B^2 - 4AC}}{2A} \tag{B.19}$$

and

$$b_1 = \frac{-B - \sqrt{B^2 - 4AC}}{2A}. \tag{B.20}$$

ξ_1 and ξ_2 are constants determined by the initial conditions.

Solving Equation B.16 then gives

$$c_2 = \xi_1 e^{a_1 \tau} + \xi_2 e^{b_1 \tau} \tag{B.21}$$

with

$$a_1 = \frac{-\left(\nu + \frac{D_M}{2} + 2\right) + \sqrt{\left(\nu + \frac{D_M}{2} + 2\right)^2 - 4\left(\frac{D_M \nu}{2} + \nu\right)}}{2} \tag{B.22}$$

$$b_1 = \frac{-\left(\nu + \frac{D_M}{2} + 2\right) - \sqrt{\left(\nu + \frac{D_M}{2} + 2\right)^2 - 4\left(\frac{D_M \nu}{2} + \nu\right)}}{2} \tag{B.23}$$

a_1 *and* b_1 depend on the ratio of volumes, ν, and the apparent Damköhler number, D_M. Neither depend on the dimensionless time, τ.

c_1 is solved for by substituting Equation B.21 into Equation B.14

$$c_1 = \frac{\xi_1 a_1}{\nu} e^{a_1 \tau} + \frac{\xi_2 b_1}{\nu} e^{b_1 \tau} + \xi_1 e^{a_1 \tau} + \xi_2 e^{b_1 \tau}. \tag{B.24}$$

To find the constants ξ_1 and ξ_2, apply the initial conditions from Equations B.3 and B.4 to Equations B.21 and B.24

$$c_2\left(t = \tau = 0\right) = c_{2(0)} = \xi_1 + \xi_2 \tag{B.25}$$

$$c_1\left(t = \tau = 0\right) = 0 = \frac{\xi_1 a_1}{\nu} + \frac{\xi_2 b_1}{\nu} + \xi_1 + \xi_2 \tag{B.26}$$

From Equation B.25

$$\xi_2 = c_{2(0)} - \xi_1. \tag{B.27}$$

Substituting in to Equation B.26

$$0 = \frac{\xi_1 a_1}{\nu} + \frac{\left(c_{2(0)} - \xi_1\right) b_1}{\nu} + \xi_1 + \left(c_{2(0)} - \xi_1\right) \tag{B.28}$$

and rearranging

$$0 = \left(\frac{a_1}{\nu} - \frac{b_1}{\nu}\right)\xi_1 + \left(\frac{b_1}{\nu} + 1\right) c_{2(0)} \tag{B.29}$$

then solving for ξ_1 gives

$$\xi_1 = \left(\frac{b_1 + \nu}{b_1 - a_1} \right) c_{2(0)} . \tag{B.30}$$

Substituting into Equation B.27 gives

$$\xi_2 = \left(1 - \frac{b_1 + \nu}{b_1 - a_1} \right) c_{2(0)} . \tag{B.31}$$

In summary, for the system shown in Figure B.1

$$c_2 = \xi_1 e^{a_1 \tau} + \xi_2 e^{b_1 \tau}$$

$$c_1 = \frac{\xi_1 a_1}{\nu} e^{a_1 \tau} + \frac{\xi_2 b_1}{\nu} e^{b_1 \tau} + \xi_1 e^{a_1 \tau} + \xi_2 e^{b_1 \tau}$$

$$a_1 = \frac{-\left(\nu + \frac{D_M}{2} + 2 \right) + \sqrt{\left(\nu + \frac{D_M}{2} + 2 \right)^2 - 4\left(\frac{D_M \nu}{2} + \nu \right)}}{2}$$

$$b_1 = \frac{-\left(\nu + \frac{D_M}{2} + 2 \right) - \sqrt{\left(\nu + \frac{D_M}{2} + 2 \right)^2 - 4\left(\frac{D_M \nu}{2} + \nu \right)}}{2}$$

$$\xi_1 = \left(\frac{b_1 + \nu}{b_1 - a_1} \right) c_{2(0)}$$

$$\xi_2 = \left(1 - \frac{b_1 + \nu}{b_1 - a_1} \right) c_{2(0)} .$$

Appendix C

Zero-Order Reaction, Configuration 1 Derivation

The results discussed previously show how a barrier membrane loaded with a model reversible reactive group responds to changes in upstream concentration. Following is a theory demonstrating how these results can be used in a real-world situation. We begin by envisioning two well-stirred volumes. The first volume, V_1, contains a reactive group which degrades contaminant with a zero-order reaction rate constant $k_{R,0}$. The second volume represents a carbon-filled membrane. The membrane has a volume, V_2, with a carbon weight percent W that follows a linear isotherm with slope K. Contaminant can transfer via diffusion between the volumes and out of the second volume. Contaminant present in the first volume is called c_1; contaminant in the second volume is called c_2.

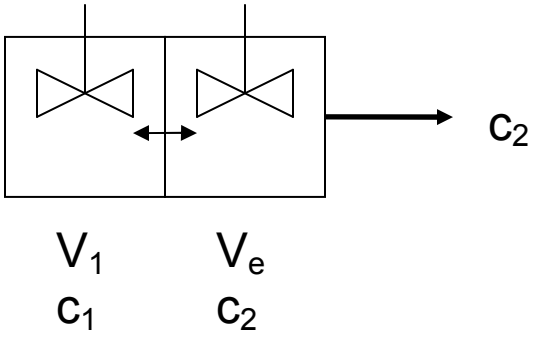

Figure C.1: Model system where a zero-order reaction takes place in V_1 and carbon is contained in V_e. Both volumes are assumed to be well-mixed.

Writing a mass balance on each volume gives

$$V_1 \frac{dc_1}{dt} = -\frac{DHA}{l/2}(c_1 - c_2) - k_{R,0} V_1 \qquad \text{(C.1)}$$

$$V_e \frac{dc_2}{dt} = \frac{DHA}{l/2}(c_1 - c_2) - \frac{DHA}{l/2}(c_2 - 0) \qquad \text{(C.2)}$$

with initial conditions

$$t = 0 \qquad c_1 = c_{1(0)} \qquad \text{(C.3)}$$

$$t = 0 \qquad c_2 = 0 \qquad \text{(C.4)}$$

where the diffusion coefficient for the contaminant is D, the partition coefficient is H, the area diffusion occurs across is A, and the length diffusion occurs across is $l/2$. Equation C.2 uses an equivalent volume V_e which takes into account the capacity of the carbon

$$V_e = V_2\left(1+\frac{KW}{V_2}\right). \tag{C.5}$$

Dividing both sides of Equations A.1 and A.2 by their respective volumes and rearranging gives

$$\frac{dc_1}{dt} = -\frac{2DHA}{V_1 l}c_1 + 2\frac{DHA}{V_1 l}c_2 - k_{R,0} \tag{C.6}$$

$$\frac{dc_2}{dt} = \frac{2DHA}{V_e l}c_1 - \frac{4DHA}{V_e l}c_2 \tag{C.7}$$

Define groups

$$k \equiv \frac{DH}{l} \tag{C.8}$$

$$\tau \equiv \frac{2kAt}{V_1} \tag{C.9}$$

$$\nu \equiv \frac{V_1}{V_e} \tag{C.10}$$

$$D_M \equiv \frac{k_{R,0}}{c_{1,(0)}kA/V_1}. \tag{C.11}$$

Note the definition of D_M is slightly different than for a first-order reaction. Looking at the units of $k_{R,0}$ shows

$$k_{R,0}[=]\frac{mole}{volume*time} \tag{C.12}$$

while k_R has the units

$$k_R[=]\frac{1}{time}. \tag{C.13}$$

The goal of defining D_M is to have a dimensionless group. To achieve this, $k_{R,0}$ must be divided by a reference concentration. The appropriate reference concentration for this system is $c_{1,0}$.

Substituting Equations C.8-C.11 into Equations C.6 and C.7 and rearranging gives

$$\frac{dc_1}{d\tau} = -c_1 + c_2 - \frac{D_M c_{1(0)}}{2} \qquad \text{(C.14)}$$

$$\frac{dc_2}{d\tau} = \nu c_1 - 2\nu c_2 \qquad \text{(C.15)}$$

Equations C.14 and C.15 are a set of coupled, linear, ordinary differential equations depending on the concentrations of contaminants in the two volumes, the ratio of volumes, ν, the initial concentration $c_{1(0)}$, and an apparent Damköhler number, D_M, which is the ratio of the rate of reaction, $\frac{k_{R,0}}{c_{1(0)}}$, and the rate of mass transfer, $\frac{kA}{V_1}$.

Solving for c_1 and c_2 allows one to predict how the volumes in Figure C.1 are affected by changes in the amount of carbon (achieved by varying ν) and increasing or decreasing the reaction rate (achieved by varying D_M).

Coupled, linear, ordinary differential equations can be transformed into a single higher order equation and solved. A second order differential equation can be found by solving Equation C.14 for c_2

$$c_2 = c_1' + c_1 + \frac{D_M c_{1(0)}}{2} \qquad \text{(C.16)}$$

and substituting into Equation C.15

$$c_1'' + c_1' = \nu c_1 - 2\nu\left(c_1' + c_1 + \frac{D_M c_{1(0)}}{2}\right) \qquad \text{(C.17)}$$

where a prime denotes a derivative with respect to τ (i.e. $c_1' = \frac{dc_1}{d\tau}$ and $c_1'' = \frac{d^2 c_1}{d\tau^2}$).

Grouping like terms gives

$$c_1'' + (1 + 2\nu)c_1' + \nu c_1 = -D_M c_{1(0)}\nu\,. \qquad \text{(C.18)}$$

This equation is of the form

$$Ax_1''+Bx_1'+Cx_1 = R \tag{C.19}$$

and has the solution

$$x_1 = \xi_1 e^{a_1 t} + \xi_2 e^{b_1 t} + \frac{R}{C} \tag{C.20}$$

where

$$a_1 = \frac{-B + \sqrt{B^2 - 4AC}}{2A} \tag{C.21}$$

and

$$b_1 = \frac{-B - \sqrt{B^2 - 4AC}}{2A}. \tag{C.22}$$

ξ_1 and ξ_2 are constants determined by the initial conditions.

Solving Equation C.18 then gives

$$c_1 = -D_M c_{1(0)} + \xi_1 e^{a_1 \tau} + \xi_2 e^{b_1 \tau} \tag{C.23}$$

with

$$a_1 = \frac{-(1+2\nu) + \sqrt{1+4\nu^2}}{2} \tag{C.24}$$

and

$$b_1 = \frac{-(1+2\nu) - \sqrt{1+4\nu^2}}{2} \tag{C.25}$$

a_1 and b_1 depend on the ratio of volumes, ν, but as opposed to the first-order reaction cases, not the apparent Damköhler number, D_M. Neither depend on the dimensionless time, τ.

c_2 is solved for by substituting Equation C.23 into Equation C.14

$$c_2 = \xi_1 a_1 e^{a_1 \tau} + \xi_2 b_1 e^{b_1 \tau} + \xi_1 e^{a_1 \tau} + \xi_2 e^{b_1 \tau} - \frac{D_M c_{1(0)}}{2}. \tag{C.26}$$

To find the constants ξ_1 and ξ_2, apply the initial conditions from Equations C.3 and C.4 to Equations C.23 and C.26

$$c_1(t = \tau = 0) = c_{1(0)} = \xi_1 + \xi_2 - D_M c_{1(0)} \tag{C.27}$$

$$c_2(t=\tau=0)=0=\xi_1 a_1+\xi_2 b_1+\xi_1+\xi_2-\frac{D_M c_{1(0)}}{2} \tag{C.28}$$

From Equation C.27

$$\xi_1 = c_{1(0)} - \xi_2 + D_M c_{1(0)}. \tag{C.29}$$

Substituting in to Equation C.28

$$0=\left(c_{1(0)}-\xi_2+D_M c_{1(0)}\right)a_1+\xi_2 b_1+c_{1(0)}+\frac{D_M c_{1(0)}}{2} \tag{C.30}$$

and rearranging

$$0=a_1 c_{1(0)}+a_1 D_M c_{1(0)}+c_{1(0)}+\frac{D_M c_{1(0)}}{2}-(a_1-b_1)\xi_2 \tag{C.31}$$

then solving for ξ_2 gives

$$\xi_2=\frac{(1+a_1)c_{1(0)}+\left(\frac{1}{2}+a_1\right)D_M c_{1(0)}}{(a_1-b_1)}. \tag{C.32}$$

Substituting into Equation C.29 gives

$$\xi_1 = c_{1(0)} - \frac{(1+a_1)c_{1(0)}+\left(\frac{1}{2}+a_1\right)D_M c_{1(0)}}{(a_1-b_1)} + D_M c_{1(0)}. \tag{C.33}$$

Region 2

Unlike a first-order reaction rate, a zero-order reaction rate does not depend on concentration. Equation C.23 is only useful until the time τ^* when $c_1 = 0$. After this time, c_1 will remain zero as any additional contaminant that enters V_1 will immediately be reacted. V_1 now acts as a perfect sink. A new mass balance must be made on the system in Figure C.1 to model the concentration of contaminant after τ^*.

For $\tau > \tau^*$ where τ^* is the time at which c_1 goes to zero

$$c_1 = 0 \tag{C.34}$$

$$V_1 \frac{dc_1}{dt} = 0 \tag{C.35}$$

$$V_e \frac{dc_2}{dt} = -\frac{DHA}{l/2}(c_2 - 0) - \frac{DHA}{l/2}(c_2 - 0). \qquad \text{(C.36)}$$

The initial condition for Equation C.36 is

$$\tau = \tau^* \qquad c_2 = c_2(\tau^*) \qquad \text{(C.37)}$$

where $c_2(\tau^*)$ is the concentration of c_2 at $\tau = \tau^*$, the instant c_1 becomes zero. Dividing Equation C.36 by V_e, and rearranging gives

$$\frac{dc_2}{dt} = -\frac{4DHA}{V_e l} c_2 \qquad \text{(C.38)}$$

Substituting Equations C.9 and C.10 gives

$$\frac{dc_2}{d\tau} = -2\nu c_2 \qquad \text{(C.39)}$$

which depends on carbon-loading, but not on the reaction rate. Solving and applying the initial condition in Equation C.37 gives

$$c_2 = c_2(\tau^*) e^{-2\nu(\tau - \tau^*)}. \qquad \text{(C.40)}$$

In summary, for the system shown in Figure C.1

For $\tau \le \tau^*$

$$c_1 = -D_M c_{1(0)} + \xi_1 e^{a_1 \tau} + \xi_2 e^{b_1 \tau}$$

$$c_2 = \xi_1 a_1 e^{a_1 \tau} + \xi_2 b_1 e^{b_1 \tau} + \xi_1 e^{a_1 \tau} + \xi_2 e^{b_1 \tau} - \frac{D_M c_{1(0)}}{2}$$

$$a_1 = \frac{-(1+2\nu) + \sqrt{1+4\nu^2}}{2}$$

$$b_1 = \frac{-(1+2\nu) - \sqrt{1+4\nu^2}}{2}$$

$$\xi_1 = c_{1(0)} - \frac{(1+a_1)c_{1(0)} + \left(\frac{1}{2} + a_1\right) D_M c_{1(0)}}{(a_1 - b_1)} + D_M c_{1(0)}$$

$$\xi_2 = \frac{(1+a_1)c_{1(0)} + \left(\frac{1}{2} + a_1\right) D_M c_{1(0)}}{(a_1 - b_1)}$$

For $\tau \geq \tau^*$

$$c_1 = 0$$

$$c_2 = c_2\left(\tau^*\right)e^{-2\nu\left(\tau-\tau^*\right)}$$

Appendix D

Zero-Order Reaction, Configuration 2 Derivation

The results discussed previously show how a barrier membrane loaded with a model reversible reactive group responds to changes in upstream concentration. Following is a theory demonstrating how these results can be used in a real-world situation. We begin by envisioning two well-stirred volumes. The upstream volume represents a carbon-filled membrane. The membrane has a volume, V_2, with a carbon weight percent W that follows a linear isotherm with slope K. Downstream of V_2 is a volume, V_1, containing a reactive group which degrades contaminant with a zero-order reaction rate constant $k_{R,0}$. Contaminant can transfer via diffusion between the volumes and also out of V_1. Contaminant present in V_e is called c_2; contaminant present in V_1 is called c_1.

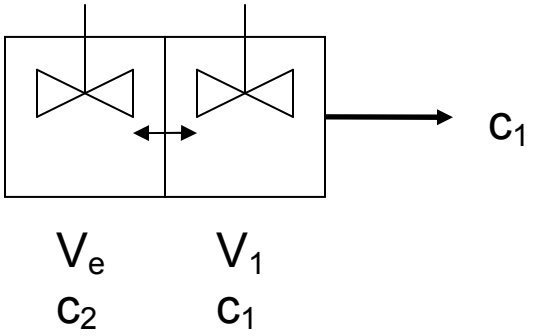

Figure D.1: Model system where carbon is contained in V_e and a first-order reaction takes place in V_1. Both volumes are assumed to be well-mixed.

Writing a mass balance on each volume gives

$$V_e \frac{dc_2}{dt} = -\frac{DHA}{l/2}(c_2 - c_1) \qquad \text{(D.1)}$$

$$V_1 \frac{dc_1}{dt} = \frac{DHA}{l/2}(c_2 - c_1) - \frac{DHA}{l/2}(c_1 - 0) - k_{R,0}V_1 \qquad \text{(D.2)}$$

with initial conditions

$$t = 0 \qquad c_2 = c_{2(0)} \qquad \text{(D.3)}$$

$$t = 0 \qquad c_1 = 0 \qquad \text{(D.4)}$$

where the diffusion coefficient for the contaminant is D, the partition coefficient is H, the area diffusion occurs across is A, and the length diffusion occurs across is $l/2$. Equation D.1 uses an equivalent volume V_e which takes into account the capacity of the carbon

$$V_e = V_2\left(1+\frac{KW}{V_2}\right). \tag{D.5}$$

Dividing both sides of Equations D.1 and D.2 by their respective volumes and rearranging gives

$$\frac{dc_2}{dt} = \frac{2DHA}{V_e l}c_1 - \frac{2DHA}{V_e l}c_2 \tag{D.6}$$

$$\frac{dc_1}{dt} = -\frac{4DHA}{V_1 l}c_1 + \frac{2DHA}{V_1 l}c_2 - k_{R,0} \tag{D.7}$$

Defining groups

$$k \equiv \frac{DH}{l} \tag{D.8}$$

$$\tau \equiv \frac{2kAt}{V_1} \tag{D.9}$$

$$\nu \equiv \frac{V_1}{V_e} \tag{D.10}$$

$$D_M \equiv \frac{k_{R,0}}{c_{2,(0)}kA/V_1} \tag{D.11}$$

Note the definition of D_M is slightly different than for a first-order reaction. Looking at the units of $k_{R,0}$ shows

$$k_{R,0}[=]\frac{mole}{volume*time} \tag{D.12}$$

while k_R has the units

$$k_R[=]\frac{1}{time}. \tag{D.13}$$

The goal of defining D_M is to have a dimensionless group. To achieve this, $k_{R,0}$ must be divided by a reference concentration. The appropriate reference concentration for this system is $c_{2,0}$.

Substituting Equations D.8-D.11 into Equations D.6 and D.7 and rearranging gives

$$\frac{dc_2}{dt} = \nu c_1 - \nu c_2 \qquad \text{(D.14)}$$

$$\frac{dc_1}{dt} = -2c_1 + c_2 - \frac{D_M}{2} \qquad \text{(D.15)}$$

Equations D.14 and D.15 are a set of coupled, linear, ordinary differential equations depending on the concentrations of contaminants in the two volumes, the ratio of volumes, ν, the initial concentration $c_{2(0)}$, and an apparent Damköhler number, D_M, which is the ratio of the rate of reaction, $\frac{k_{R,0}}{c_{2(0)}}$, and the rate of mass transfer, $\frac{kA}{V_1}$.

Solving for c_1 and c_2 allows one to predict how the volumes in Figure D.1 are affected by changes in the amount of carbon (achieved by varying ν) and increasing or decreasing the reaction rate (achieved by varying D_M).

Coupled, linear, ordinary differential equations can be transformed into a single higher order equation and solved. A second order differential equation can be found by solving Equation D.15 for c_2

$$c_2 = c_1' + 2c_1 + \frac{D_M c_{2(0)}}{2} \qquad \text{(D.16)}$$

and substituting into Equation D.14

$$c_1'' + 2c_1' = \nu c_1 - \nu c_1' - 2\nu c_1 - \frac{D_M c_{2(0)} \nu}{2} \qquad \text{(D.17)}$$

where a prime denotes a derivative with respect to τ (i.e. $c_2' = \frac{dc_2}{d\tau}$ and $c_2'' = \frac{d^2 c_2}{d\tau^2}$).

Grouping like terms gives

$$c_1'' + (2+\nu)c_1' + \nu c_1 = -\frac{D_M c_{2(0)} \nu}{2}. \qquad \text{(D.18)}$$

This equation is of the form

$$Ax_2''+Bx_2'+Cx_2 = R \tag{D.19}$$

and has the solution

$$x_2 = \xi_1 e^{a_1 t} + \xi_2 e^{b_1 t} + \frac{R}{C} \tag{D.20}$$

where

$$a_1 = \frac{-B+\sqrt{B^2-4AC}}{2A} \tag{D.21}$$

and

$$b_1 = \frac{-B-\sqrt{B^2-4AC}}{2A}. \tag{D.22}$$

ξ_1 and ξ_2 are constants determined by the initial conditions.

Solving Equation D.18 then gives

$$c_1 = -\frac{D_M c_{2(0)}}{2} + \xi_1 e^{a_1 \tau} + \xi_2 e^{b_1 \tau} \tag{D.23}$$

with

$$a_1 = \frac{-(2+\nu)+\sqrt{4+\nu^2}}{2} \tag{D.24}$$

$$a_1 = \frac{-(2+\nu)-\sqrt{4+\nu^2}}{2} \tag{D.25}$$

a_1 *and* b_1 depend on the ratio of volumes, ν, but as opposed to the first-order reaction cases, not the apparent Damköhler number, D_M. Neither depend on the dimensionless time, τ.

c_2 is solved for by substituting Equation D.23 into Equation D.16

$$c_2 = \xi_1 a_1 e^{a_1 \tau} + \xi_2 b_1 e^{b_1 \tau} + 2\xi_1 e^{a_1 \tau} + 2\xi_2 e^{b_1 \tau} - \frac{D_M c_{2(0)}}{2}. \tag{D.26}$$

To find the constants ξ_1 and ξ_2, apply the initial conditions from Equations D.3 and D.4 to Equations D.23 and D.26

$$c_1(t=\tau=0)=0=\xi_1+\xi_2-\frac{D_M c_{2(0)}}{2} \tag{D.27}$$

$$c_2(t=\tau=0)=c_{2(0)}=\xi_1 a_1+\xi_2 b_1+2\xi_1+2\xi_2-\frac{D_M c_{2(0)}}{2} \tag{D.28}$$

From Equation D.27

$$\xi_1=\frac{D_M c_{2(0)}}{2}-\xi_2 . \tag{D.29}$$

Substituting in to Equation D.28

$$c_{2(0)}=\frac{a_1 D_M c_{2(0)}}{2}-a_1\xi_2+\xi_2 b_1+\frac{D_M c_{2(0)}}{2} \tag{D.30}$$

and rearranging

$$c_{2(0)}=\frac{D_M c_{2(0)}}{2}(a_1+1)+\xi_2(b_1-a_1) \tag{D.31}$$

then solving for ξ_2 gives

$$\xi_2=\frac{c_{2(0)}-\frac{D_M c_{2(0)}(a_1+1)}{2}}{(b_1-a_1)} . \tag{D.32}$$

Substituting into Equation B.27 gives

$$\xi_1=\frac{D_M c_{2(0)}}{2}-\frac{c_{2(0)}-\frac{D_M c_{2(0)}(a_1+1)}{2}}{(b_1-a_1)} \quad . \tag{D.33}$$

Region 2

Unlike a first-order reaction rate, a zero-order reaction rate does not depend on concentration. For this system, as contaminant from V_e begins to transfering into V_1, c_1 will begin to rise. The presence of the zero-order reaction, along with transfer out of the system, will cause c_1 to decrease. Equation D.23 is only useful until the time τ^* when $c_1=0$. Equation D.4 shows $c_1=0$ when $t=\tau=0$ therefore τ^* is defined for the

$\tau > 0$ root. After this time, c_1 will remain zero as any additional contaminant that enters V_1 will immediately be reacted. V_1 now acts as a perfect sink. A new mass balance must be made on the system in Figure D.1 to model the concentration of contaminant after τ^*.

For $\tau > \tau^*$ where τ^* is the time at which c_1 goes to zero

$$c_1 = 0 \tag{D.34}$$

$$V_1 \frac{dc_1}{dt} = 0 \tag{D.35}$$

$$V_e \frac{dc_2}{dt} = -\frac{DHA}{l/2}(c_2 - 0). \tag{D.36}$$

The initial condition for Equation D.36 is

$$\tau = \tau^* \qquad c_2 = c_2(\tau^*) \tag{D.37}$$

where $c_2(\tau^*)$ is the concentration of c_2 at $\tau = \tau^*$, the instant c_1 becomes zero. Dividing Equation D.36 by V_e, and rearranging gives

$$\frac{dc_2}{dt} = -\frac{2DHA}{V_e l} c_2. \tag{D.38}$$

Substituting Equations D.9 and D.10 gives

$$\frac{dc_2}{d\tau} = -\nu c_2 \tag{D.39}$$

which depends on carbon-loading, but not on the reaction rate. Solving and applying the initial condition in Equation D.37 gives

$$c_2 = c_2(\tau^*) e^{-\nu(\tau - \tau^*)}. \tag{D.40}$$

In summary, for the system shown in Figure D.1

For $\tau \le \tau^*$

$$c_1 = -\frac{D_M c_{2(0)}}{2} + \xi_1 e^{a_1 \tau} + \xi_2 e^{b_1 \tau}$$

$$c_2 = \xi_1 a_1 e^{a_1 \tau} + \xi_2 b_1 e^{b_1 \tau} + 2\xi_1 e^{a_1 \tau} + 2\xi_2 e^{b_1 \tau} - \frac{D_M c_{2(0)}}{2}$$

$$a_1 = \frac{-(2+\nu) + \sqrt{4+\nu^2}}{2}$$

$$b_1 = \frac{-(2+\nu)-\sqrt{4+\nu^2}}{2}$$

$$\xi_1 = \frac{D_M c_{2(0)}}{2} - \frac{c_{2(0)} - \frac{D_M c_{2(0)}(a_1+1)}{2}}{(b_1 - a_1)}$$

$$\xi_2 = \frac{c_{2(0)} - \frac{D_M c_{2(0)}(a_1+1)}{2}}{(b_1 - a_1)}$$

For $\tau \geq \tau^*$

$$c_1 = 0$$

$$c_2 = c_2(\tau^*)e^{-\nu(\tau-\tau^*)}$$